WADC TECHNICAL REPORT 55-29
PART V

HYDRAULIC SERVO CONTROL VALVES—PART 5, ANALOG SIMULATION, PRESSURE CONTROL, AND HIGH-TEMPERATURE TEST FACILITY DESIGN

LESLIE R. AXELROD
DELMAR R. JOHNSON
WAYNE L. KINNEY

COOK RESEARCH LABORATORIES
A DIVISION OF COOK ELECTRIC COMPANY

AUGUST 1958

FLIGHT CONTROL LABORATORY
CONTRACT NO. AF 33(616)-5136
PROJECT NO. 1385
TASK 82128

WRIGHT AIR DEVELOPMENT CENTER
AIR RESEARCH AND DEVELOPMENT COMMAND
UNITED STATES AIR FORCE
WRIGHT-PATTERSON AIR FORCE BASE, OHIO

FOREWORD

This report, Hydraulic Servo Control Valves - Part 5, Analog Simulation, Pressure Control, and High-Temperature Test Facility Design, was prepared under the direction of B. A. Johnson, project engineer and T. J. Dunsheath, technical director of the Automatic Controls Section of Cook Research Laboratories, Morton Grove, Illinois. This work was done under Air Force Contract No. AF 33(616)-5136, and this report is the first of two parts to be prepared under this contract. It also is a continuation of previous work on related subjects and is Part 5 of the series entitled Hydraulic Servo Control Valves. Incluced is a means of analog simulation for the internal characteristics of a servo valve, analysis of a pressure control valve including development and experimental verification of its transfer function, and design of a high-temperature valve test facility. Part 6 of this series will contain information on the effects of oil contamination on valve operation, an analysis of factors influencing valve life and reliability, results of standard tests on certain newly developed valves, and a study of the effects of gamma radiation on servo valves and control systems.

Personnel involved in the program included L. R. Axelrod, W. L. Kinney, D. R. Johnson, J. A. Scheid, E. D. Schumann, and A. D'Andrea. Mr. Axelrod developed the equations necessary for analog simulation of the valve and was assisted in the actual simulation by Mr. Scheid. Mr. Schumann performed the necessary experimental work on the two valves that were simulated. Mr. Kinney developed the pressure control valve transfer function and was assisted in laboratory verification of the results by Mr. D'Andrea. Mr. D. R. Johnson performed a major portion of the work in the design of the high-temperature test facility.

The work was administered under the direction of the Flight Control Laboratory, WADC, with Mr. V. R. Schmitt as initiator. This document is unclassified.

ABSTRACT

This report is divided into three sections, analog computer simulation of an electrohydraulic servo valve, investigation of pressure control valves, and design of a high-temperature test facility. In the first section, analytical relations are developed which describe the internal nonlinear operations of the valve. These equations are then mechanized on an analog computer and the results verified for static conditions.

The advisability of using a pressure control valve as opposed to a flow control valve in closed loop operation is investigated in the second section. Included is the development of a pressure control valve transfer function and experimental verification of the analytical results. In the third section, the requirements for a valve testing facility capable of providing and utilizing oil at 750°F, and an ambient temperature up to 1200°F, are presented. Such a facility is designed and described.

PUBLICATION REVIEW

This report has been reviewed and is approved.

FOR THE COMMANDER:

C. R. Bryan
for DONALD S. DUNLAP
Colonel, USAF
Chief, Flight Control Laboratory

TABLE OF CONTENTS

TABLE OF CONTENTS (cont'd)

LIST OF ILLUSTRATIONS

LIST OF ILLUSTRATIONS (cont'd)

LIST OF ILLUSTRATIONS (cont'd)

LIST OF ILLUSTRATIONS (cont'd)

LIST OF ILLUSTRATIONS (cont'd)

LIST OF TABLES

CHAPTER 1

INTRODUCTION

A. Purpose

This is an interim report and covers the results of work carried out under the following three tasks:

(1) A Servo Valve Analog Study

(2) Investigation of Pressure Control Valves

(3) Requirements and Design of a High-Temperature Hydraulic Test Facility.

Four other tasks, conducted under this same contract, will be covered in Technical Report 55-29, Part 6. These are:

(1) Investigation of the Effect of Nuclear Radiation on Electro-hydraulic Servo Valves and Associated Equipments

(2) Investigation of the Effects of Oil Contamination on Servo Valves

(3) Study of Life and Reliability of Servo Valves

(4) Test of Three Electrohydraulic Servo Valves.

The purpose of the Servo Valve Analog Study was to simulate on an electronic analog computer the complete operational characteristics of an electrohydraulic servo valve, excluding certain transient flow phenomena. Such a simulation is useful for investigating how various valve parameters affect the over-all valve performance and can be used to optimize the various elements within the valve to provide the best combination of valve characteristics.

Manuscript released by the author 8 August 1958 for publication as a WADC Technical Note.

The object of the Pressure Control Valve Investigation was to determine the types of applications or loads for which the pressure control valve was more suited than the flow control valve and to determine the extent of its superiority, if any. Another objective of this task was to study and compare various designs of pressure control valves and to determine their transfer functions.

The purpose of the High-Temperature Facility phase was to ascertain the high-temperature requirements of present and contemplated aircraft and missiles, to determine the requirements of a facility for testing components which will operate under high oil and ambient temperatures, and to formulate a preliminary design of such a facility. A brief survey of high-temperature facilities currently in operation or under construction was also required.

B. Organization of the Report

Each of the various tasks is included as a separate integral chapter of this report. Chapter II and Appendixes I through IV cover the Servo Valve Analog Study. Chapter III and Appendix V discuss the Investigation of Pressure Control Valves. Chapter IV and Appendix VI deal with the High-Temperature Facility Study.

CHAPTER II

ANALOG COMPUTER SIMULATION OF AN ELECTROHYDRAULIC SERVO VALVE

A. Introduction

1. Background

In the comparison of electrohydraulic servo valves the question often arises, "Why does one valve have better dynamic response than another?" It is doubtful if the valve manufacturers themselves can answer the question in its entirety. A complete answer would require a thorough understanding of the internal operation of the valve itself; this is difficult to obtain either analytically or intuitively because of the great number of nonlinearities associated with the valve.

For example, in a typical two-stage valve with a flapper-nozzle first stage and a spring-restrained output stage, the torque motor possesses at least two nonlinearities; the saturation of the force vs. differential current characteristic, and hysteresis in the magnetic core material. The flapper is actuated by nonlinear flow forces which are proportional to the product of the flow and square root of the first-stage differential pressure; coulomb friction of the flapper can generally be ignored. The characteristics of the flapper orifices are also nonlinear, according to the Bernoulli relationship $Q = kx\sqrt{\Delta P}$ where x is flapper displacement, ΔP is the differential pressure across the orifice and k is a constant. Thus, the first stage has four significant nonlinearities if coulomb friction is neglected and if magnetic torque vs. flapper displacement can be considered linear over the range of operation.

The second stage also exhibits the flow force and orifice nonlinearities previously mentioned, as well as spool coulomb friction and stiction which cannot be neglected as may be possible in the case of the flapper. All these nonlinearities are associated with the static characteristics of the valve. Added to these are flow saturation of the first stage and dynamic lags occurring in the torque motor, flapper, passages between the flapper and the output spool, the output spool assembly, etc., which further complicate the problem.

It can readily be seen that a valve defies exact analysis unless a great number of simplifying and linearizing assumptions are made. The work conducted to date utilizing these assumptions has not been particularly encouraging.

The method of small perturbations, which was employed successfully in the analysis of valve-controlled systems (References (1) and (2)), could not be used for analyzing the valve itself: the variations in the significant parameters were so large that the various nonlinear relationships in the valve became amplitude sensitive, hence prohibiting small signal analysis.

The describing function approach was not used because to do so would have required the assumptions that the input to the nonlinear element was sinusoidal and that the output of the nonlinear element was periodic, with only the fundamental making a significant contribution to the response.

Actually, most of the equations describing the valve's operation can be formulated analytically even though they are nonlinear and not readily solvable. It was this fact that suggested a third approach, the one that was actually used. It was decided to simulate a servo valve itself on an analog computer.

2. Plan of Attack

Once it was decided to simulate the valve, it became necessary to prepare a detailed plan for accomplishing the simulation. It was decided to simulate two valves and judge the success of their simulation by the closeness of agreement between the analog data and the measured valve characteristics. The two valves were purposely chosen to be different from each other; the Moog 942 is an uncompensated low flow valve, whereas the Moog 9126 is a gain compensated high flow model. For each valve, the simulation program consisted of three phases: an experimental phase, an analytical phase, and a simulation phase.

The experimental phase consisted of three tasks. First, physical dimensions and valve constants were measured; second, operating characteristics of the first stage were obtained; third, over-all characteristics of the valve were experimentally determined.

Concurrent with the experimental phase was the analytical phase, which consisted of two tasks. First, analytical relationships in the

form of equations and graphs were derived from theoretical considerations; second, these relations were verified, as far as possible, by comparison with the data obtained in the experimental phase.

The simulation phase itself began when the other two phases were completed. First, the equations were used to construct a block diagram; second, a computer wiring diagram was prepared from the block diagram and used to mechanize the equations of the valve; third, the complete analog was built up by obtaining correspondence between analog and experimental data for each stage before adding the next stage to the analog setup.

In this manner, an analog of each valve was obtained which compared closely with the actual valve.

B. Experimental Phase

1. Measurement of Physical Dimensions and Valve Constants

Resistance and inductance of the torque motor coils were measured using the procedures described in Reference (1). The various physical dimensions were determined optically with a Gaertner Toolmaker's Microscope M-2001, which can read to 0.0001 inch. For readily accessible parts, micrometer measurements were also taken. The spools and springs were weighed on a standard analytical balance. The actual computation of various valve constants from the significant valve parameters is described in Appendixes I through IV. Specifically:

(1) Appendix I describes the determination of torque motor parameters.

(2) Appendix II describes the determination of flapper parameters.

(3) Appendix III describes the determination of first-stage parameters.

(4) Appendix IV describes the determination of second-stage parameters.

2. Determination of Operating Characteristics of the First Stage

a. General

The following tests were conducted to provide a satisfactory description of first-stage operation:

(1) Measurement of first-stage leakage flow

(2) Measurement of spool end null pressures (with zero differential current)

(3) Measurement of spool differential pressure vs. differential current, with zero spool flow (blocked load test)

(4) Measurement of drain pressure

(5) Measurement of spool flow vs. differential current, spool differential pressure a parameter

(6) Measurement of spool flow vs. spool differential pressure, differential current a parameter.

b. Experimental Setup

A special valve manifold was installed on one of the static test stands to facilitate first-stage tests. This manifold had provisions for measuring the pressures on each end of the valve spool by utilizing the special taps which are found on Moog valves. Figure 1 shows schematically the piping layout. First-stage flow was measured by employing an actuator in series with the flow path and measuring its velocity.

The actuator was a Curtiss double-ended model with a 4 inch stroke. On one end of the actuator shaft was fastened a marker which was positioned over a ruler which was in turn fastened to the test bed. The area of the O-ring sealed piston was 4.21 in^2.

Both V_1 and V_2 were Marsh needle valves. The Helicoid

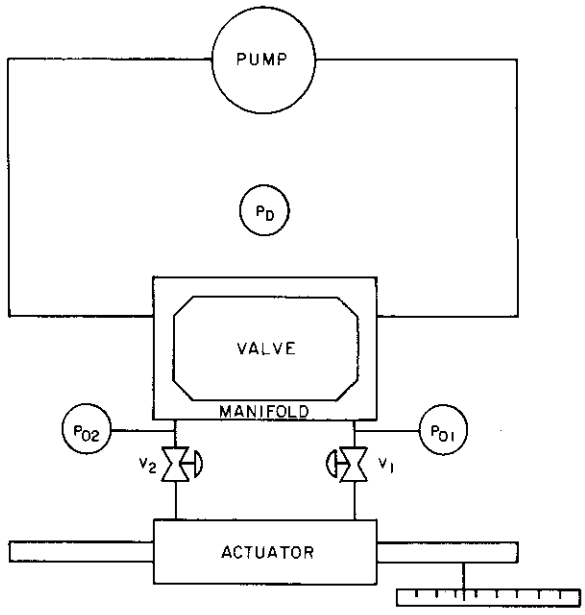

Figure 1. Schematic of First-Stage Test Installation

pressure gages had a range of 0-3000 psi.

A Moog valve torque motor cover was drilled to accommodate a pressure tap, thus permitting measurement of drain pressure.

c. Experimental Procedures

First-stage leakage flow for each valve was obtained from the standard quiescent flow test prescribed by Reference (1).

Spool end null pressures were measured by closing V_1 and V_2 and reading the pressure gages with differential current adjusted to provide the pressure null.

The blocked load test was run by closing both V_1 and V_2 and measuring the spool end pressures for various values of applied differential current.

The first-stage pressure-flow tests were run by measuring all three pressures and first-stage load flow for various valve openings and a fixed value of differential current. Runs were made at ± 2, ± 4, ± 6, and ± 8 ma.

3. Determination of Over-all Characteristics of the Valve

The tests used for determing over-all valve characteristics consisted mainly of the standard tests described in Reference (1).

They were:

(1) Measurement of Quiescent Flow

(2) Measurement of Load Differential Pressure vs. Differential Current at Zero Load Flow (Pressure Gain)

(3) Measurement of Valve Flow vs. Differential Current, Load Differential Pressure a Parameter (Flow Gain)

(4) Measurement of Valve Load Flow vs. Load Differential Pressure, Differential Current a Parameter.

A system for measuring instantaneous spool position was also provided. The movable core of a Schaevitz Linear Variable

Differential Transformer was mechanically coupled to the spool. The input winding was excited by a 5 kc constant amplitude carrier. The output signal, after demodulation, was a varying voltage with an instantaneous amplitude proportional to the displacement of the movable core and hence to spool position.

C. Analytical Phase

1. Introduction

In the analytical phase, the numerous equations describing valve operation were obtained from theoretical considerations. These inherently nonlinear relationships were then solved graphically to yield numerical values and characteristic curves which could be readily verified by direct measurement.

The derivation of these equations was relatively straightforward, involving for the most part fundamental principles of electricity, mechanics, and fluid dynamics. Each equation will be examined in some detail in Part C2 of this chapter. Figure 2, a simplified sketch of a typical two-stage valve, indicates the valve constants and variables which are referred to in the equations that follow.

As a subsidiary part of this phase, various parameters (orifice coefficients, torque motor constants, flow force coefficients, etc.) had to be assigned numerical values. This aspect of the analytical phase, including analysis of the magnetic circuit, will be deferred to Appendixes I through IV.

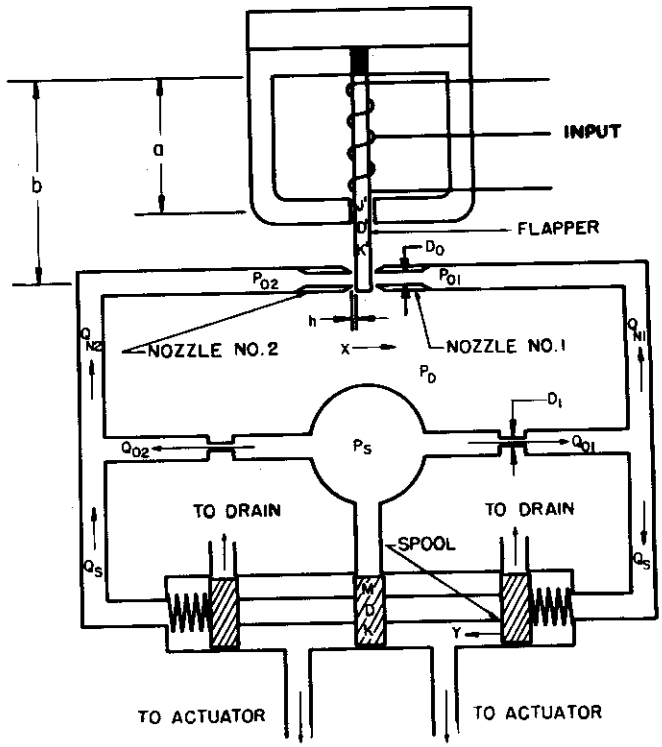

Figure 2. Typical Two-Stage Servo Valve

2. Equations of Valve Characteristics

Summing the voltages in the torque motor circuit,

$$e = R\Delta I + L\dot{\Delta I} + K_v \dot{x}' \qquad (1)^*$$

where R includes the plate resistance of the output stage and the resistance of the torque motor and where $K_v \dot{x}'$ represents the flapper-induced back emf. Summing the torques acting on the flapper,

$$aKm\ \Delta I - b(A_f \Delta P - F_F) = J' \ddot{\theta} + D' \dot{\theta} + K' \theta \qquad (2)$$

where we have defined, for convenience of notation,

$$\Delta P = P_{O_1} - P_{O_2} \qquad (3)$$

and where F_F, the flapper flow forces, can be expressed as the change in momentum of the fluid impinging on the flapper. That is,

$$F_F = (Q_{N1}\ u_1 - Q_{N2} u_2)\rho$$

Since the velocity $u = Q/A$, we can write that

$$F_F = (Q_{N1}^2 - Q_{N2}^2)\ \rho / A_f \qquad (4)$$

Since the angular displacement of the flapper is small,

$$\theta = \frac{x'}{a} = \frac{x}{b} \qquad (5)$$

Application of Bernoulli's principle to the various first-stage orifices results in the following equations:

$$Q_{01} = K_0 \sqrt{P_s - P_{01}} \qquad (6)$$

$$Q_{02} = K_0 \sqrt{P_s - P_{02}} \qquad (7)$$

$$Q_{N1} = K_N h\ (1 - x/h)\sqrt{P_{01} - P_D} \qquad (8)$$

$$Q_{N2} = K_N h\ (1 + x/h)\sqrt{P_{02} - P_D} \qquad (9)$$

---

* See Table 1 for list of symbols

$$Q_L = K_D\sqrt{P_D} \tag{10}$$

From continuity considerations, we can write

$$Q_{01} = Q_{N1} + Q_s \tag{11}$$

$$Q_{02} = Q_{N2} - Q_s \tag{12}$$

Equations (6) and (7) can be solved explicitly for pressure, a step which anticipates the computer mechanization.

$$P_{01} = P_s - (Q_{01}/K_0)^2 = f_1(Q_{01}) \tag{13}$$

$$P_{02} = P_s - (Q_{02}/K_0)^2 = f_2(Q_{02}) \tag{14}$$

Summing the forces on the spool, we obtain

$$A_s\Delta P = M\ddot{y} + D\dot{y} + Ky + K_B P_v y \pm F_c \tag{15}$$

where the last terms on the right hand side are the Bernoulli, or reaction, force on the spool and spool coulomb friction. We can also write the equation of continuity for the spool as

$$Q_s = A_s\dot{y} + K_c\dot{\Delta P} + K_L\Delta P \tag{16}$$

The relation between valve flow and spool displacement can be written as

$$Q_v = K_F y\sqrt{P_s - P_L(y/|y|)} \tag{17}$$

only as long as spool displacement is greater than the underlap. However, when the spool displacement is less than the underlap, the valve behaves like an open-centered valve, and the pressure-flow curves can be approximated with sufficient accuracy by the following relationship

$$Q_v = C_1 y - C_2 P_L \tag{18}$$

For convenience, both (17) and (18) can be written as

$$Q_v = f_3(y, P_L) \tag{19}$$

Actually, valves of the type which were simulated are designed for zero lap, but spool manufacturing tolerances can introduce either

underlaps or overlaps of about 0.0002 inch; since there are two orifices in series, there even exists the possibility that one could be overlapped and one underlapped. However, since these tolerances exist radially as well as axially, the over-all effect is for the valve to have the flow characteristics of an open-center valve at small spool displacements. Determination of the exact spool-sleeve configuration can best be obtained from an examination of the plots of blocked and short-circuited load pressure vs. differential current, as discussed in Reference 1.

The relation between load pressure and valve flow depends on the nature of the load. Assuming a viscous load, we can write in a form analagous to (15).

$$A_a P_L = B_v \dot{\theta}_0 \tag{20}$$

Again applying the principle of continuity, this time to the actuator, we obtain

$$Q_v = A_a \dot{\theta}_0 + K_3 \dot{P}_L + K'_2 P_L \tag{21}$$

If we let $x/h = 0$, then $P_{01} = P_{02} = P_0$ and likewise

$Q_{01} = Q_{02} = Q_{N1} = Q_{N2} = Q_L/2$. Equations (6) through (10) then reduce to the following matrix equation

$$\begin{bmatrix} K_N^2 h^2 + K_0^2 & -K_N^2 h^2 \\ 4K_0^2 & K_D^2 \end{bmatrix} \begin{bmatrix} P_0 \\ P_D \end{bmatrix} = K_D^2 P_s \begin{bmatrix} 1 \\ 4 \end{bmatrix} \tag{22}$$

Now, letting

$$d = K_D/K_O \tag{23}$$

and

$$r = K_0/K_N \tag{24}$$

the solution of (22) for null pressure P_0 and drain pressure P_D can be written after suitable rearrangement as

$$P_0 = \frac{d^2 + 4h^2/r^2}{d^2 + (d^2 + 4)\, h^2/r^2} P_s \tag{25}$$

$$P_D = \frac{4h^2/r^2}{d^2 + (d^2 + 4)\, h^2/r^2} \quad P_s \tag{26}$$

The determination of first-stage pressure-flow curves required an extensive graphical procedure. This procedure can best be understood by first considering the solution of (11) and (12) for Q_s and the subsequent substitution of (6) - (9) into the resulting equations. The final result is

$$Q_s = K_0 \sqrt{P_s - P_{01}} \quad - K_N h(1 - x/h \sqrt{P_{01} - P_D} \tag{27}$$

$$Q_s = -K_0 \sqrt{P_s - P_{02}} \quad + K_N h(1 + x/h \sqrt{P_{02} - P_D} \tag{28}$$

The right hand side of (27) was plotted with Q_s as ordinate, P_{01} as abscissa, and x/h as a parameter; a similar plot was made for the right hand side of (28). Then for any given value of x/h and for various values of Q_s, corresponding values of P_{01} and P_{02} were read off the graphs. Making use of (3), a graph of Q_s vs. ΔP was constructed with x/h as a parameter. This family of curves can be described symbolically as

$$Q_s = f_4(\Delta P,\ x/h) \tag{29}$$

From the magnetic circuit analysis in Appendix I, it was possible to evaluate the static relation existing among ΔP, ΔI and x/h:

$$\Delta P = \frac{aKm}{bA_f} \quad \Delta I - \frac{K'h}{b^2 A_f} \quad x/h \tag{30}$$

Then, for a given ΔI and x/h, ΔP was determined from (30). For the same x/h and the derived ΔP, Q_s was determined from (29). Hence, it was possible to proceed point by point and plot Q_s vs. ΔP with ΔI as a parameter. The equations for the first-stage pressure-flow curves which were obtained in the manner just described can be very closely approximated by

$$Q_s = K_1 \Delta I - K_2 \Delta P, \tag{31}$$

a relationship that will be used later in the analysis of the dynamic characteristics of the valve.

The determination of blocked load characteristics was accomplished by letting $Q_s = 0$ and solving (6) and (8) for P_{01} and (7) and (9) for P_{02}. Making use of (3), there finally resulted an expression for ΔP as a function of x/h.

$$\Delta P = \frac{4 (P_s - P_D) (h^2/r^2) (x/h)}{\left[1 + \frac{h^2}{r^2} (1 - \frac{x}{h})^2\right]\left[1 + \frac{h^2}{r^2} (1 + \frac{x}{h})^2\right]} \tag{32}$$

Combining (30) and (32), it was possible to obtain a graphical relation between x/h and ΔI

$$x/h = f(\Delta I) \tag{33}$$

Using (32) and (33), there ultimately resulted the desired blocked load characteristic, a plot of ΔP vs. ΔI.

No-load response was determined by solving simultaneously the Laplace transforms of (15), (16), and (31) under no-load conditions. Neglecting spool coulomb friction under these conditions,

$$A_s \overline{\Delta P} = (Ms^2 + Ds + K^*) \overline{y} \tag{34}$$

$$\overline{Q}_s = A_s s\overline{y} + (K_c s + K_L) \overline{\Delta P} \tag{35}$$

$$\overline{Q}_s = K_1 \overline{\Delta I} - K_2 \overline{\Delta P} \tag{36}$$

where for convenience of notation in (34)

$$K^* = K + K_B P_s$$

with $K_B P_s$ the value of the Bernoulli forces at no-load. The bars over the variables serve to indicate that they are the Laplace transforms of the actual variables and, hence, are functions of s rather than t. Equations (34), (35), and (36) finally yield

$$\frac{y}{\Delta I}(s) = \frac{A_s K_1/K_c M}{s^3 + \left[\frac{K_L + K_2}{K_c} + \frac{D}{M}\right] s^2 + \left[\frac{A_s^2}{K_c M} + \frac{K_L + K_2}{K_c} \frac{D}{M} + \frac{K^*}{M}\right] s + \frac{K_L + K_2}{K_c} \frac{K^*}{M}} \tag{37}$$

It was found that K*/M was much smaller numerically than either of the other two coefficients of s. Neglecting K*/M and factoring the cubic denominator results in

$$\frac{y}{\Delta I}(s) = \frac{A_s K_1/K_c M}{\left[s + \frac{(K_L + K_2) K^*}{A_s^2 + (K_L + K_2) D}\right]\left[s^2 + \left(\frac{K_L + K_2}{K_c} + \frac{D}{M}\right) s + \left(\frac{A^2}{K_c M} + \frac{K_L + K_2}{K_c} \frac{D}{M}\right)\right]} \tag{38}$$

Replacing s by jω to obtain conventional frequency response information, we find that the linear factor has a break frequency of the order of 10 - 100 cps; the quadratic factor has a resonant frequency of several kilocycles. The first order break frequency can be written as

$$f_1 = \frac{1}{2\pi} \quad \frac{K^*}{D + \frac{A_s^2}{K_L + K_2}} \tag{39}$$

but if viscous damping and spool leakage can be neglected, as is usually the case, a very simple equation for predicting the valve's approximate bandwidth results

$$f_1 = \frac{1}{2\pi} \quad \frac{K^* K_2}{A_s^2} \tag{40}$$

Equation (37) can be solved to give a relation between y and ΔI under static conditions. Letting s = 0, we obtain

$$y = \frac{A_s K_1}{(K_L + K_2)K^*} \quad \Delta I \tag{41}$$

a relation which is essential for obtaining numerical values of K_F (see Appendix IV).

The next section will consider the simulation phase, during which the exact equations and curves derived in this section were mechanized.

D. Simulation Phase

1. Preliminary Considerations

a. Preparation of Block Diagram of the Valve Equations

The equations which were derived in Section C became the basis of the valve simulation. A block diagram of the equations was prepared as a necessary first step. For

convenience of notation, the Laplace transforms of the various differential equations were used; these equations in operational form are listed below with only a minimum of comment. As before, transformed variables are indicated by the presence of a bar over them.

Transforming (1) and rearranging terms,

$$\overline{e} - K_v s\overline{x}' = (R + L\ s)\ \overline{\Delta I} \tag{42}$$

From (2) and (5),

$$aK_m\overline{\Delta I} - b(A_f\overline{\Delta P} - \overline{F_f}) = (J' s^2 + D' s + K')\ \frac{\overline{x}'}{a} \tag{43}$$

and

$$\overline{x} = \frac{b}{a}\ \overline{x}' \tag{44}$$

Transforming (15) and rearranging terms,

$$A_s\ \overline{\Delta P} - K_B\ (\overline{P_v y}) \pm F_c = (Ms^2 + Ds + K)\overline{y} \tag{45}$$

Similarly operating on (16),

$$\overline{Q}_s = A_s s\overline{y} + (K_c s + K_L)\ \overline{\Delta P} \tag{46}$$

Equations (42) through (46), together with the various other equations derived in Chapter III, were then graphed, using standard signal flow, or block diagram, procedures.

The complete block diagram, Figure 3, has two unconventional aspects which warrant close considerations. First, the block labelled "Dead Zone" was incorporated to represent hysteresis of the torque motor, a factor not explicitly accounted for in the theoretical analysis of the torque motor. Second, the presence of the blocks to represent multiplication or squaring of variables and generalized functional relationships indicates the extreme nonlinearity of the equations describing valve operation.

After the block diagram was completed, but before the computer wiring diagram could be prepared, it was necessary to determine values for the computer components. The block diagram had to be scaled in order to obtain reasonable resistor

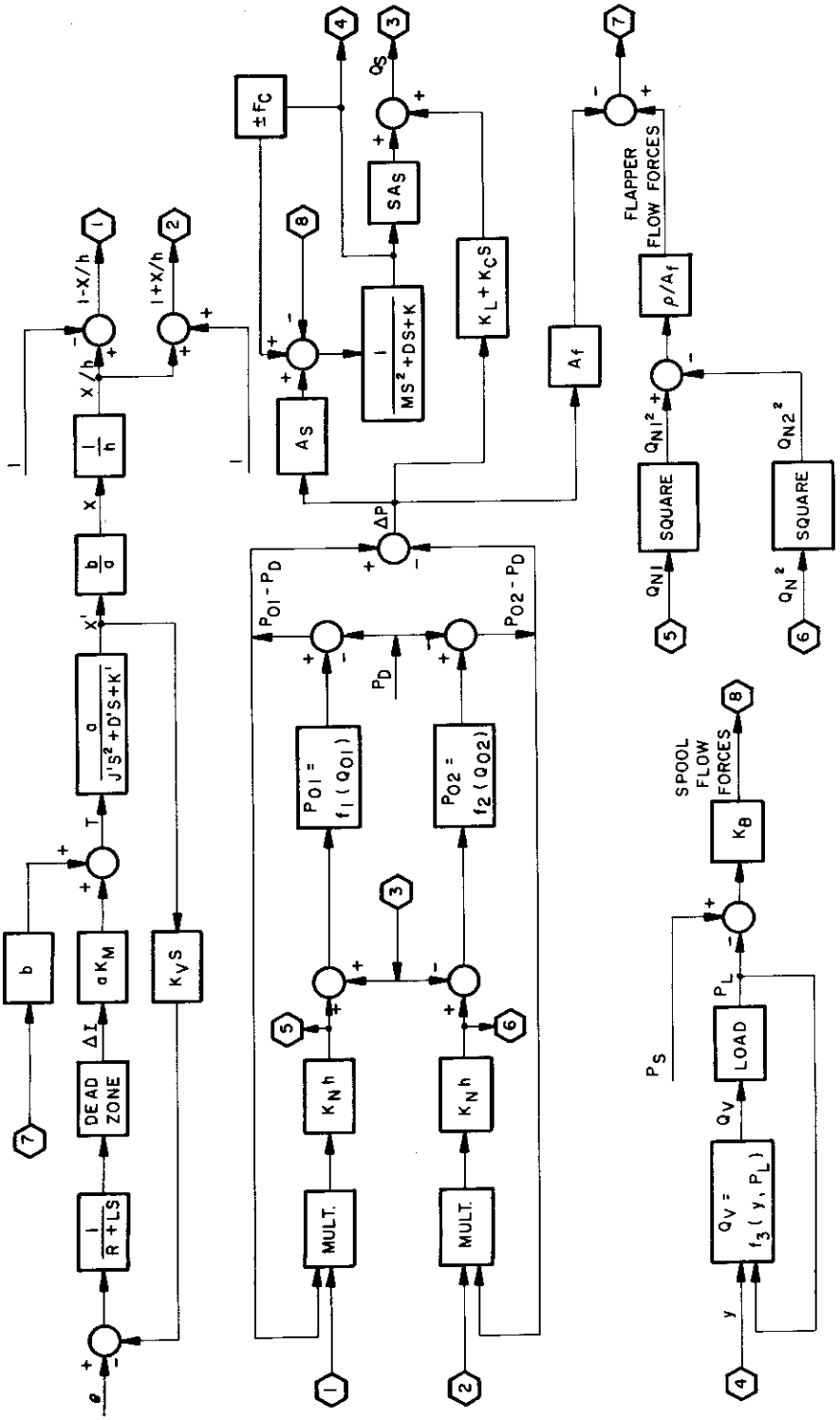

Figure 3. Block Diagram of Valve Relations

and capacitor sizes; the procedure followed will be discussed in the next section of this chapter.

b. Determination of Computer Scale Factors

Once numerical values for all the constants were inserted in the block diagram, it became quickly evident that the problem could not be run in real time. The presence of resonant frequencies as high as 10 kc dictated a time-scale change of 1000 to 1. Under this scale change, a 10 kc resonance appeared on the computer at 10 cps.

The criteria for the determination of amplitude scale factors were: amplifier inputs had to be large enough to produce favorable signal-to-noise ratios; amplifier outputs could not exceed ± 100 volts. For simplicity and ease of interpretation, and in order to handle the wide range of values some of the variables possessed, the method described in Reference 3 was used for scaling the problem.

Using this system,

1 machine unit = 1 volt (47)

For example, nozzle pressures are typically about 140 psi, whereas load differential pressure can range from - 3000 psi to + 3000 psi. To satisfy the criteria established earlier, the outputs of amplifiers representing nozzle pressures had the "value" $0.1\ P_{01}$ and $0.1\ P_{02}$, whereas the outputs of amplifiers representing load pressure had the "value" $0.01\ P_L$.

One more example will serve to illustrate the method. Nozzle flows are about 0.15 in^3/sec, but output flows are about 15 in^3/sec. Hence, on the computer nozzle flow amplifiers represent 100 Q_N, but output flow amplifiers only represent 1.0 Q_v.

This system of scale factor (or perhaps more appropriately, amplifier output) selection worked very well; the only precaution necessary was for all inputs to summing points to be of the same power of 10.

A new block diagram was then prepared, taking into account the values of the scaled variables.

c. Preparation of Computer Wiring Diagram

The analog computer wiring diagram was prepared from the scaled block diagram using conventional computer circuitry as applicable to the specific equipment available. That is, on the L3 GEDA, adjustable plug-in resistors were used to produce coefficient units, but on the modified Heath Analog Computer fixed resistors and output attenuators were used for the same type of unit. Figure 4 compares the two procedures for a unit

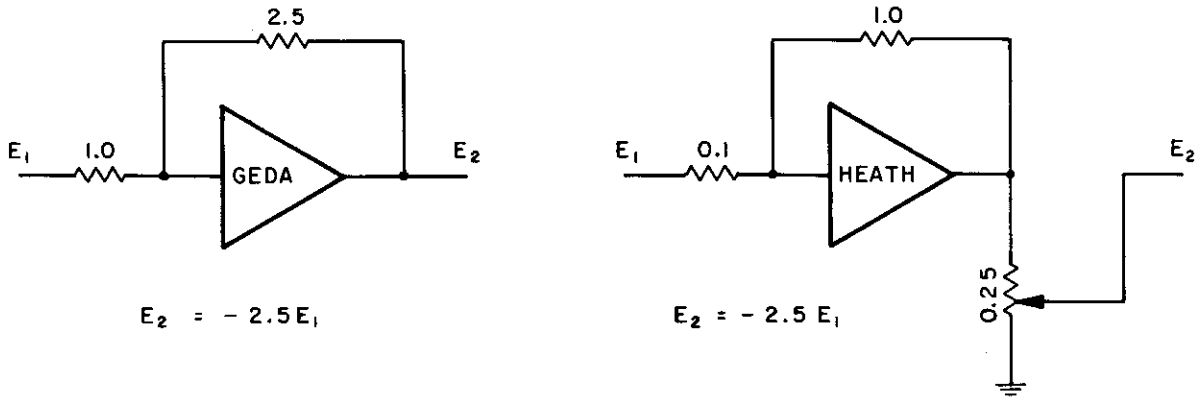

Figure 4. Comparison of Coefficient Units

whose output voltage is 2.5 times the input voltage.

Figure 5 is the final computer wiring diagram for simulation of the Moog 9126; this diagram resulted from making the various adjustments described in the next section.

2. Simulation Procedure

a. Equipment Used

The linear relationships previously derived were set up on a GEDA L3 Analog Computer; however, because the GEDA had an insufficient number of amplifiers, certain subsidiary relations were set up on a Heath Analog Computer modified by the use of chopper-stabilized Philbrick K2X operational amplifiers. (Heath amplifiers are indicated on the computer wiring diagram by a number with the prefix H.) The nonlinear relations were

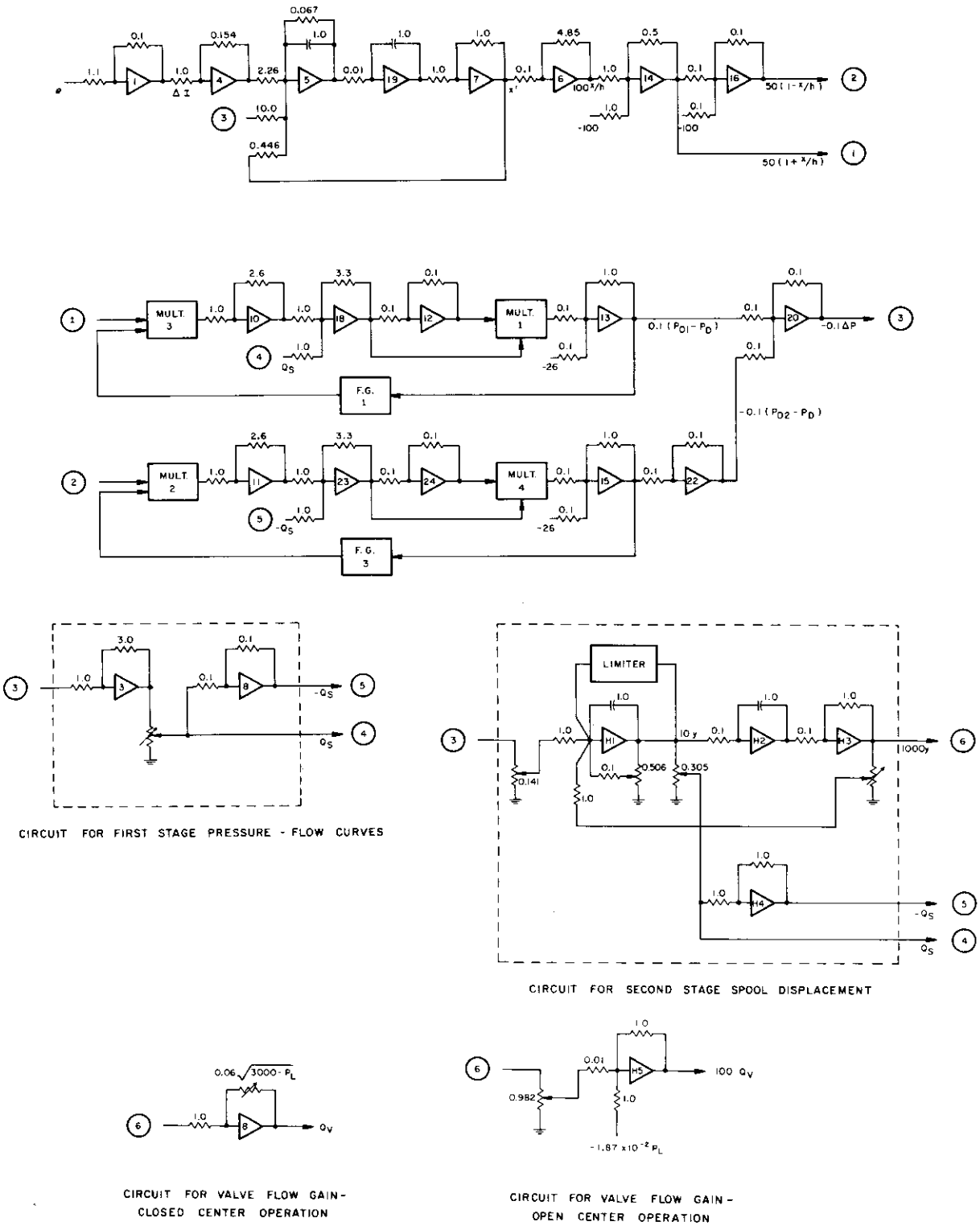

CIRCUIT FOR FIRST STAGE PRESSURE - FLOW CURVES

CIRCUIT FOR SECOND STAGE SPOOL DISPLACEMENT

CIRCUIT FOR VALVE FLOW GAIN - CLOSED CENTER OPERATION

CIRCUIT FOR VALVE FLOW GAIN - OPEN CENTER OPERATION

Figure 5. Final Analog Computer Wiring Diagram

generated on Electronics Associates Model 16-7J Electronic Multipliers and Model 16-16B Diode Function Generators.

b. Setup and Initial Adjustments

In what follows, the discussion will be primarily limited to simulation of the 9126; a similar process was used for the 942.

The equations of the torque motor were first mechanized. It was found that the effects of flapper back emf and torque motor inductance could be neglected, thereby simplifying the circuitry.

Next, the equations of the first stage at blocked load ($Q_S = 0$) were added to the simplified torque motor equations. It was found that the flapper flow forces could be neglected without noticeably affecting system response.

At this point, initial gain adjustments were made. No voltage was applied to the torque motor (e = 0); gains on 14 and 16 (underscored numbers refer to computer amplifier numbers) were adjusted to yield exactly 50 volts output from each. The inputs to 20 were grounded and each loop was then adjusted individually.

Considerable difficulty was encountered in attempting to adjust these loops. Since the equations were algebraic, the loops did not have the usual low-pass filter characteristics of a closed-loop system and went unstable, ringing at about 10 kc. The problem was solved by reducing the number of amplifiers to a minimum and placing 100 μμf and 0.01 μf capacitors in the feedback paths of critical summing amplifiers. The resultant configuration gave satisfactory results for static tests; however, its dynamic response was not as satisfactory because of the low cutoff frequency introduced by the extra capacitors.

One possible means of improving the bandwidth would have been to make a further time-scale change; however, to do so would have required the use of frequencies from 0.001 cps to 0.03 cps, which were below the lower limits of existing oscillators and recorders. Another alternative would have been to measure the response of the compensated computer circuitry and use the dynamic lags as part of the simulated valve lags. The calculation or experimental determination of such corrections would have been quite tedious and time-consuming because of

the presence of parallel feed-forward paths and multiple feedback paths in the system. There was insufficient time to attempt this approach.

Loop 1 was adjusted by setting the gains on 10, 18, and 13 to yield simultaneously $Q_{N1} = 0.14$ in^3/sec and $(P_{01} - P_D) = 140$ psi. The procedure was essentially systematic "knob twiddling". Loop 2 was adjusted in a similar manner.

Once the two loops were adjusted properly, the inputs to 20 were reconnected and the spool was unblocked by feeding back Q_S to 18 and 23 (with the appropriate polarities for each); the computer was ready for running first-stage pressure-flow tests.

c. Final Adjustments and Tests

(1) First-Stage Pressure-Flow Tests

With differential current at 8 ma, the feedback on 4 was adjusted so that ΔP would be 350 psi, an experimentally obtained value, with $Q_S = 0$. As the output of 3 was varied, corresponding values of ΔP and Q_S were read. Because of the inaccuracies necessarily inherent in the estimate of flapper parameters, the first plot of Q_S vs. ΔP did not match the theoretical curves. By judicious trial-and-error adjustment of the flapper spring rate, the final plot practically coincided with the experimental curves over the entire range.

(2) Output Stage Flow Gain Tests - Closed Center

Once the first-stage tests were run, the dynamics of the spool were added. It was determined that leakage and compressibility across the spool lands, as well as spool coulomb friction, could be neglected, further simplifying the computer circuits.

For an 8 ma input and for a given load pressure, the spool spring rate was adjusted so that the experimental value of Q_V was obtained on the output of 8. Then, differential current was varied from +8 to -8 and the resultant Q_V measured.

Because of insufficient time, it was not possible to obtain output stage pressure-flow curves, but such data were available by making a cross-plot from the flow gain curves.

(3) Output Stage Flow Gain Tests - Open Center

For a 0.2 ma input and with P_L = 2900 psi, the attenuated input to H5 was adjusted to give zero valve flow. Then for various given load pressures, ΔI was varied from +0.2 to -0.2 ma. The intercepts on the ΔI axis of the low-flow curves yielded points on the pressure gain curves.

3. Comments on the Simulation Phase

The analog described in this chapter accounted for all static operational characteristics of the valve. No attempt was made to simulate the unsteady flow conditions which can cause instability in the case of certain spool geometries (5); it was assumed that the valve had been designed to prevent these instabilities.

The transition from closed center to open center operation of the output spool was not performed, but a suitable analog circuit for simulating this transition is shown in Figure 6. Time did not permit the checkout of this circuit.

One no-load frequency response run was made. The results of this test were unsatisfactory and indicated that the dynamic lags in the computer circuitry would have to be taken into account if an accurate dynamic simulation was to be obtained. This matter is discussed more fully in Section D 2b of this chapter.

E. Discussion of Results

1. Physical Dimensions and Valve Constants

Table 1 contains a list of all symbols which were used in the analytical phase of the analog study. Those constants obtained from theoretical and graphical analyses have as an entry the number of the equation in which they first appear; those obtained by direct measurement have, in addition, an asterisk to indicate this fact.

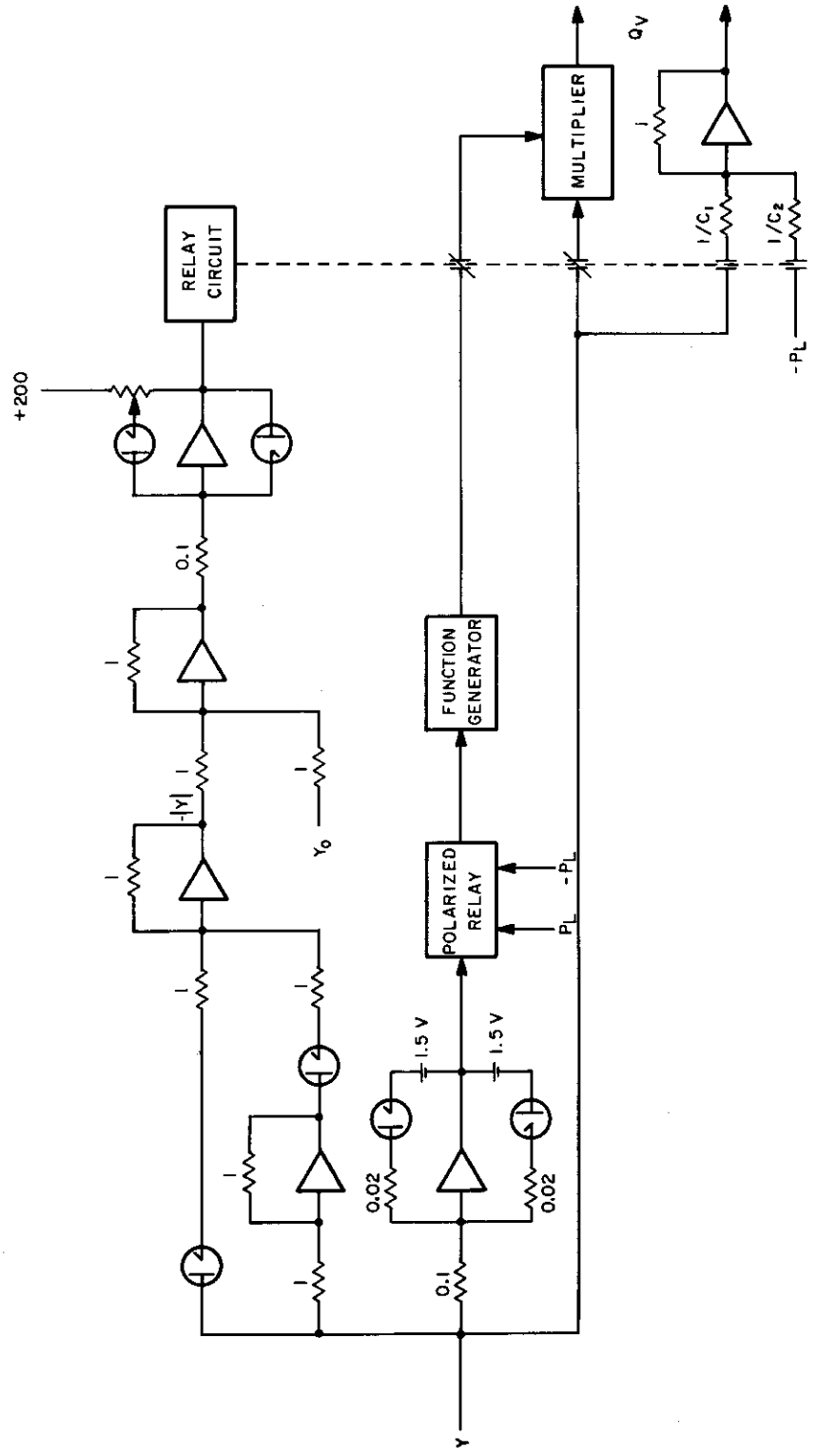

Figure 6. Computer Circuit for Simulating Valve Flow

TABLE 1

LIST OF SYMBOLS

Symbol	Description	Dimensions	Direct Measurement and Equation Number	Numerical Value 9126	Numerical Value 942
e	Magnet Torque Arm	in.	2*	0.551	0.500
A_a	Actuator cross-section area	in^2	20	Various	
A_f	Flapper cross-section area	in^2	2	2.54×10^{-4}	3.14×10^{-4}
A_g	Movable air gap area	in^2	I-3	0.0195	0.0184
A_M	Magnet cross-section area	in^2	I-7	0.163	0.163
A_s	Spool cross-section area	in^2	15	3.05×10^{-2}	3.14×10^{-2}
b	Nozzle torque arm	in.	2*	0.713	0.660
B_{em}	Flux density in air gap due to electromagnet	gauss	I-4		
B_{pm}	Flux density in air gap due to permanent magnet	gauss	I-4		
B_m	Flux density of permanent magnet	gauss	I-7		
B_v	Actuator viscous damping	lb-sec/in	20	Various	
B_1	Flux density in air gap between flapper and pole piece 1	gauss	I-3		
B_2	Flux density in air gap between flapper and pole piece 2	gauss	I-3		
C_1	$Q_v/y \ @ \ P_L = 0$	in^2/sec	18	982	1100
C_2	$\partial Qv/\partial P_L @ y$ = constant	$in^5/lb\text{-}sec$	18	1.87×10^{-4}	2.9×10^{-4}
d	Ratio of drain orifice constant to upstream orifice constant	numeric	23	4.95	10.1
D	Spool viscous damping	lb-sec/in	15	0.11	0.13
D'	Flapper viscous damping	in-lb-sec/rad	2	3.22×10^{-3}	4.34×10^{-3}
D_D	Drain orifice diameter	in.	III-4*	1.37×10^{-2}	2.03×10^{-2}
D_o	Nozzle diameter	in.	III-5*	1.94×10^{-2}	2.0×10^{-2}
D_1	Upstream orifice diameter	in.	III-3*	6.2×10^{-3}	6.4×10^{-3}
e	Voltage applied to the torque motor	volts	1	Various	
f_1	No-load break frequency	cps	39	110	65
F_c	Spool coulomb friction	lb	15		
F_F	Flapper flow forces	lb	2		
h	Nominal nozzle-flapper clearance	in.	8*	1.5×10^{-3}	2.7×10^{-3}
H_m	Magnetizing force of permanent magnet	oersted	I-8		
H_{pm}	Magnetizing force in air gap due to permanent magnet	oersted	I-8		
ΔI	Differential current in torque motor	ma	1	Variable	

TABLE 1 (cont'd)

LIST OF SYMBOLS

Symbol	Description	Dimensions	Direct Measurement and Equation Number	Numerical Value 9126	942
J'	Flapper moment of inertia	$in\text{-}lb\text{-}sec^2/rad^2$	2	6.81×10^{-7}	5.96×10^{-7}
K	Spring rate of spool restraining springs	lb/in	15	570	675
K'	Flapper spring rate	$in\text{-}lb/_{rad}$	2	21	31
K^*	Total spool spring rate at no-load	lb/in	34		
K_B	Spool flow force spring rate constant	in.	15	0.133	0.135
K_c	Spool compressibility coefficient	$in^5/_{lb}$	16	3.33×10^{-8}	4.22×10^{-8}
K_D	Drain orifice constant	$in^4/sec\sqrt{lb}$	10	1.5×10^{-2}	3.3×10^{-2}
K_F	Output valve flow constant	$in^3/sec\sqrt{lb}$	17	60	20
K_L	Spool leakage coefficient	$in^5/lb\text{-}sec$	16	9.3×10^{-5}	9.1×10^{-5}
K_M	Torque motor constant	lb/amp	2	25	17
K_N	Nozzle constant	$in^3/sec\sqrt{lb}$	8	4.85	
K_o	Upstream orifice constant	$in^4/sec\sqrt{lb}$	6	3.03×10^{-3}	3.27×10^{-3}
K_v	Flapper back emf constant	volt-sec/in	1	2.54	
K_1	$Q_s/\Delta I$ @ $\Delta P = 0$	$in^3/ma\text{-}sec$	31	2.20×10^{-2}	2.24×10^{-2}
K_2	$\partial Q_s/\partial \Delta P$@ ΔI = constant	$in^5/lb\text{-}sec$	31	5.36×10^{-4}	4.6×10^{-4}
K_2'	Actuator leakage coefficient	$in^5/lb\text{-}sec$	21	Various	
K_3	Actuator compressibility coefficient	in^5/lb	21	Various	
l_o	Length of air gap between flapper and upper pole piece	in.	I-16*		
l_1	Length of air gap between flapper and lower pole piece	in.	I-17*		
L	Torque motor inductance	henry	1*	0.7	1.0
L_g	Total air gap length	in.	I-8*		
L_m	Total length of magnet	in.	I-8*		
M	Spool mass	$lb\text{-}sec^2/in$	15*	2.17×10^{-5}	5.1×10^{-6}
M_m	Mmf of permanent magnet	gilbert	I-14		
N	Number of turn on torque motor	numeric	I-11	4500	
P_D	Drain pressure	lb/in^2	8	400	89
P_L	Load differential pressure	lb/in^2	17	Variable	
P_o	Spool end null pressure	lb/in^2	22	537	555
P_{01}	Pressure at nozzle 1	lb/in^2	3	Variable	
P_{02}	Pressure at nozzle 2	lb/in^2	3	Variable	
P_s	Supply pressure	lb/in^2	6	3000	3000
P_v	Valve pressure drop $P_s - P_L$	lb/in^2	15	Variable	
ΔP	Spool differential pressure	lb/in^2	2	Variable	

TABLE 1 (cont'd)

LIST OF SYMBOLS

Symbols	Description	Dimensions	Direct Measurement and Equation Number	Numerical Value 9126	942
Q_L	First-stage leakage flow	in^3/sec	10*	0.28	0.33
Q_{N1}	Flow from nozzle 1	in^3/sec	4	Variable	
Q_{N2}	Flow from nozzle 2	in^3/sec	4	Variable	
Q_{01}	Flow through fixed orifice 1	in^3/sec	6	Variable	
Q_{02}	Flow through fixed orifice 2	in^3/sec	7	Variable	
Q_s	Spool flow	in^3/sec	11	Variable	
Q_v	Valve flow	in^3/sec	17	Variable	
r	Ratio of upstream orifice constant to nozzle constant	in.	24	6.25×10^{-4}	6.55×10^{-4}
R	Effective resistance of torque motor	ohms	1*	11×10^3	11×10^3
$\mathcal{R}$	Reluctance of either upper air gap	gilberts/maxwell	I-14		
$\mathcal{R}_1$	Reluctance of air gap at pole piece 1	gilberts/maxwell	I-14		
$\mathcal{R}_2$	Reluctance of air gap at pole piece 2	gilberts/maxwell	I-14		
s	Laplace operator	rad/sec	34		
u	Velocity	in/sec	III-8	Variable	
x	Position of flapper referred to nozzles	in.	8	Variable	
x'	Position of flapper referred to pole pieces	in.	1	Variable	
y	Position of spool	in.	15	Variable	
β	Bulk modulus of oil	lb/in^2	III-8	2.2×10^{-2}	2.2×10^{-2}
θ	Angular displacement of flapper	rad	2	Variable	
θ_o	Position of actuator shaft	in.	20	Variable	
μ	Magnetic permeability	gauss/oersted	I-11	1	1
σ_{em}	Electromagnet leakage factor	numeric	I-11	3	
σ_{pm}	Permanent magnet leakage factor	numeric	I-7	7	
ϕ_1	Flux linking flapper and pole piece 1	lines	I-14	Variable	
ϕ_2	Flux linking flapper and pole piece 2	lines	I-15	Variable	
ρ	Mass density of oil	$lb\text{-}sec^2/in^4$	4	78×10^{-6}	78×10^{-6}

2. Comparison of Theoretical and Experimental Results

a. First Stage

Table 2 compares the theoretical and experimental values

TABLE 2

COMPARISON OF THEORETICAL AND EXPERIMENTAL VALUES

	Moog 9126			Moog 942		
Quantity	Theor.	Exp.	% Diff.	Theor.	Exp.	% Diff.
P_o (psi)	537	540	0.50	555	550	0.91
P_D (psi)	400	370	8.10	89	100	11.0
Q_L (in^3/sec)	0.30	0.28	7.14	0.32	0.33	3.04
f_1 (cps)	110	115	4.35	65	70	7.14

of P_O, P_D, Q_L, and f_1 for the 9126 and for the 942. It can be seen that the differences between theoretical and experimental values of P_O were much less than those for P_D. It is believed that the discrepancies in P_D are the result of slight errors in the measurement of the nozzle geometry, which affect (26) more than (25).

It was observed experimentally that P_D remained practically constant over the entire range of applied differential currents and spool differential pressures, thus corroborating the fact that first-stage leakage flow is essentially constant in two-stage servo valves.

The value of the theoretical break frequency f_1 is actually good for one amplitude only, as it tends to decrease with increasing differential current. Although the reduction in K_2 with increasing ΔI is a contributing factor to the change in f_1, it is actually less important than the change caused by so-called first-stage flow saturation. Flow saturation and its effect on no-load response will be discussed in the next two paragraphs.

From the geometry of the valve, it can be seen that the greatest possible value spool flow can assume would be first-stage leakage flow, Q_L. Also, since spool flow is proportional to spool velocity and since spool velocity is proportional to frequency, it follows that spool flow will be proportional to frequency. For any given amplitude of applied differential current, there will occur a maximum attainable spool flow and a corresponding maximum attainable spool velocity. The frequency at which this flow-limited velocity will occur (f_L) has a profound effect on no-load response.

For large amplitude signals (100 percent ΔI), f_L will be smaller than f_1 and will contribute heavily to the observed experimental break frequency. For small amplitude signals (10 percent ΔI), f_L will be much greater than f_1 and will have little effect on the low-frequency no-load response. Spool stiction and coulomb friction will, however, cause a decrease in the experimental break frequency, as well as a decrease in no-load flow. Also, load stiction and coulomb friction are even more significant factors in bandwidth reduction at low amplitudes because full supply pressure is not available for moving the load. For medium amplitude signals (30 to 70 percent of ΔI), flow saturation occurs at higher frequencies; stiction effects also have little influence on the no-load response. Hence, the valve characteristics most closely represent a first order lag. This can be seen by examining no-load curves for various valves; the curve for 60 percent ΔI invariably has the best frequency response characteristic, when compared with the 10 percent and 100 percent curves. It is this curve which comes closest to matching the theoretical break frequency obtained in (39).

3. Simulation Results

a. First Stage

As stated previously, the first-stage pressure-flow curves of the simulated valves coincided almost exactly with the theoretical ones and very closely with the experimental ones. Examination of these curves indicates that the asymmetry of the actual valve characteristics (caused by null shifts, differences in nozzle diameters, etc.) was not accounted for in this simulation. It was felt that to do so would have introduced unnecessary complications and obscured, rather than revealed, information about valve operation.

The curves of the blocked load test and flow gain test were obtained by cross-plotting from the pressure-flow curves; once for Q_s = O and again for constant values of ΔP. These curves agreed fairly well with those obtained experimentally. They are presented as Figures 7 through 12 for the 9126 and Figures 13 through 18 for the 942.

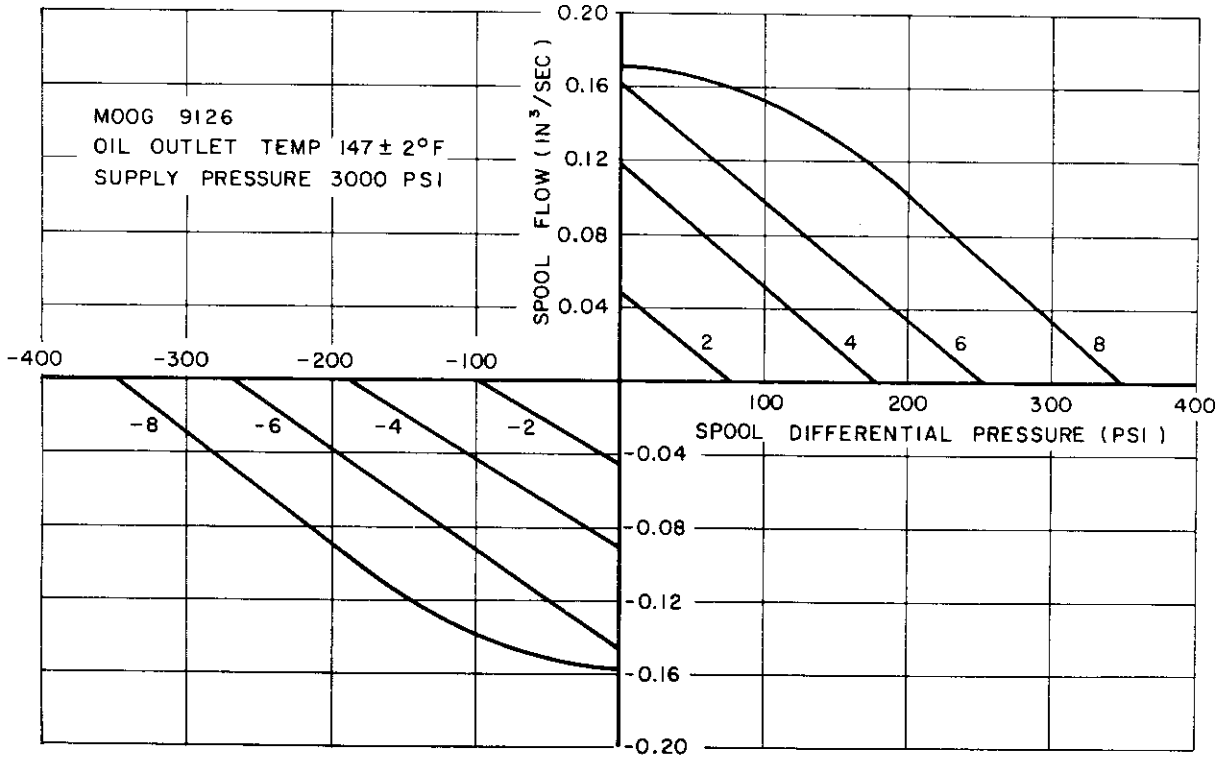

Figure 7. Experimental First-Stage Pressure vs. Flow - Moog 9126

b. Second Stage

Output stage flow gain curves (closed center) agreed fairly well with experimental ones. The curves for open center operation had never been obtained experimentally, but the good agreement of the pressure gain curves verified the resultant low-flow curves. (See Figures 19 through 25 for the 9126 and Figures 26 through 32 for the 942.)

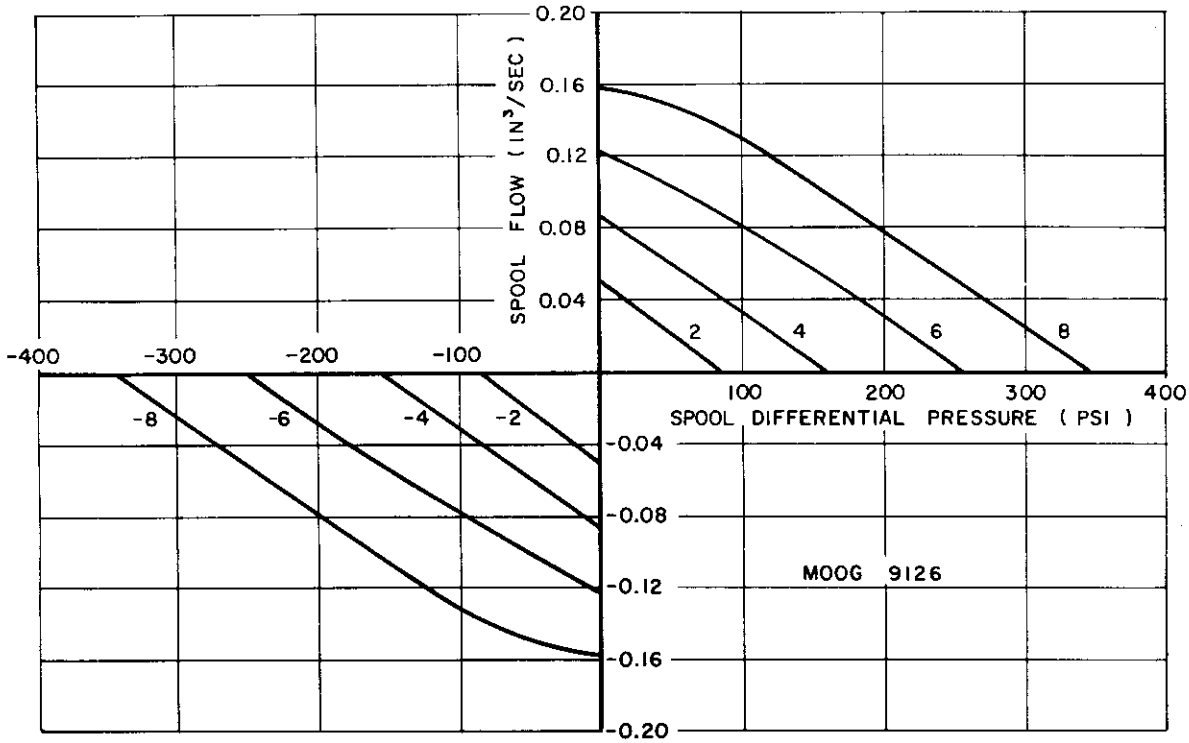

Figure 8. Theoretical and Analog First-Stage Pressure vs. Flow - Moog 9126

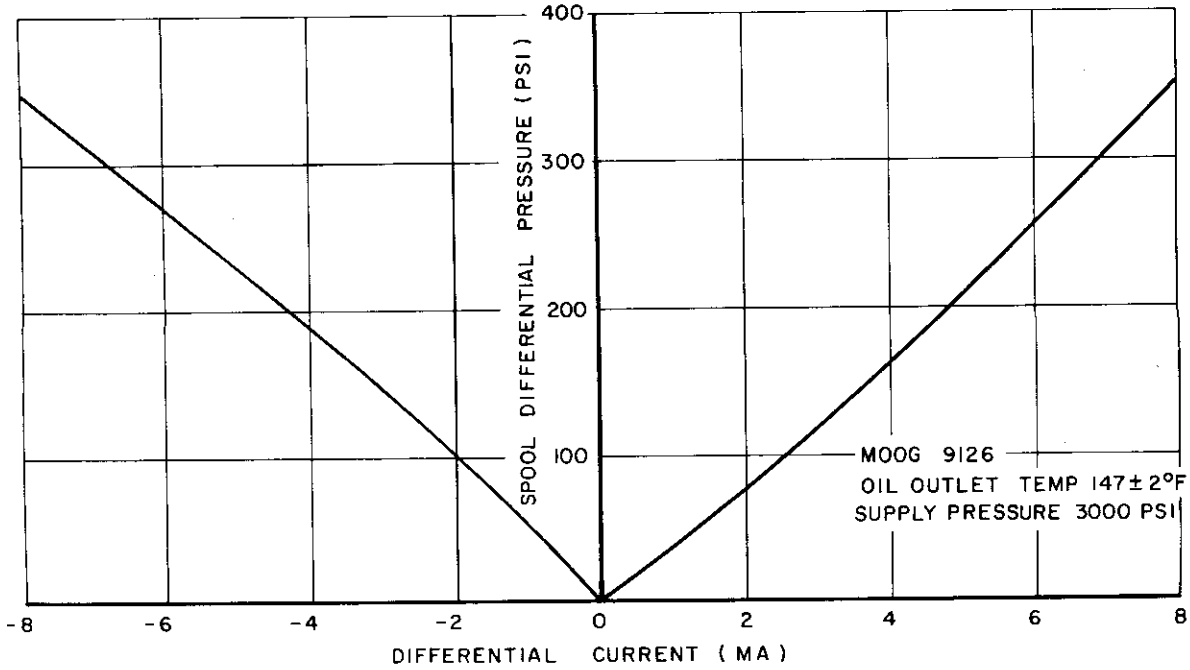

Figure 9. Experimental Blocked Load Characteristic - Moog 9126

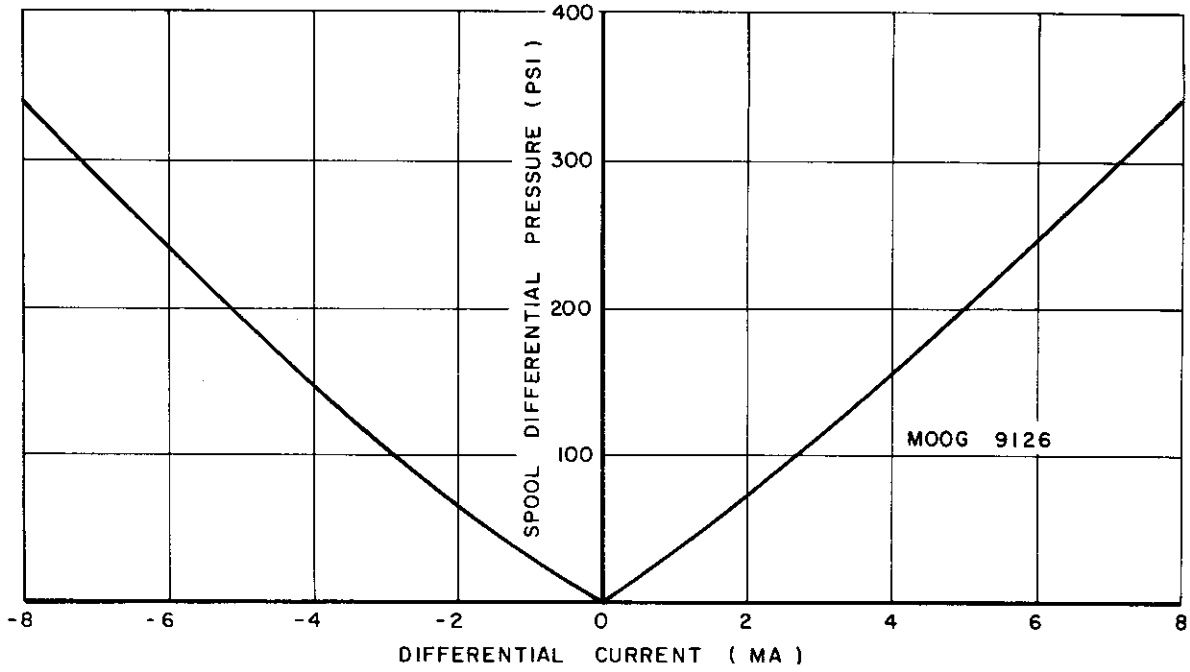

Figure 10. Theoretical and Analog Blocked Load Characteristics - Moog 9126

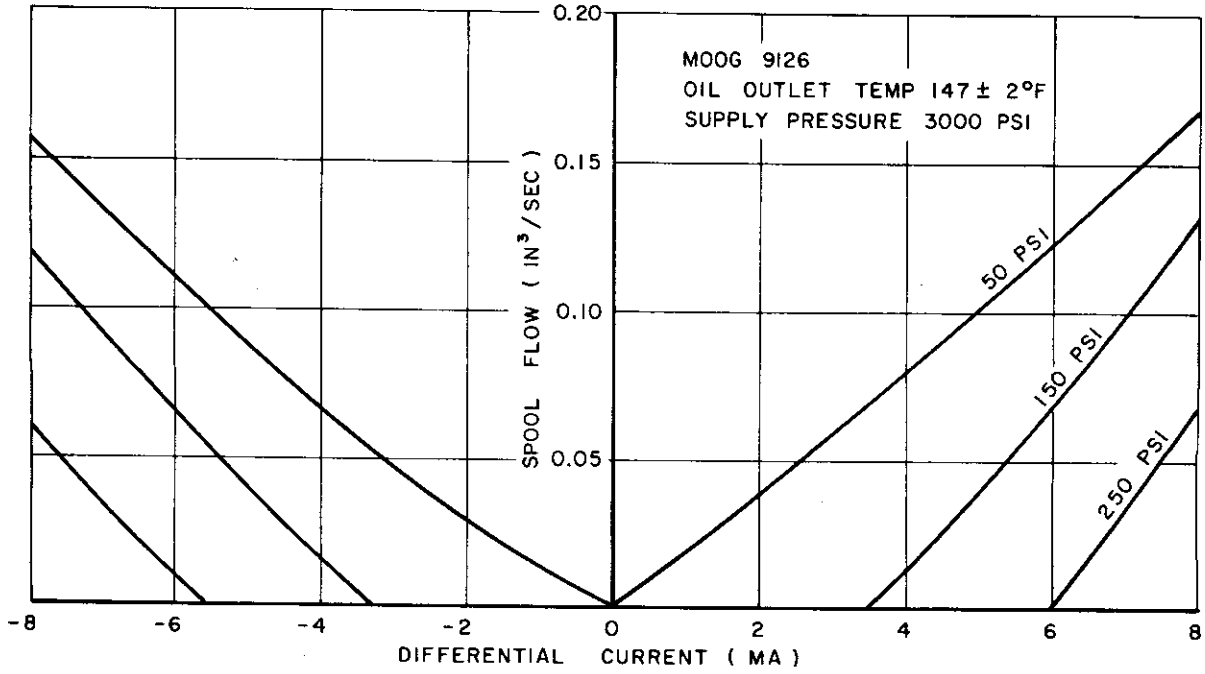

Figure 11. Experimental First-Stage Flow Gain - Moog 9126

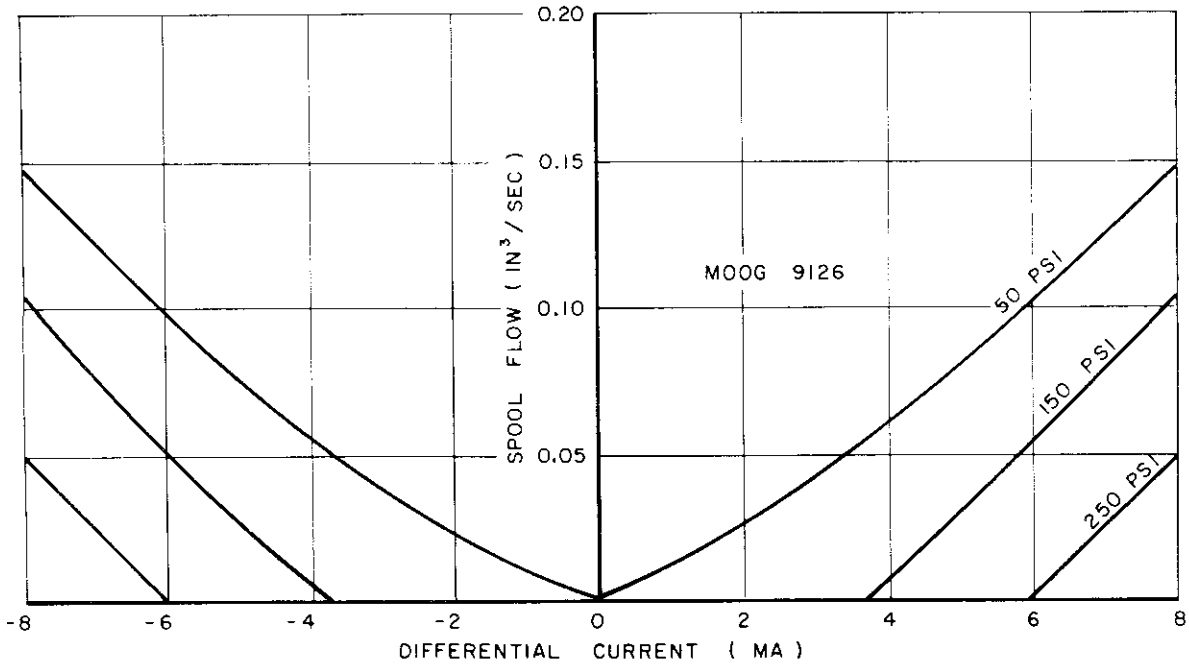

Figure 12. Theoretical and Analog First-Stage Flow Gain - Moog 9126

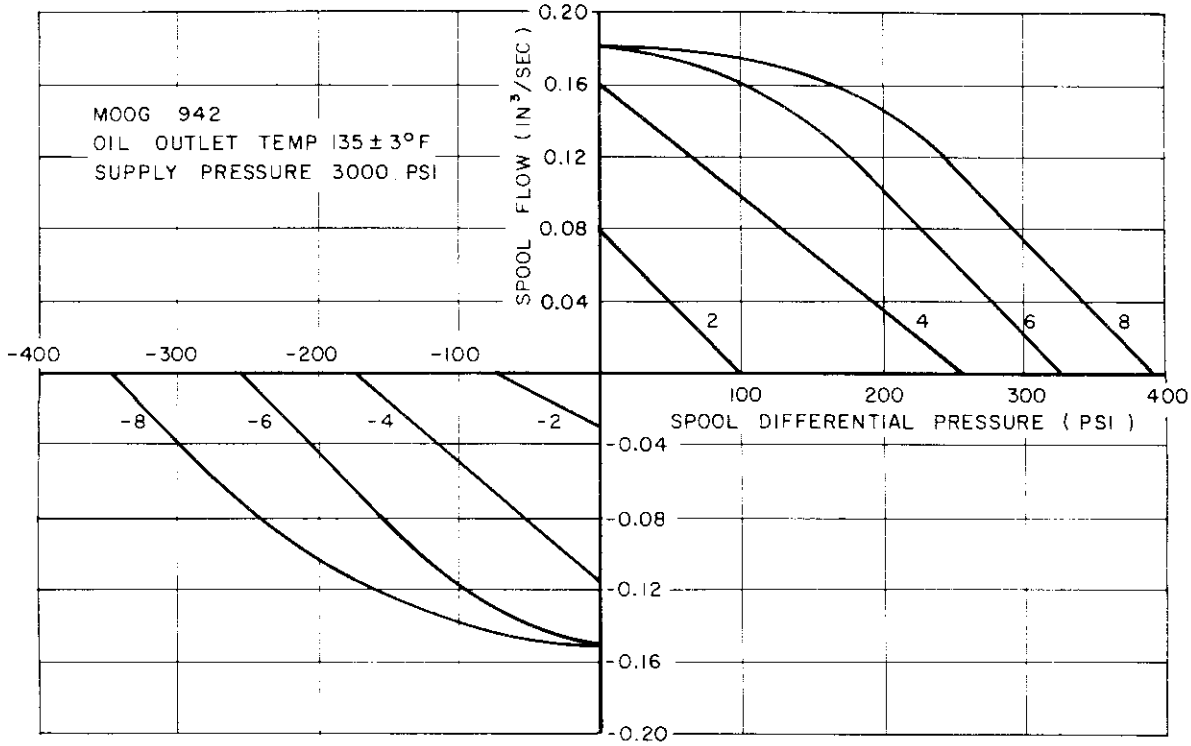

Figure 13. Experimental First-Stage Pressure vs. Flow - Moog 942

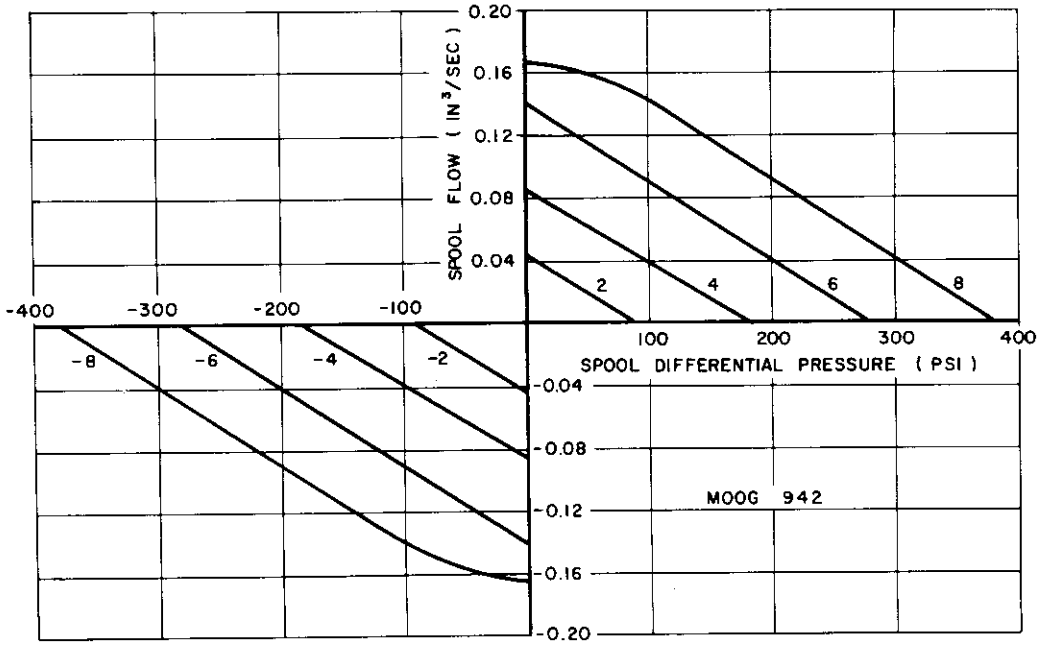

Figure 14. Theoretical and Analog First-Stage Pressure vs. Flow - Moog 942

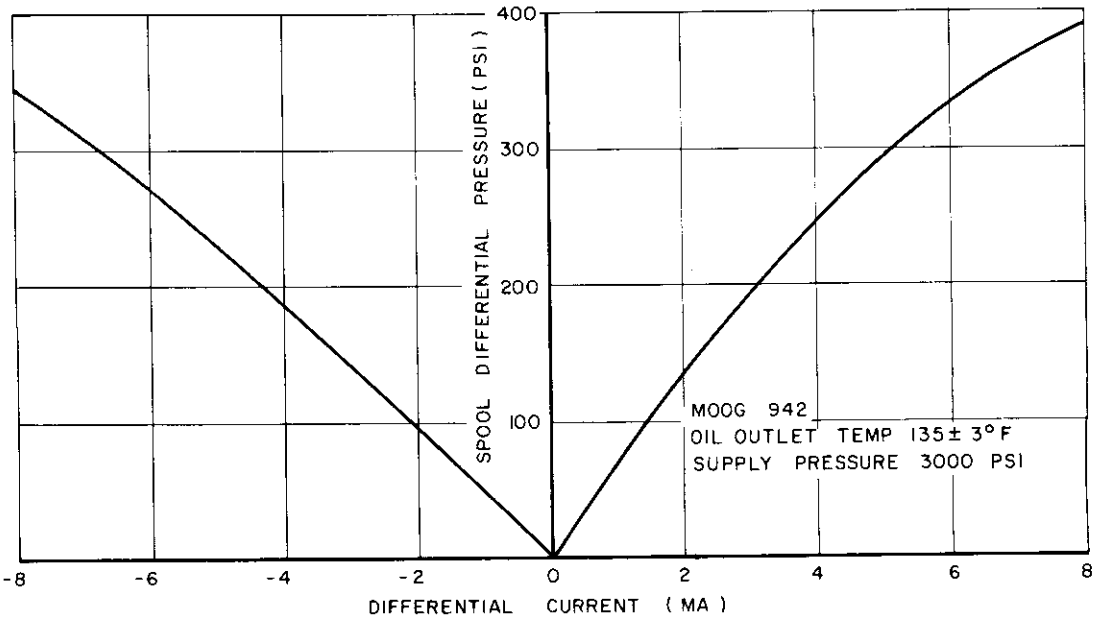

Figure 15. Experimental Blocked Load Characteristic - Moog 942

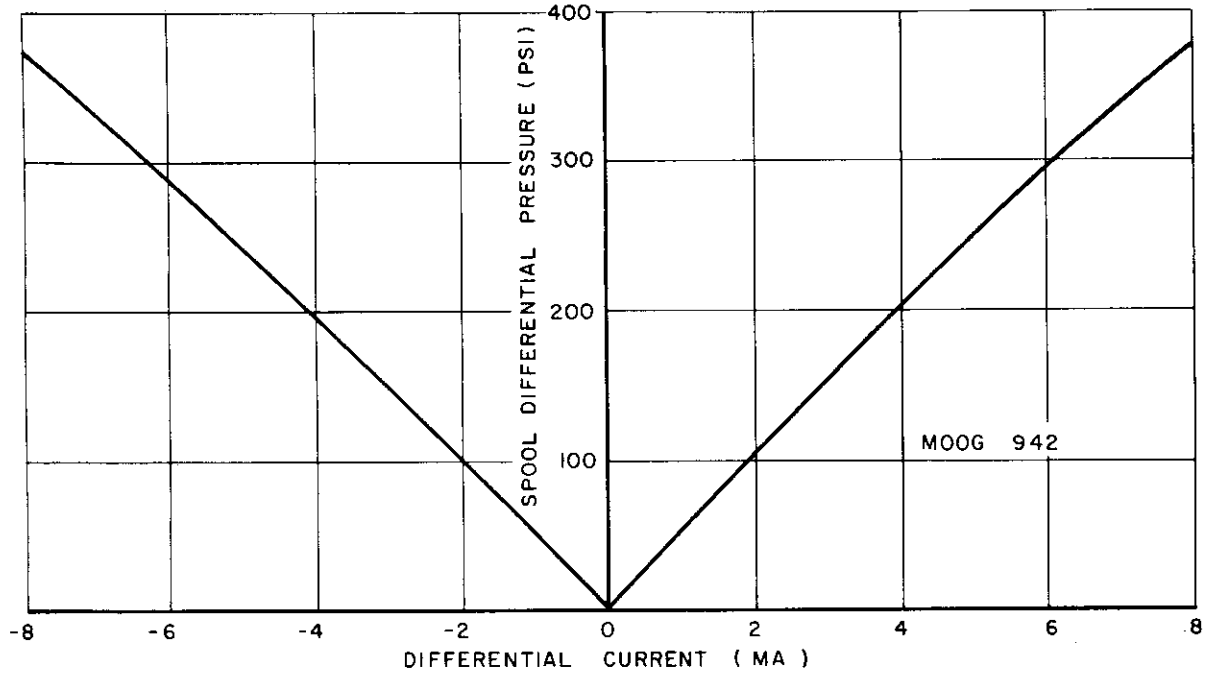

Figure 16. Theoretical and Analog Blocked Load Characteristic - Moog 942

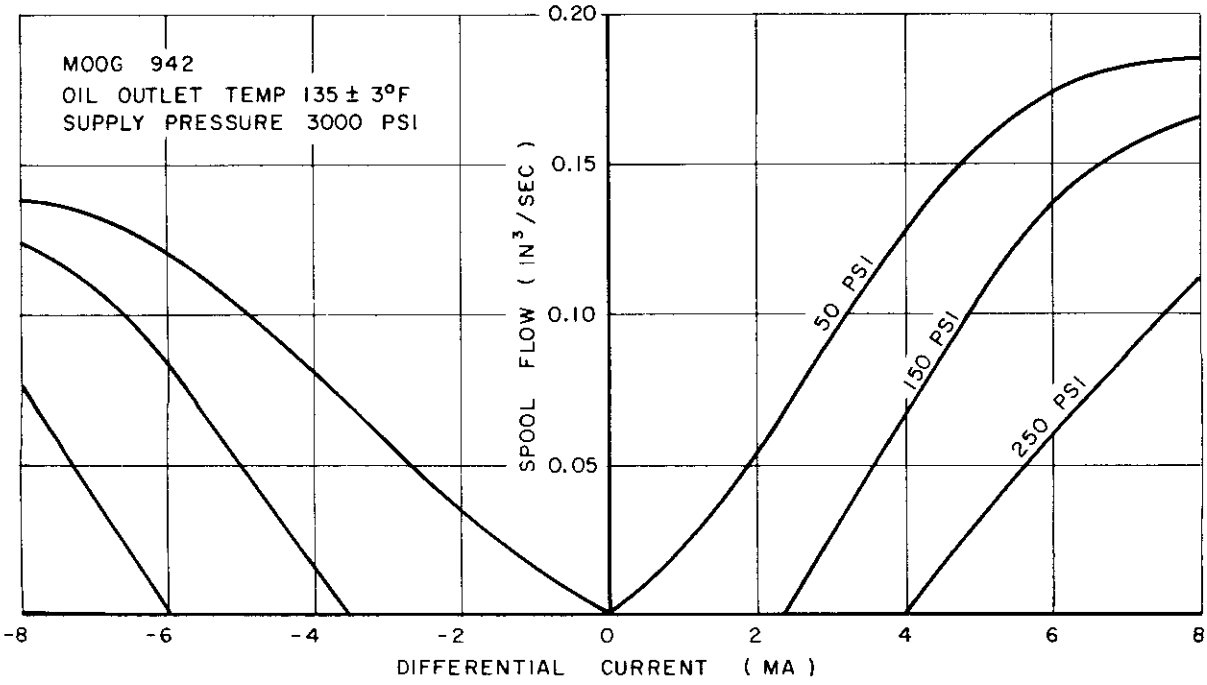

Figure 17. Experimental First-Stage Flow Gain - Moog 942

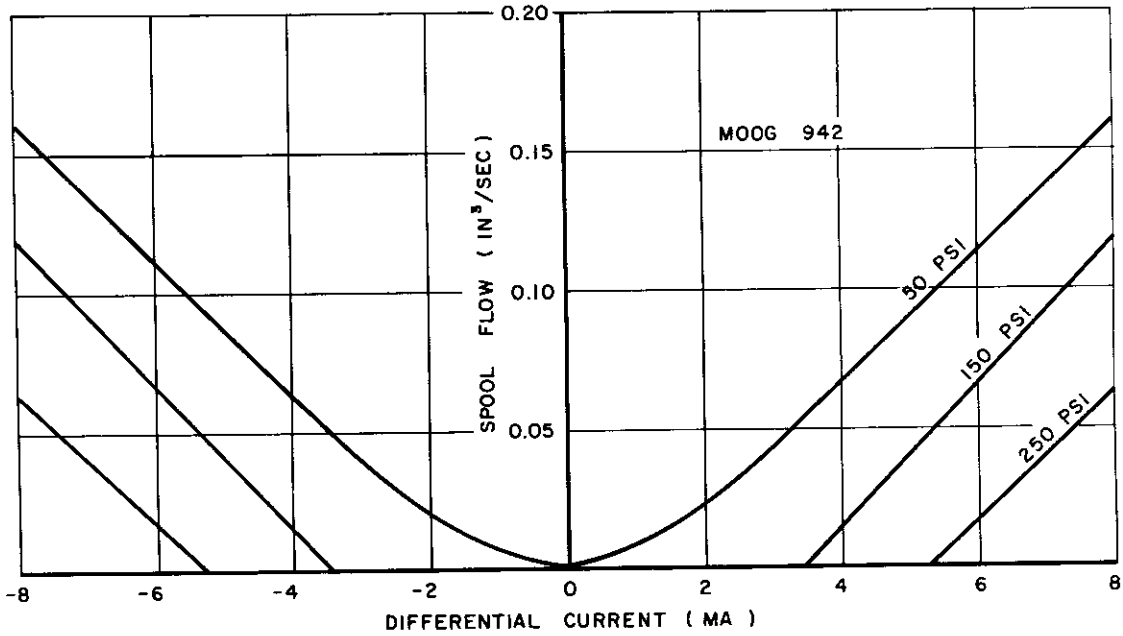

Figure 18. Theoretical and Analog First-Stage Flow Gain - Moog 942

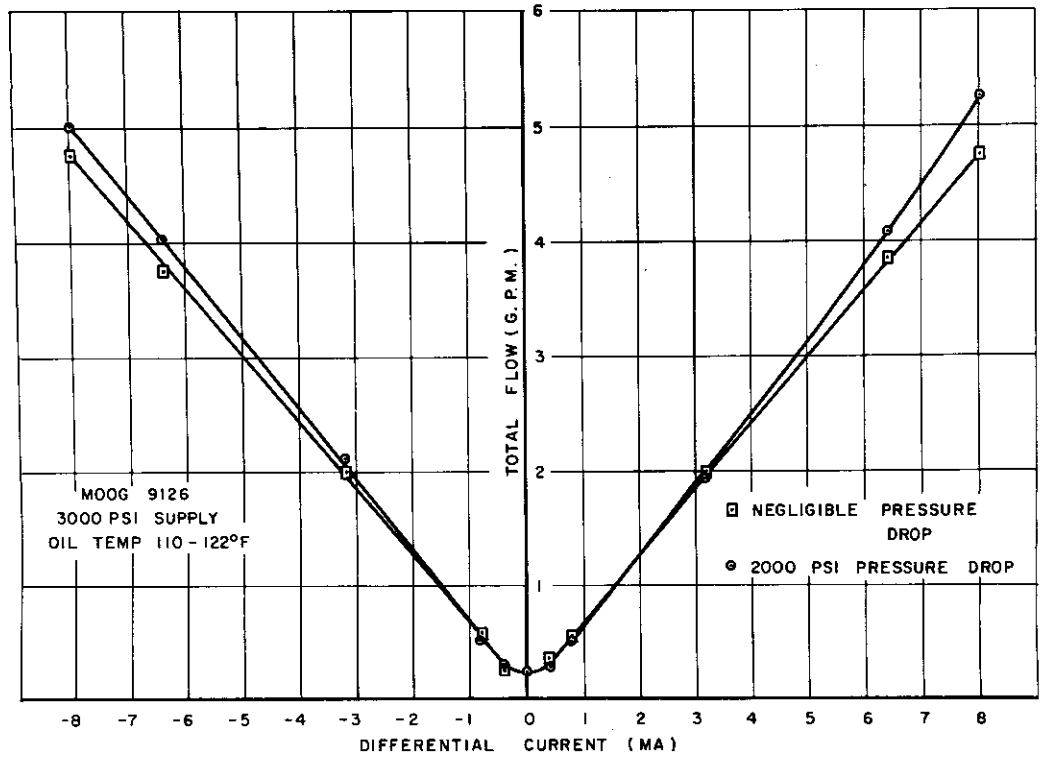

Figure 19. Experimental Flow Gain Characteristic - Moog 9126

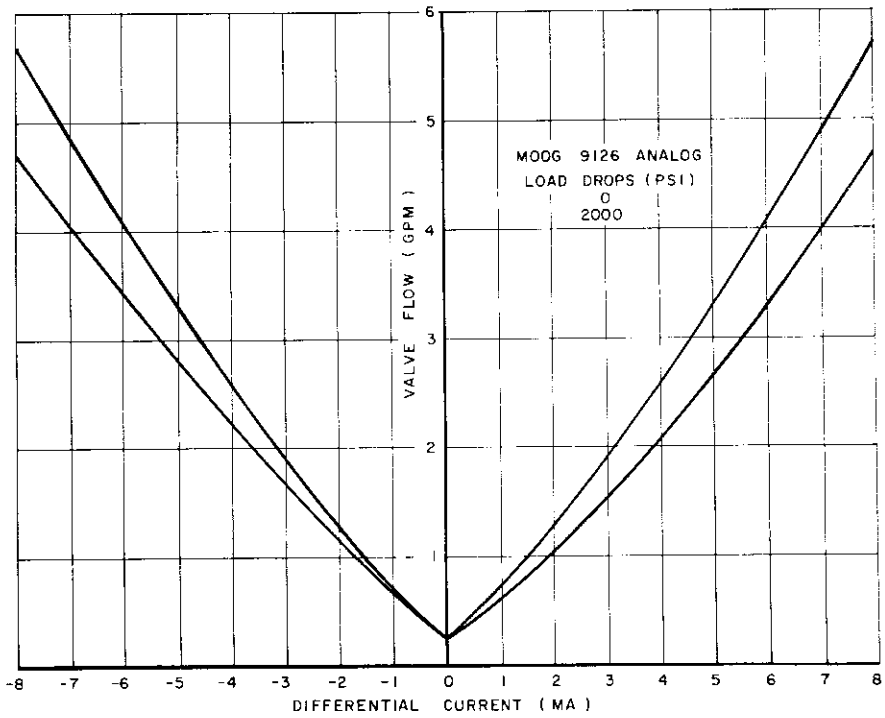

Figure 20. Analog Flow Gain Characteristic - Moog 9126

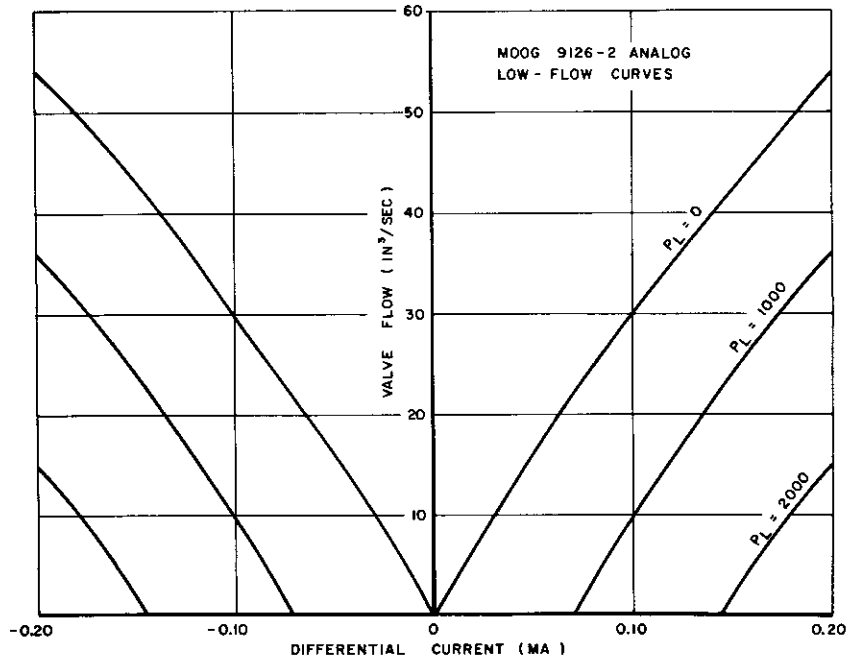

Figure 21. Analog Low Flow Characteristic - Moog 9126

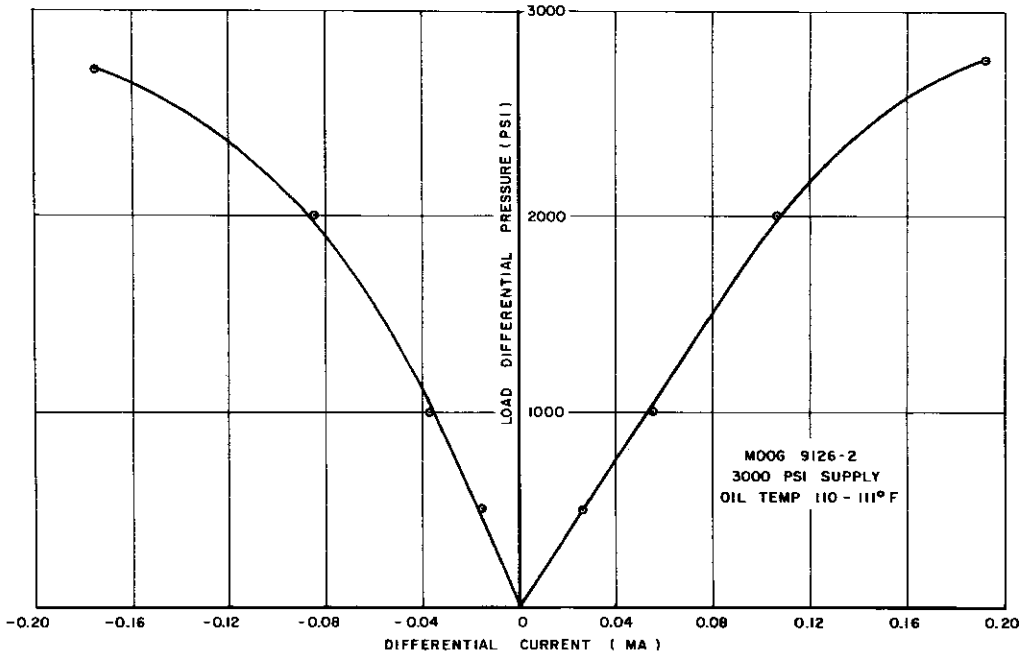

Figure 22. Experimental Pressure Gain Characteristic - Moog 9126

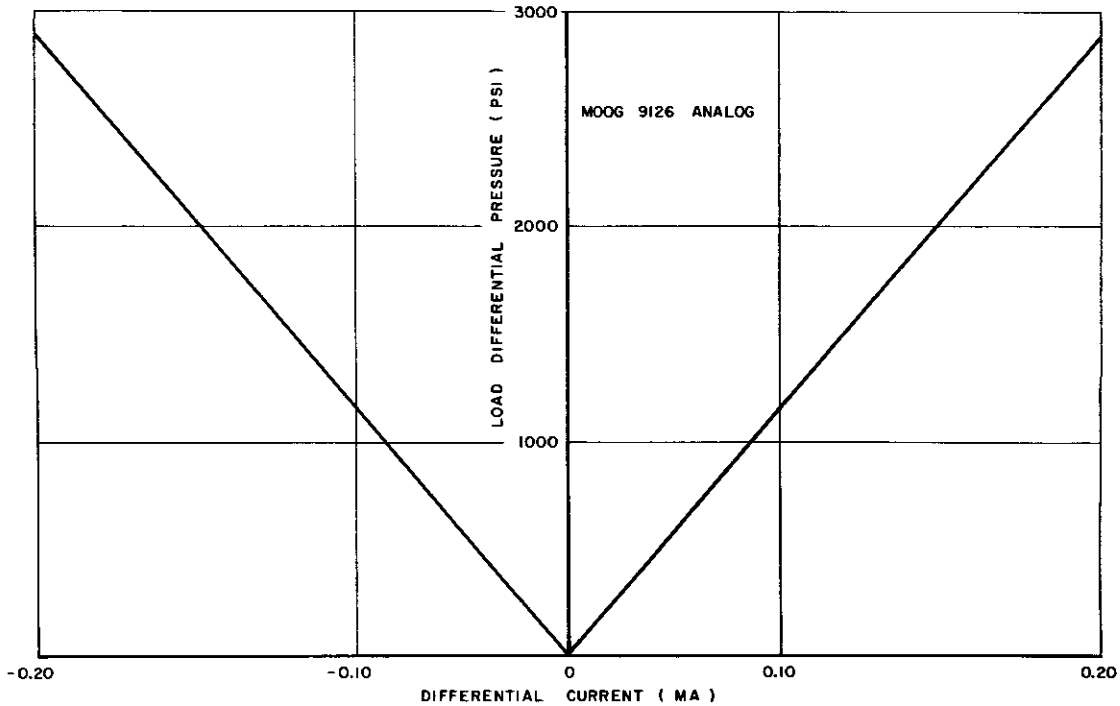

Figure 23. Analog Pressure Gain Characteristic - Moog 9126

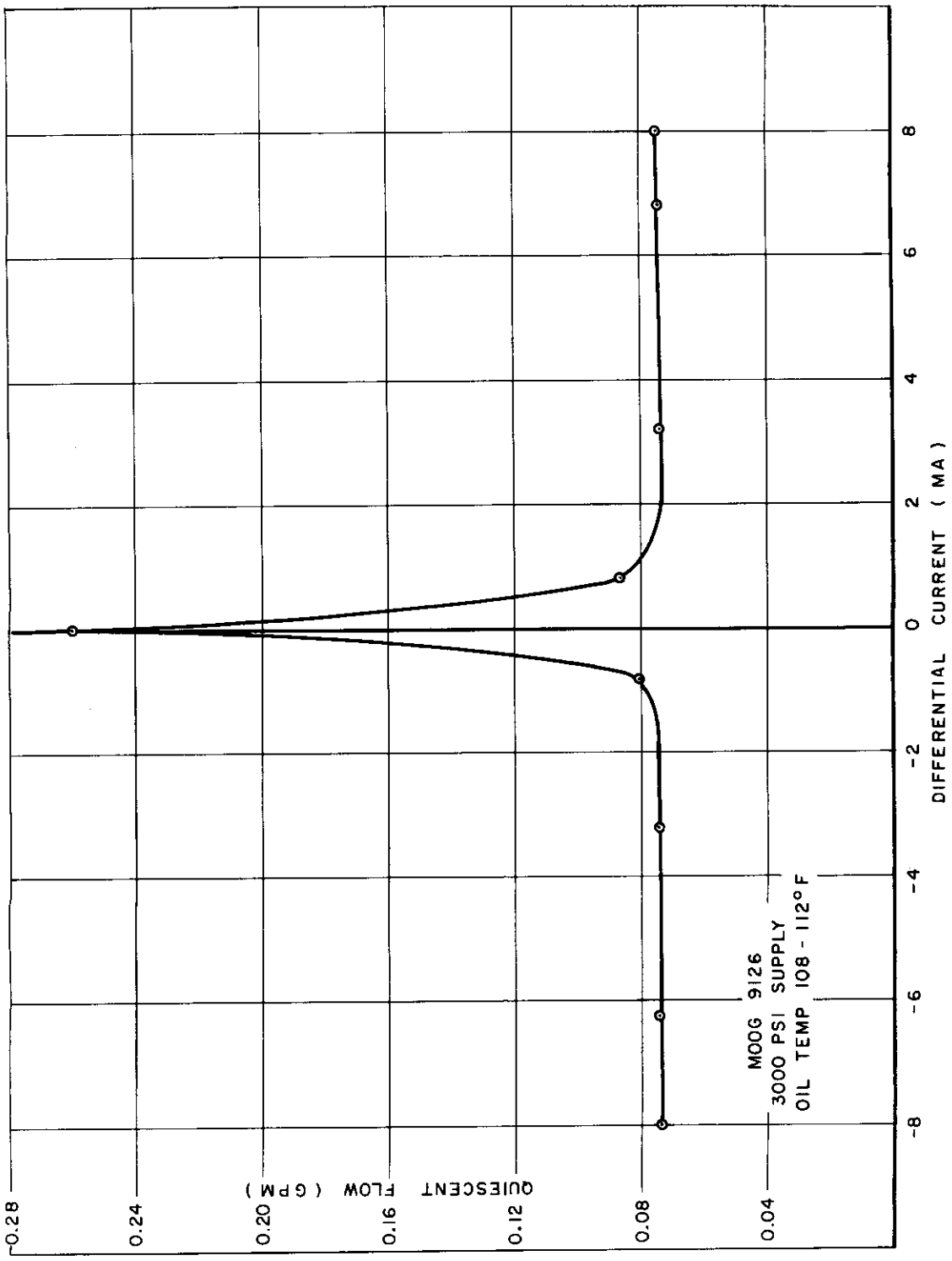

Figure 24. Quiescent Flow vs. Differential Current - Moog 9126

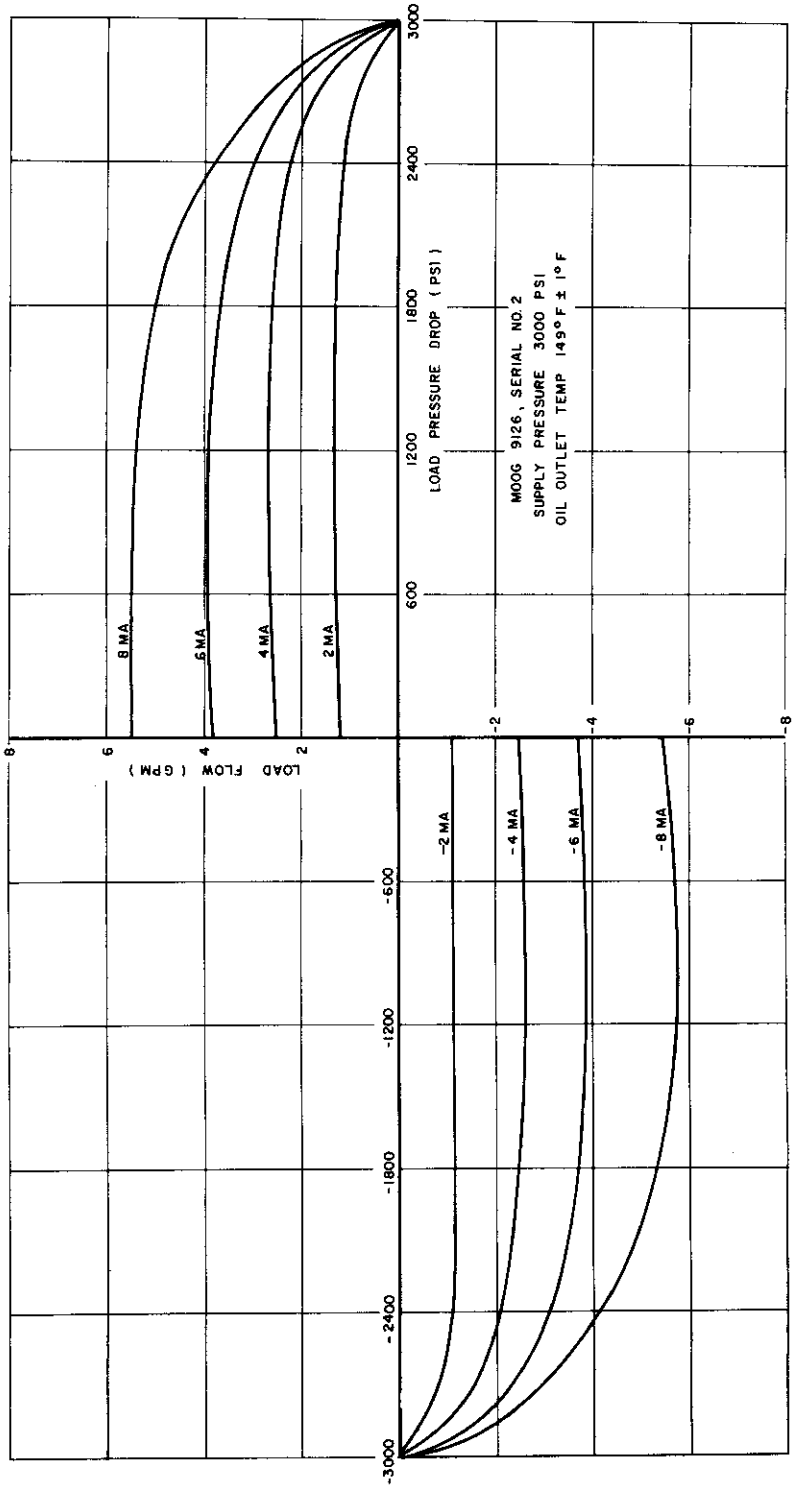

Figure 25. Output Load Pressure vs. Load Flow - Moog 9126

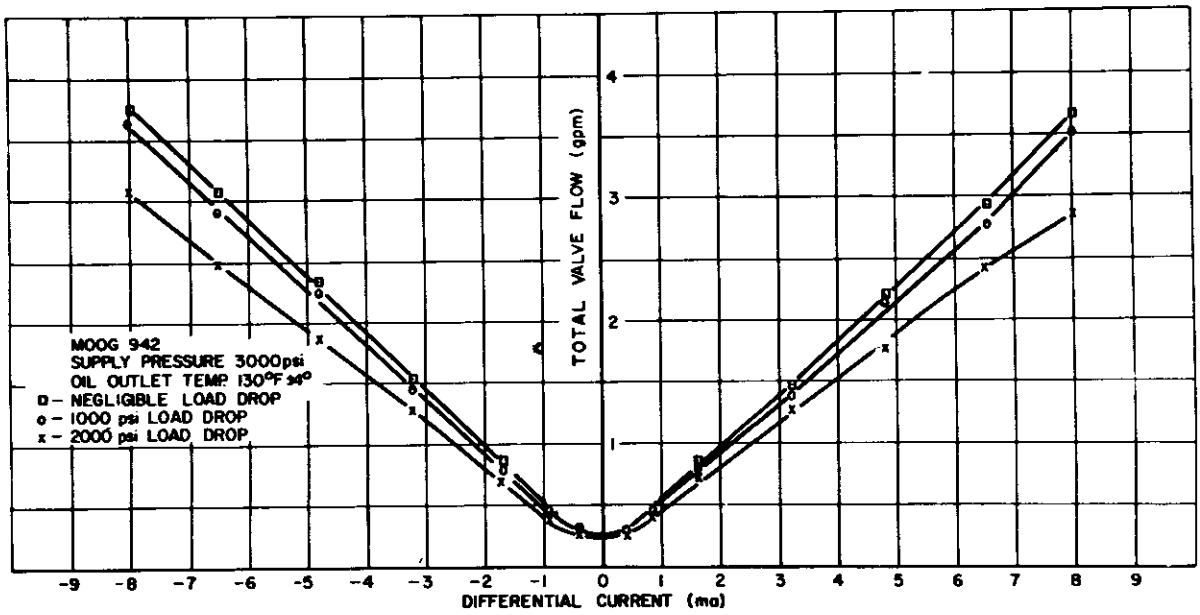

Figure 26. Experimental Flow Gain Characteristic - Moog 942

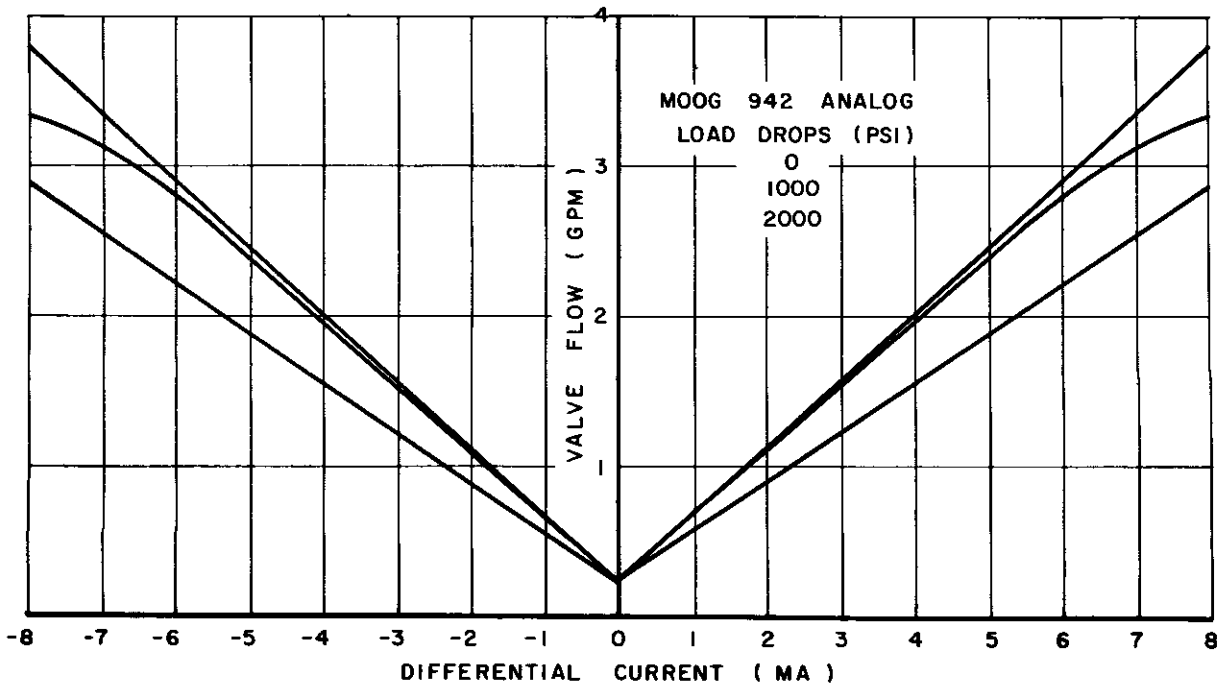

Figure 27. Analog Flow Gain Characteristic - Moog 942

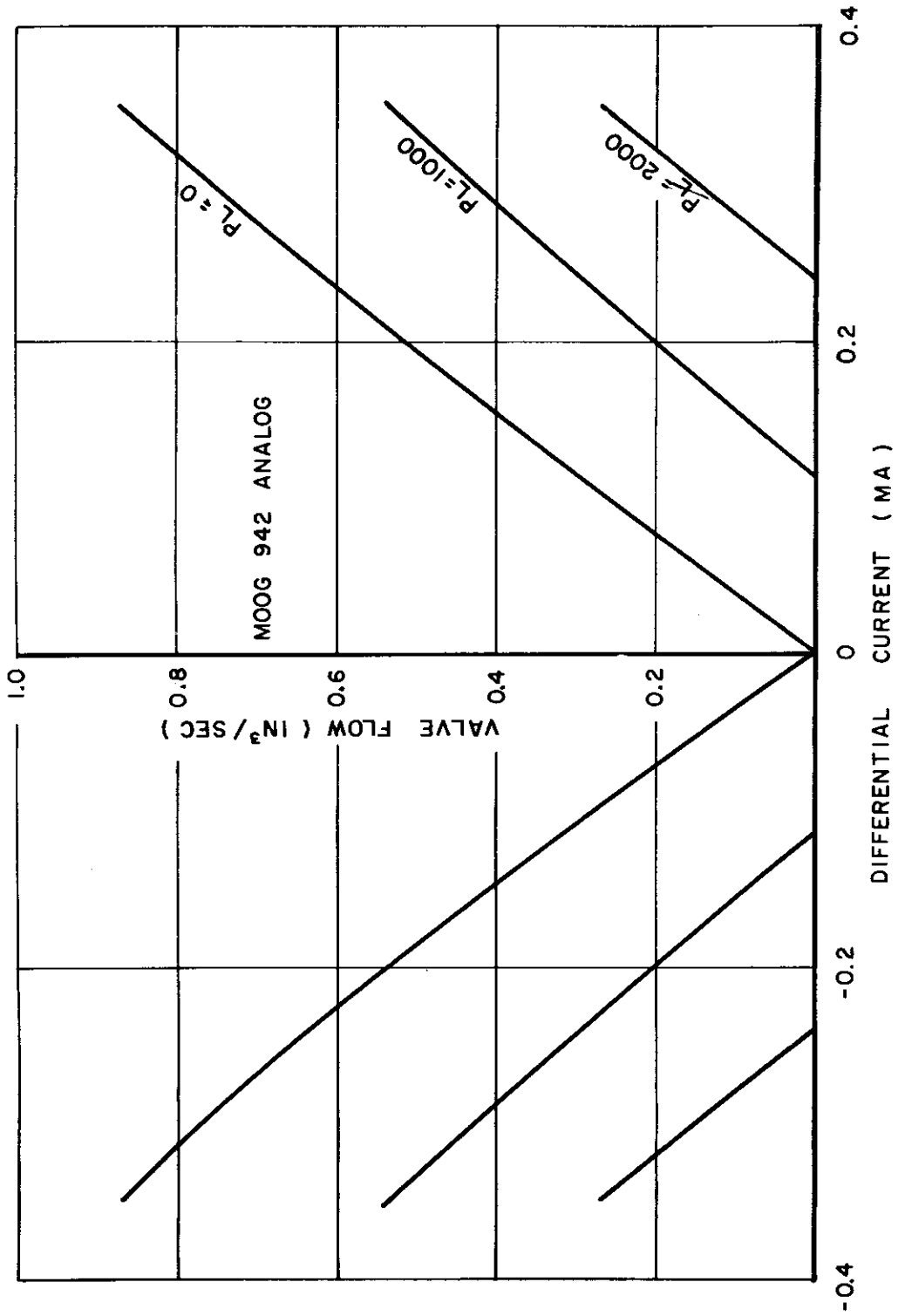

Figure 28. Analog Low Flow Characteristic - Moog 942

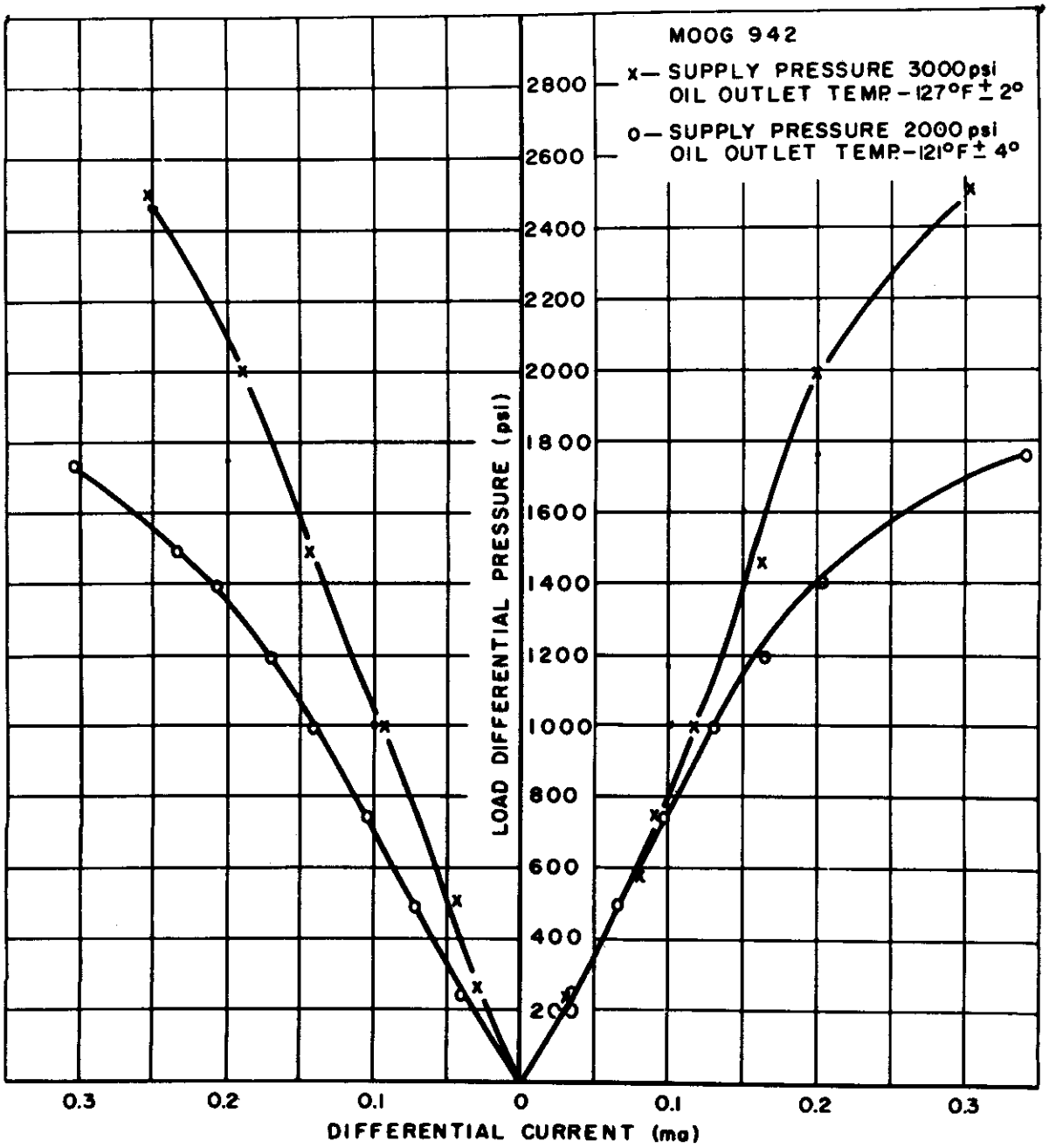

Figure 29. Experimental Pressure Gain Characteristic - Moog 942

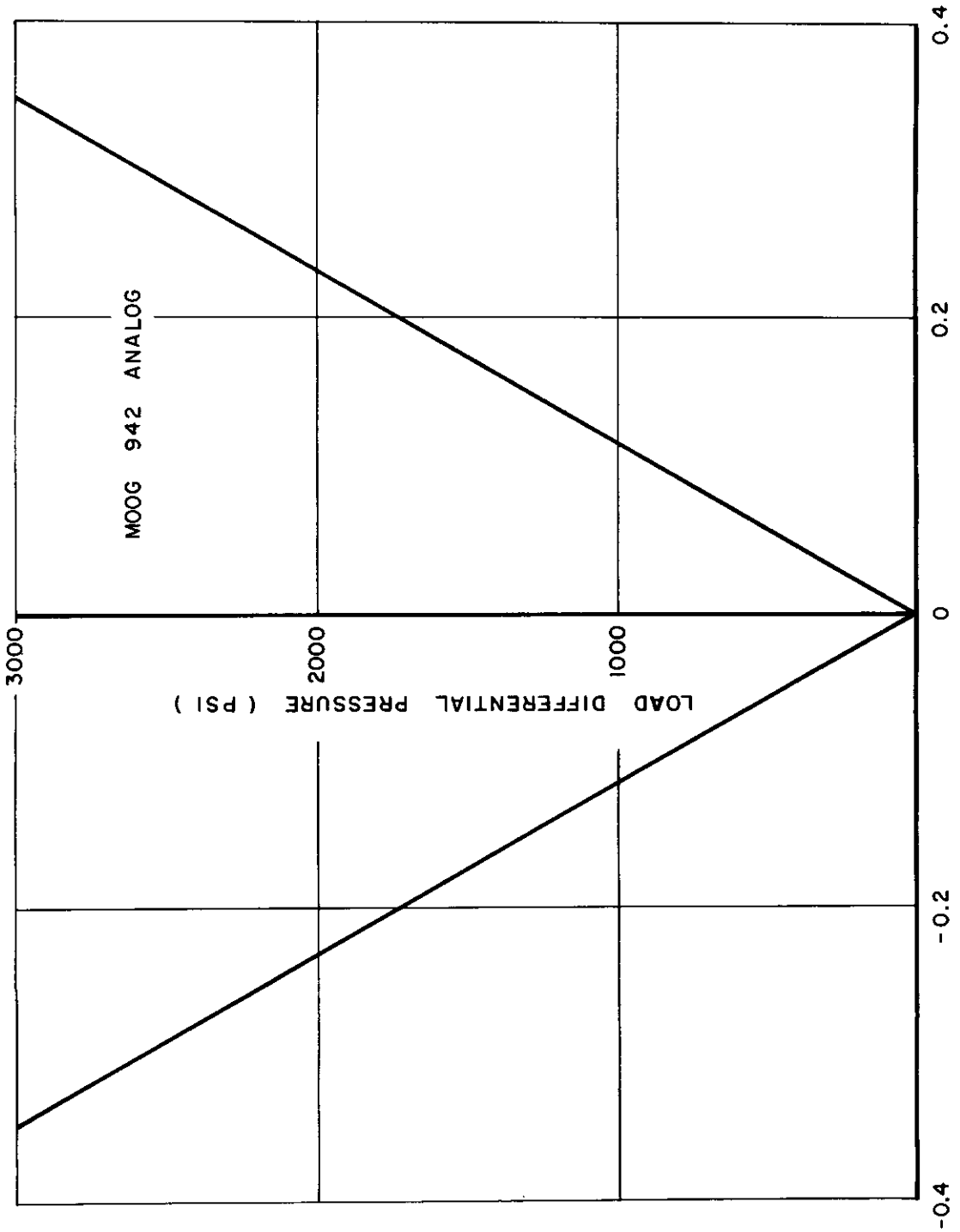

Figure 30. Analog Pressure Gain Characteristic - Moog 942

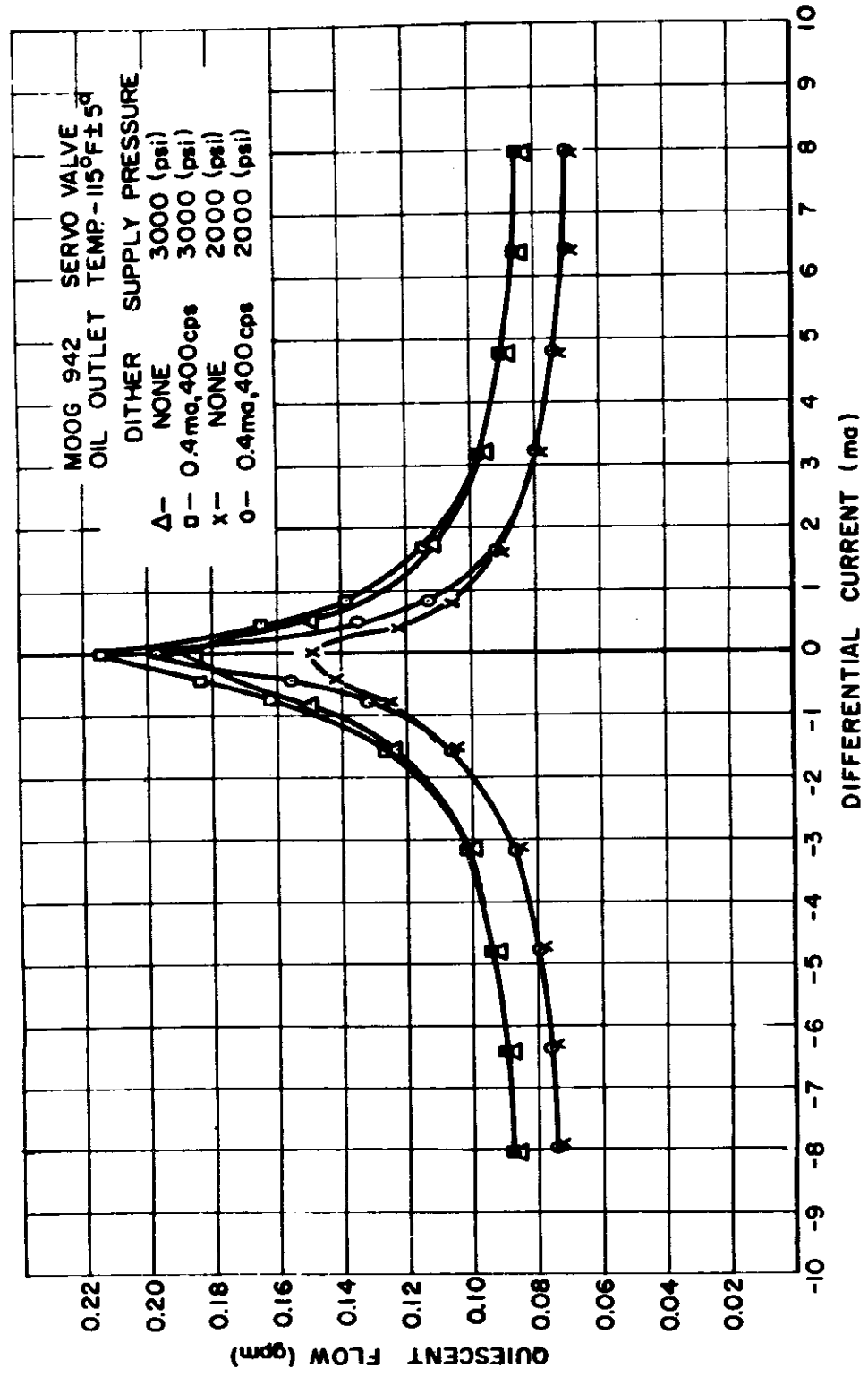

Figure 31. Quiescent Flow vs. Differential Current - Moog 9126

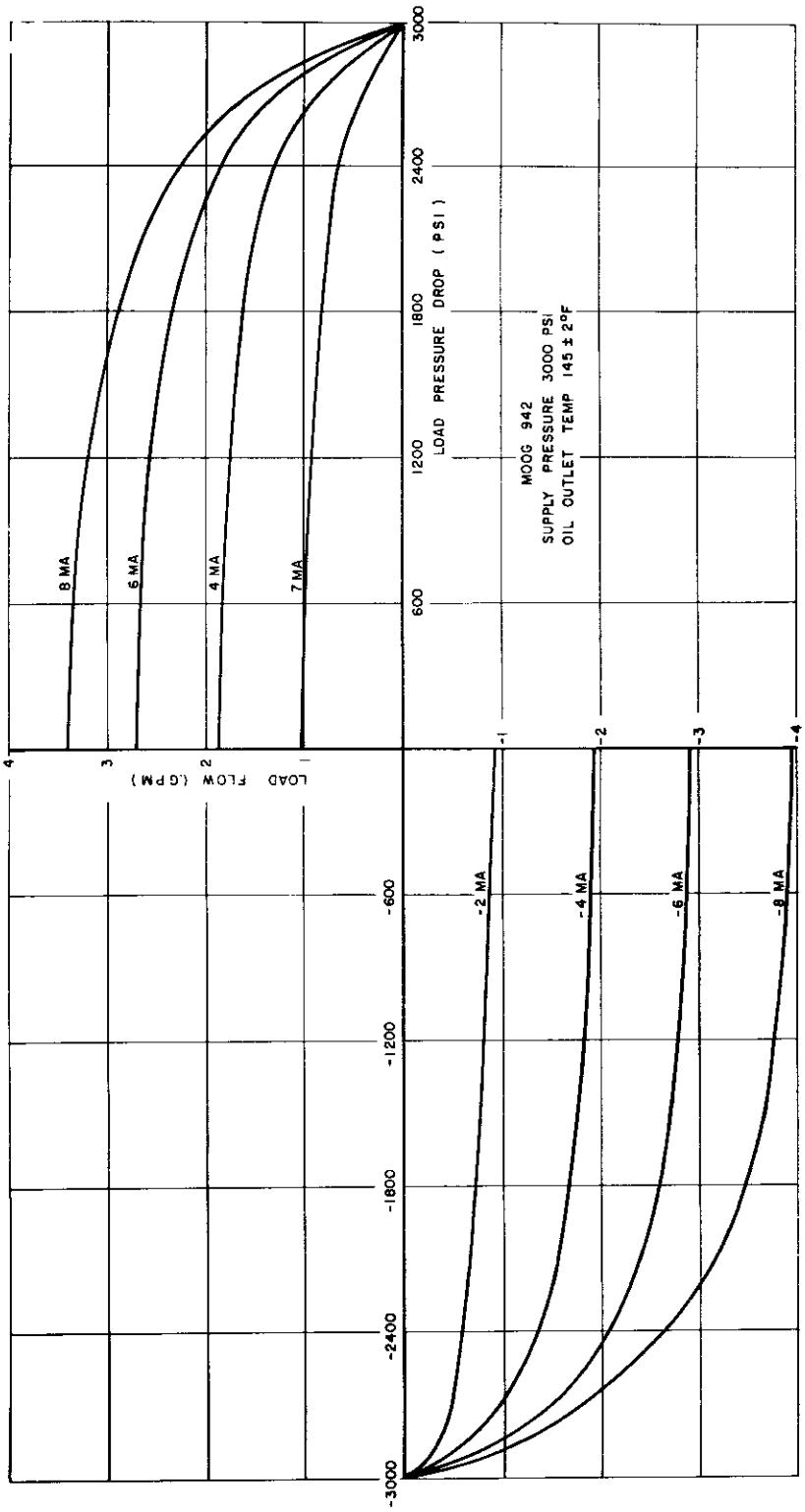

Figure 32. Output Load Pressure vs. Load Flow - Moog 942

F. Conclusions

As mentioned in the Introduction to this chapter, an electrohydraulic servo valve contains many nonlinearities which render analysis of the valve difficult. Those mentioned, such as orifice nonlinearities, velocity saturation, coulomb friction, etc., can be successfully simulated on an electronic analog computer, either alone or in combination. Since these nonlinearities essentially define the valve's general operational characteristics, it is logical to assume that the valve, too, can be simulated on an analog computer. The results of this study have shown this to be true, to a degree. The static characteristics of the first and second stages of the valve, as simulated, compared within 10 to 20 percent of those measured experimentally. While time did not permit a complete evaluation of the dynamic characteristics of the simulated valve, results of previous analog studies (see Reference 2) indicate the same order of accuracy for the dynamic simulation. Actually, the present simulation should be much superior because of the inclusion of the effects of pressure gain and flow saturation.

The questions then arise: what limits of accuracies are attainable in the present simulation? Is it possible to obtain higher accuracies economically? Is the simulation, as developed under this study, sufficiently accurate to permit its use as a design tool for valve design and development?

First, the main difficulty in analoging a valve is in ascertaining what the actual valve characteristics are initially. Because the valve operates at very high pressures, clearances are exceedingly small and, therefore, variations in the clearances are difficult if not impossible, to measure sufficiently accurately for precise simulation. For instance, rounding of the first-stage nozzle edges can cause nonlinearities which are difficult to analog over all ranges of operation. Rounding and variations in the axial to radial clearances of the spool can be even more serious. Then friction and stiction effects are not constant but vary with temperature, load pressure, time of operation, oil contamination level, etc.

While it is theoretically possible to simulate these variations in characteristics, it does not appear to be feasible, practically. For instance, the amount of nonlinear equipment required would be greatly increased, further complicating the problem of maintaining stable loops within the computer, a major simulation problem in itself. The use of larger time scales increases the drift problems in computing elements and input and output devices.

From consideration of the accuracies obtained in the current study, it does appear that the simulation as presently set up would be useful in

assisting in the design of the valve. The interrelationships between various elements within the valve can be determined merely by varying potentiometer settings on the computer and noting how the various characteristics are influenced. Much about the valve's over-all characteristics can be learned in a very short time without the need for building and testing out designs, an expensive procedure. The experimental development could then be limited to much narrower areas of investigation.

It appears desirable to include variability of the torque motor characteristics in the simulation, also, since small changes in the torque motor configuration can influence valve performance drastically. This was not done in the present program because only one set of characteristics, those of the valve being simulated, was needed.

CHAPTER III

INVESTIGATION OF PRESSURE CONTROL VALVES

A. Introduction

Under ideal conditions, proportional hydraulic control can be accomplished through flow control, pressure control, or a combination of both. If a flow control valve is used,*

$$Q_L = K_f \Delta I \tag{1}$$

and $$\Delta P_L = Q_L/K_3 S - A_L \theta_o/K_3. \tag{2}$$

Since $$A_L \Delta P_L = (M_L S^2 + B_L S + K_L)\, \theta_o, \tag{3}$$

the resulting transfer function is

$$\frac{\theta_o}{\Delta I} = \frac{A_L K_1/K_3}{S(M_L S^2 + B_L S + K_L + A_L{}^2/K_3).} \tag{4}$$

If an ideal pressure control valve is used

$$\Delta P_L = K_p \Delta I, \tag{5}$$

and the resulting transfer function is

$$\frac{\theta_o}{\Delta I} = \frac{A_L K_p}{M_L S^2 + B_L S + K_L}. \tag{6}$$

In the ideal situation, one advantage of the pressure control valve is therefore apparent, as the flow control valve will have a minimum of 90 degrees phase shift for all frequencies while a system using a pressure control valve would have no phase shift until the region of the load spring-mass resonance is reached.

---

* List of symbols appears on pages 74 and 75

An additional advantage for the pressure control valve is indicated when this type of valve is operated in a closed loop system. In a position servo system employing a flow control valve, there will always be some finite value of gain, K_1, at which the system becomes unstable. However, since the ideal pressure control valve system contains only two open loop poles, it can theoretically be designed to have any desired closed loop bandwidth by the simple expedient of changing the loop gain.

As the result primarily of flow forces within the valve, it has been impossible to manufacture a valve whose output is entirely independent of flow such as was assumed in the above analysis. Because of this fact, certain factors inherent in systems using flow control valves must also be considered with practical pressure control valves, and the advantages of pressure control are therefore appreciably weakened. Two pressure control valves are presently available commercially and to illustrate the considerations inherent in their use, a system transfer function was developed using each type of valve. One of each of the two valves was obtained and tested both statically and dynamically with various loads.

An attempt was made in WADC Technical Report 55-29, Part 4, written by Cook Research Laboratories, to utilize a transfer function, as previously developed for flow control valves, to also describe operation of a pressure control valve. Although the steep slope of the pressure-flow curves of the pressure control valve necessitated use of a large value for C_1 in this transfer function, the results obtained were not entirely satisfactory. Calculated resonant frequency was within 7 percent of the experimentally obtained frequency. The calculations also indicated that the system should be highly overdamped ($\zeta = 2.5$); however, experimental damping ratios of less than 0.2 were measured. The following development essentially results in a modification of the previously derived transfer function. Use of this modified function results in closer agreement with experimental findings for system damping ratio.

B. Transfer Function Development

1. Cadillac Gage Company - PC-2 Valve

A schematic diagram of this valve is shown in Figure 33. In operation, a differential current applied to the torque motor results in a differential first-stage pressure. This pressure tends to move the two spools in opposite directions, thus opening a pressure port to one side of the load and a drain port to the opposite side of the load. A portion of the resulting differential output pressure is then

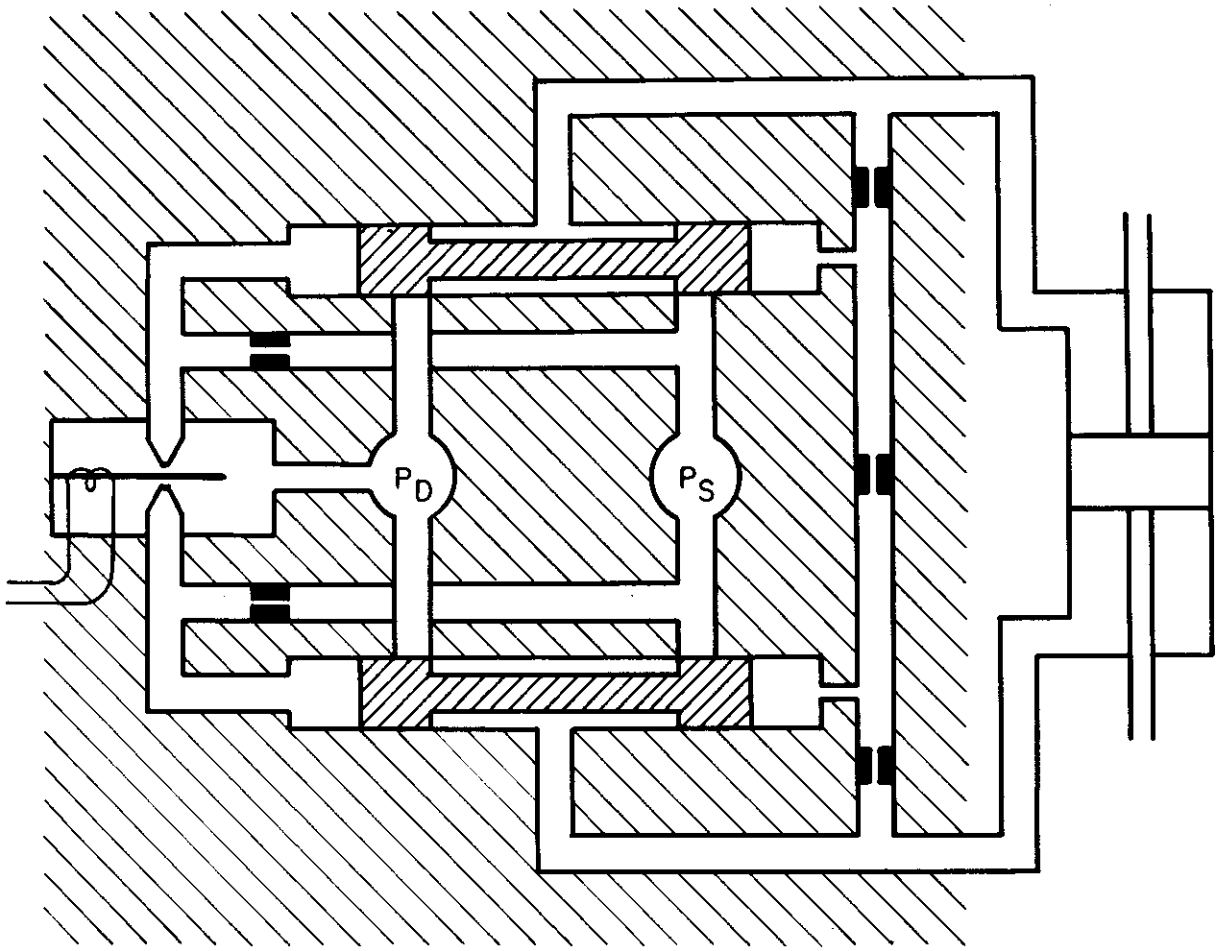

Figure 33. Schematic of Cadillac Gage PC-2 Valve

applied to the spool ends in a manner to oppose first-stage differential pressure. When the force produced by feedback pressure plus the flow forces on the spools equals the force due to first-stage pressure, the spools will cease to move and an output pressure proportional to input current will result.

Equations describing this action are

$$Q_1 = K_1\Delta I - C_3\Delta P_1 = A_s\theta_s S, \tag{7}$$

$$A_s\Delta P_1 = K_s\theta_s + A_sK_2\Delta P_L + B_v\theta_s A_s S, \tag{8}$$

and

$$Q_L = K_4\theta_s - C_4\Delta P_L = A_L\theta_o S + C_2\Delta P_L + K_3\Delta P_L S. \quad (9)$$

From these basic equations, a relationship among ΔP_L, ΔP_1, and Q_L can be developed such that

$$\left(1 + \frac{C_4 B_v A_s}{K_4 A_s K_2 + C_4 K_s} S\right)\Delta P_L = \frac{K_4 A_s}{K_4 A_s K_2 + C_4 K_s}\ \Delta P_1 - \frac{K_s}{K_4 A_s K_2 + C_4 K_s}\left(1 + \frac{A_s B_v}{K_s} S\right) Q_L. \quad (10)$$

This equation can be simplified to the form

$$(1 + T_2 S)\ \Delta P_L = C_7\Delta P_1 - \frac{1}{C_1}\ (1 + T_1 S)\ Q_L. \quad (11)$$

From Equations (7) and (8)

$$\left[K_s + \left(\frac{A_s^2}{C_3} + B_v A_s\right) S\right]\Delta P_1 = \left(\frac{K_1}{C_3}\right)\ (K_s + B_v A_s S)\ \Delta I + \left(\frac{A_s^2 K_2}{C_3}\ S\right)\ \Delta P_L \quad (12)$$

$\frac{A_s^2}{C_3}$ is appreciably less than $B_v A_s$ in magnitude and may be neglected. Therefore,

$$\Delta P_1 \approx \frac{K_1}{C_3}\ \Delta I + \frac{\left[\frac{A_s^2 K_2}{C_3}\right](\Delta P_L S)}{K_s + B_v A_s S} \quad \text{or} \quad (13)$$

$$\Delta P_1 = a\ \Delta I + \frac{\beta P_L S}{1 + T_a S} \quad (14)$$

Substituting (14) in (12) one obtains the relationship

$$\left[(1 + T_2S)(1 + T_aS) - C_7\beta S\ \Delta P_L\right] = C_7\alpha\,(1 + T_aS)\,\Delta I - \frac{1}{C_1}\,(1 + T_aS)\,(1 + T_1S)\,Q_L \tag{15}$$

Since $C_7\beta$ is small with respect to T_2 plus T_a, this equation may be further simplified to

$$(1 + T_{2_c}S)\,\Delta P_L = K_1\Delta I - \frac{1}{C_1}\,(1 + T_{1_c}S)\,Q_L. \tag{16}$$

If a load containing mass, viscous damping, and a spring is used

$$A_L\Delta P_L = (M_LS^2 + B_LS + K_L)\,\theta_o \tag{17}$$

From Equations (9), (16), and (17), one can then develop a transfer function for the PC-2 valve where

$$\frac{\theta_o}{\Delta I} = \frac{C_1K_5A_L/K_3M_LT_1}{D} \tag{18}$$

and

$$D = S^4 + \left[\frac{C_2}{K_3} + \frac{B_L}{M_L} + \frac{1}{T_{1_c}} + \frac{C_1}{K_3}\cdot\frac{T_{2_c}}{T_{1_c}}\right]S^3$$

$$+\left[\frac{C_1+C_2}{K_3T_{1_c}} + \frac{B_LC_2+A_L^2}{K_3M_L} + \frac{K_L}{M_L} + \frac{B_L}{M_LT_{1_c}} + \frac{B_L\,C_1}{K_3M_L}\cdot\frac{T_{2_c}}{T_{1_c}}\right]S^2$$

$$+\left[\frac{B_L(C_1 + C_2) + A_L^2}{K_3\,M_L\,T_{1_c}} + \frac{K_L}{M_LT_{1_c}} + \frac{C_2K_L}{K_3M_L} + \frac{C_1K_L}{K_3M_L}\cdot\frac{T_{2_c}}{T_{1_c}}\right]S$$

$$+\left[\frac{(C_1 + C_2)\,K_L}{K_3M_L\,T_{1_c}}\right]. \tag{19}$$

Open loop transfer function of this valve operating with a spring-mass load containing viscous damping exhibits a fourth order characteristic equation rather than a second order as ideal theory would predict. If flow forces on the valve spools were negligible, resulting in $C_1 = \infty$, $T_1 = \infty$, and $T_2 = 0$, the ideal situation would exist. Substitution of these relationships into Equation (11) results

in the desired second order characteristic equation, thereby clearly showing the differences existing between an ideal pressure control valve and the PC-2 valve.

2. Moog Valve Company Pressure Control Valve

A schematic diagram of this valve is shown in Figure 34.

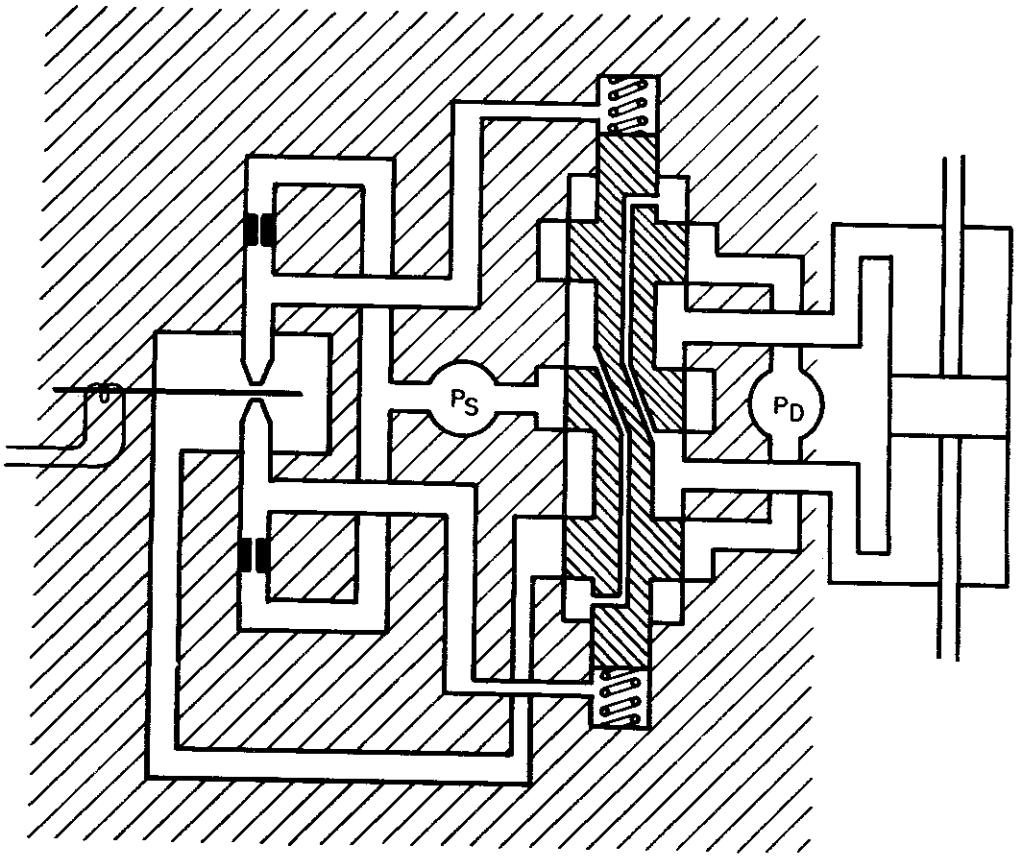

Figure 34. Schematic of Moog Pressure Control Valve

Operation of this valve is similar to that of the Cadillac PC-2 valve in that output pressure is fed back to the spool; however, this is accomplished in a somewhat different manner. Only one spool is employed with essentially two sets of end areas. First-stage differential pressure is applied to one end area set causing initial motion of the spool. Full output pressure is then fed back through openings in

the spool to the other set of areas; the spool continues to move until the force on the spool due to feedback pressure plus flow forces equals force produced by first-stage differential pressure. No leakage path is used in this valve such as was required in the Cadillac valve to reduce magnitude of feedback pressure.

Equations describing operations of this valve with a mass-spring load containing viscous damping are:

$$Q_1 = K_1 \Delta I - C_3 \Delta P_1 = A_s \theta_s S, \tag{20}$$

$$A_s \Delta P_1 = K_s \theta_s + A_f \Delta P_L, \tag{21}$$

$$Q_L = K_4 \theta_s - C_4 \Delta P_1 = A_L \theta_o S + C_2 \Delta P_L + K_3 \Delta P_L S, \text{ and} \tag{22}$$

$$A_L \Delta P_L = (MS^2 + B_L S + K_L)\, \theta_o. \tag{23}$$

Therefore,

$$\Delta P_1 = \frac{K_1 K_s \Delta I + A_s A_f \Delta P_L S}{C_3 K_s + A^2{}_s S} = \frac{K_a \Delta I + K_b \Delta P_L S}{1 + T_3 S} \tag{24}$$

$$\Delta P_L = K_5 \Delta P_1 - \frac{1}{C_1} Q_L \tag{25}$$

and

$$\left[1 + (T_3 - K_5 K_b) S\right] \Delta P_1 = K_s K_a \Delta I - \left(\frac{1}{C_1}\right)(1 + T_3 S)\, Q_L, \tag{26}$$

or

$$(1 + T_{2_m} S)\, \Delta P_L = K_1 \Delta I - \frac{1}{C_1} (1 + T_{1_m})\, Q_L. \tag{27}$$

This relationship results in a transfer function for a system using the Moog pressure control valve which is identical in form to that obtained for the Cadillac PC-2 valve. The values of T_{1_m} and T_{2_m} are roughly equal in magnitude to T_{1_c} and T_{2_c}, respectively, and this fact results in two valves which are in this respect essentially theoretically equal in performance.

C. Theoretical Performance Analysis

1. Comparison with Flow Control Valves

The similarity between a theoretical analysis of a system using a pressure control valve as opposed to a flow control valve can be readily seen by examining the characteristic equation for a system using mass with viscous damping with each type of valve. For a pressure control valve this equation is:

$$D = S^3 + \left[\frac{C_2}{K_3} + \frac{B_L}{M_L} + \frac{1}{T_1} + \frac{C_1}{K_3} \cdot \frac{T_2}{T_1}\right] S^2$$

$$+ \left[\frac{C_1 + C_2}{K_3\, T_1} + \frac{B_L C_2 + A_L^2}{K_3\, M_L} + \frac{B_L}{M_L T_1} + \frac{B_L C_1}{K_3 M_L} \cdot \frac{T_2}{T_1}\right] S$$

$$+ \left[\frac{B_L\ (C_1 + C_2) + A_L^2}{K_3 M_L T_1}\right] \qquad (28)$$

For a flow control valve, the characteristic equation including the no-load time constant, T_1, is

$$D = S^3 + \left[\frac{C_2}{K_3} + \frac{B_L}{M_L} + \frac{1}{T_1} + \frac{C_1}{K_3}\right] S^2$$

$$+ \left[\frac{C_1 + C_2}{K_3\ T_1} + \frac{B_L C_2 + A_L^2}{K_3\, M_L} + \frac{B_L}{M_L T_1} + \frac{B_L C_1}{K_3 M_L}\right] S$$

$$+ \left[\frac{B_L (C_1 + C_2) + A_L^2}{K_3 M_L T_1}\right] \qquad (29)$$

In form, both equations are identical except for the ratio T_2/T_1 multiplying one factor in each of the S^2 and S terms of the pressure control valve equation, which ratio does not appear in the flow control valve equation. Both systems will therefore exhibit a third order response; however, this response will vary in accordance with the magnitudes of C_1, T_1, and T_2, all of which are functions of the particular valve being employed. All other parameters included in the equations are functions of the actuator or load.

In a flow control valve, the first-stage time constant is effectively isolated from the second-stage load system and can be so considered mathematically. As was shown in WADC Technical Report 55-29 Pt IV, the expression for resonant frequency in such a system is:

$$\omega_n = \left[\frac{(C_1 + C_2)\quad B + A_L^2}{K_3 \quad M} \right]^{1/2} \tag{30}$$

and

$$2 \quad \zeta \quad \omega_n = \frac{C_1 + C_2}{K_3} + \frac{B}{M} \tag{31}$$

A pressure control valve does not exhibit the same property of first-stage isolation because of pressure feedback to the second-stage spool. As a result, value of the time constant for the system first order lag is influenced by load characteristics and no simple expression can be derived for ω_n and ζ. Relative effects on ω_n and ζ produced by variation of M and K_3 will be the same for both types of systems, although magnitude of the changes produced by equivalent variation will usually be somewhat different.

In a majority of the flow control valves produced to date of 10 gpm capacity or less, the value of T_1, first-stage time constant, is approximately 0.002 second and slope of the valves' pressure flow curves, C_1, in the useful region is about 1×10^{-5} in ^{5}/lb-sec. For both the Cadillac and Moog pressure control valves, the value of T_1 is approximately 0.02 second and T_2 0.002 second. C_1 for the Cadillac PC-2 valve tested is 7.5×10^{-2} in ^{5}/lb-sec. It should be noted in this regard that for a perfect flow control valve $C_1 = 0$ while in an ideal pressure control valve $C_1 = \infty$.

2. Comparison of System Loads

a. Representative Systems

Since differences between the transfer functions of systems using practical flow and pressure control valves are a matter of relative magnitude of similar terms, a useful method of presenting these differences is to analyze system open loop performance with various types of loads. It is difficult to choose system parameter constants which are representative of a

majority of flight control systems in missiles and aircraft. The following values are believed indicative of possible applications as well as being capable of simulation in the laboratory.

C_1 (flow control) - 1×10^{-5} $in^3/lb\text{-}sec$

C_1 (pressure control) - $7.5 \times 10^{-3}/lb\text{-}sec$

T_1 (flow control) - 2×10^{-3} sec

T_1 (pressure control) - 2×10^{-2} sec

T_2 -1.7×10^{-3} sec

C_2 -2.7×10^{-4} $in^5/lb\text{-}sec$

B_L $-10^{lb\text{-}sec/in}$

A_L -0.96 in^2

K_3 -5.26×10^{-6}, 1.32×10^{-5}, 2.63×10^{-5} in^5/lb

M_L -0.375, 0.125 $lb\text{-}sec^2/in$

K_L -0 lb/in

Open loop system characteristics resulting from each of the six possible load combinations listed above are tabulated in Table 3. As indicated, both a flow control and pressure control valve are compared for each situation.

b. Analysis of Theoretical Results

Table 3 shows certain similarities and some differences between systems using flow control vs. pressure control valves. In both systems, increasing mass as well as a larger oil volume (larger K_3) result in a lower resonant frequency. Values of this resonance are within the same range for both systems, although in all situations shown use of the pressure control valve resulted in a resonance 25 to 50 percent higher in frequency than would be obtained with a flow control valve.

In flow control valve systems, a change in mass has little effect on damping ratio although a decrease in oil volume has the

TABLE 3

TYPICAL SYSTEM OPEN LOOP CHARACTERISTICS

Valve	Compressibility Constant (in^5/lb)	Load Mass ($lb\text{-}sec^2/in$)	ω_c (rad/sec)	ω_n (rad/sec)	Damping Ratio
FC	5.26×10^{-6}	0.125	500	1185	0.06
PC	5.26×10^{-6}	0.125	59	1460	0.53
FC	5.26×10^{-6}	0.375	500	685	0.05
PC	5.26×10^{-6}	0.375	36	1080	0.68
FC	1.32×10^{-5}	0.125	500	751	0.07
PC	1.32×10^{-5}	0.125	59	925	0.36
FC	1.32×10^{-5}	0.375	500	433	0.05
PC	1.32×10^{-5}	0.375	36	584	0.54
FC	2.63×10^{-5}	0.125	500	530	0.08
PC	2.63×10^{-5}	0.125	59	659	0.20
FC	2.63×10^{-5}	0.375	500	306	0.06
PC	2.63×10^{-5}	0.375	36	483	0.34

effect of slightly decreasing damping ratio. Over the entire range of values examined, however, the open loop transient response would be expected to be quite oscillatory.

In a pressure control valve system, a decrease in mass tends to result in a smaller damping ratio although the change is relatively small. A change in oil volume, however, may be expected to produce an appreciable change in damping ratio with a decrease in volume causing an increase in this ratio. With the smaller oil volumes, damping ratios greater than 0.5 may be expected and, in general, systems using pressure control valves should have higher damping ratios than those with flow control valves.

As was stated previously, changes in the system load do not affect the first order lag time constant in the flow control system, while they may have a considerable effect on the time constant in a pressure control valve system. Over the range of values used, however, the break frequency resulting from this time constant was less than 10 cps for the pressure control valve while it was 80 cps for the flow control valve system.

c. Coulomb Friction Effects

Coulomb friction may be defined as that force existing in physical systems between two contacting surfaces in relative motion, which is constant in magnitude and acts in a direction such as to resist the motion. Mathematically, this effect may be expressed as follows:

$$M_L\ddot{\theta} + B_L\dot{\theta} + F_c \frac{\dot{\theta}}{|\dot{\theta}|} = PA_L \qquad (32)$$

A nonlinear equation of this type may be investigated through use of the describing function approach. This function is defined as the ratio of the output signal to the input signal where a sinusoidal input is used, and the output is considered to contain only the fundamental component of the input. Such a function in the case of coulomb friction relates output force to input velocity. When a sinusoidal velocity is assumed, the resulting coulomb friction force is a square wave. Fourier series expansion of this waveform shows the coefficient of the fundamental to be $4 F_c/\pi$ $\dot{\theta}$. The desired describing function is therefore

$$\frac{\theta_i}{\theta} = \frac{4Fc}{\pi\ |\dot{\theta}|} \tag{33}$$

Considering sinusoidal signals only,

$$\frac{\theta_i}{\theta_o} = \frac{j\ 4Fc}{\pi\ |\theta_o|} \tag{34}$$

With this same consideration, the open loop transfer function for an electrohydraulic servo valve with a mass load is of the form

$$j\omega\ \frac{\theta_o}{\theta_i} = \frac{K}{(-A\omega^2 + C)\ +\ j\ (-\omega^3 + B\omega)} \tag{35}$$

When coulomb friction is added, one obtains a function of the form

$$j\omega\ \frac{\theta_o}{\theta_i} = \frac{K}{(-A\omega^2 + C)\ +\ j\ (-\omega^3 + B\omega + \frac{4Fc}{\pi|\theta_o|})\ .} \tag{36}$$

From this expression, it can be seen that coulomb friction will tend to add a fixed value of phase lag to the system at all frequencies and will similarly tend to reduce the output magnitude. Both effects are a function of the magnitude of output position and will become more pronounced at small signal amplitudes.

Dynamically, it appears that coulomb friction in this system can be approximated by an increase in the time constant of the first order lag. The effect of the change is a decrease in closed loop system gain and an increase in phase lag. At relatively high frequencies, the valve output pressure amplitude decreases rapidly and other nonlinear effects become appreciable. Eventually insufficient pressure is produced to overcome the stiction force and no output motion can occur.

3. Optimum Loads

Transfer functions, G(S), have been developed which describe the open loop operation of both flow control and pressure control

valves with conventional mechanical loads. When these systems are operated closed loop the characteristic equation becomes

$$G(S)_c = 1 + G(S)_o \tag{37}$$

Root-locus techniques were applied to this equation to study closed loop system operation. Loci for each of three representative systems using both flow and pressure control valves are plotted on Figures 35, 36, and 37.

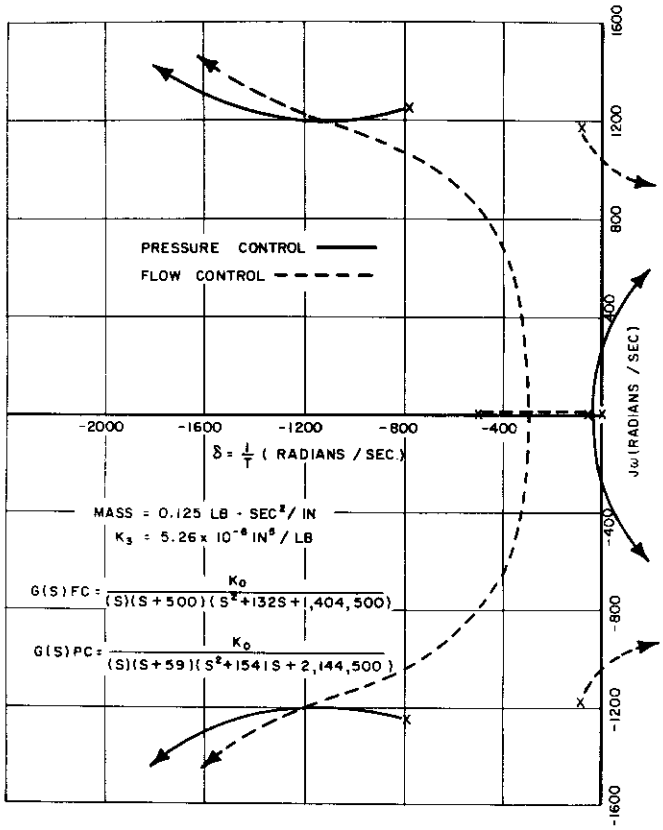

Figure 35. Root Locus Plot of Hydraulic Position Servo System

Figure 35 represents conditions existing in a position servo system containing a relatively small oil volume, small load mass, and no mechanical springs. These loci are, however, generally similar in shape to those of all uncompensated position servos within the range of loads considered in Table 3. Analysis of this figure shows that a flow control valve will have two first order time constants plus one resonance if a relatively low loop gain is employed. Break frequency of the two time constants can be made to be approximately 50 cps and the damping ratio of the resonance with the same system gain will then be approximately 0.06. Use of higher system gain will have little effect on the original resonance noted but will cause combination of the two time constants into a relatively highly damped low-frequency resonance.

A pressure control valve used in this system with any appreciable closed loop gain results in a poorly damped resonance at a frequency three to four octaves lower in frequency than the resonance

produced in the same system with a flow control valve. Another resonance of much higher frequency would also exist but would be of no practical consequence due to the frequency limitations imposed by the first resonance mentioned.

Although the two first order time constants with break frequencies near 50 cycles may limit somewhat the performance of the flow control system, the low-frequency resonance of the pressure control system makes it appear to be the least desirable of the two valves in an uncompensated position control servo system.

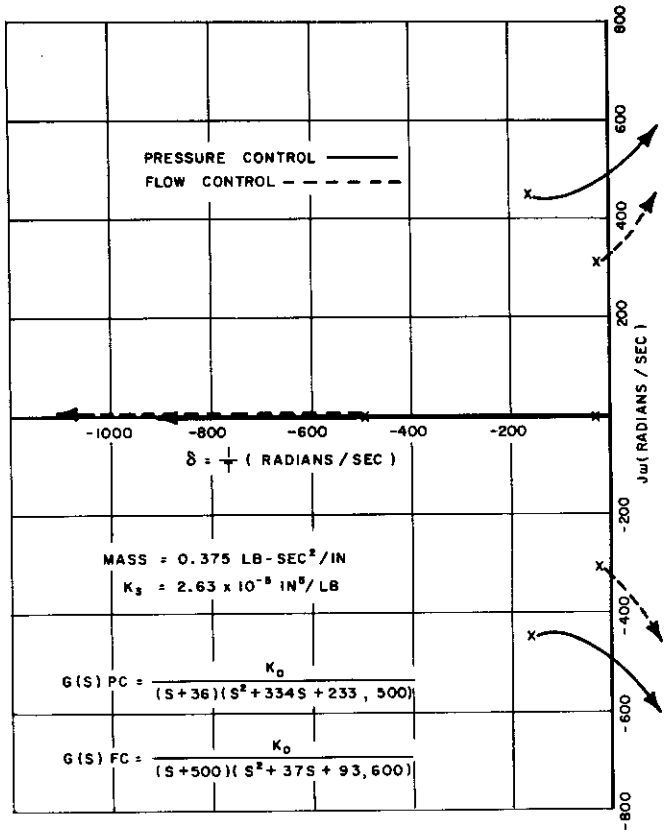

Figure 36. Root Locus Plot of Large Mass Hydraulic Velocity Servo System

Figures 36 and 37 show the root loci of pressure and flow control valves used in uncompensated velocity servo systems. It can be seen that in general both systems exhibit one first order lag plus a single resonance. In general, the frequency of resonance with a pressure control valve will be up to 40 cycles higher than that obtained from a flow control valve system. Also, the flow control valve system will be highly oscillatory at all usable values of loop gain while somewhat greater damping ratios can be obtained with a pressure control valve at the expense of loop gain.

Although the pressure control velocity servo system will exhibit a lower frequency lag than will the flow control system, this effect can be relieved by a lead network or acceleration feedback. It appears, therefore, that the dynamic response of a velocity servo using a pressure control valve can be made superior to that of a flow control valve system. The pressure control system will, however, be more

susceptible to load pressure disturbances which in some systems may be an important factor. Although loop gain of the pressure control system can be made greater than could be done in an equivalent flow control system for purpose of reducing such disturbances, these effects should be considered in evaluating each prospective system.

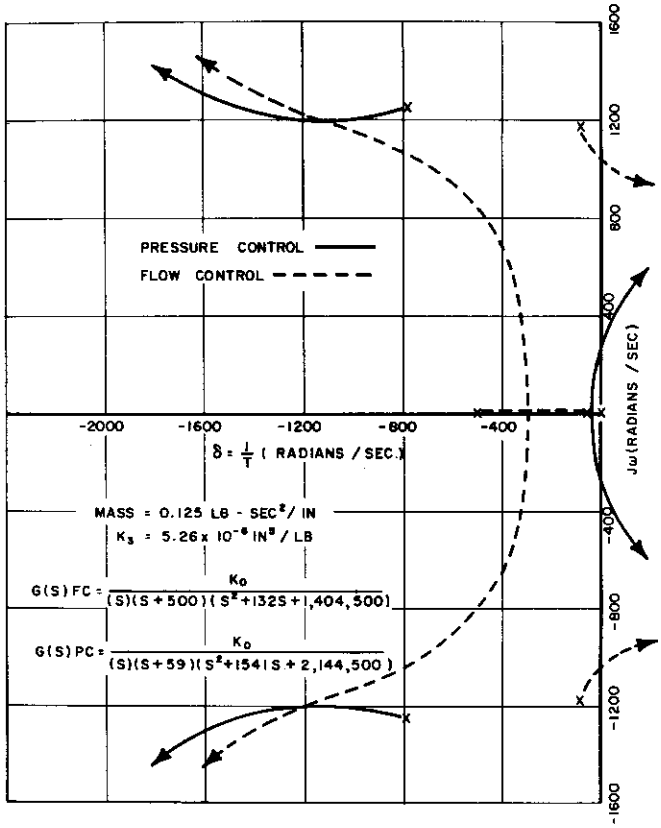

Figure 37. Root Locus Plot of Small Mass Hydraulic Velocity Servo System

If compensation is considered in a position servo, performance of a pressure control valve can be appreciably improved. Figure 38 represents the root loci of a velocity compensated pressure control position servo vs. a noncompensated flow control servo. Constants have been chosen to show optimum performance for the pressure control valve, but the general effect of adding velocity compensation can be readily seen. In essence, the low-frequency resonance has been removed and replaced by a single first order lag which has a cutoff frequency somewhere above 30 cycles, dependent on closed loop gain. The remaining resonance is roughly equal in frequency to that produced by a flow control valve in the same system but may be somewhat more highly damped. Use of velocity compensation with a pressure control position servo can, therefore, result in a system whose dynamic response is equal or in some cases somewhat better than that produced by a flow control valve in the same system. Further, at the expense of reduced damping, the pressure control system loop gain can be made considerably higher than can be used with a flow control system.

D. Experimental Results

1. Valve Tests

Each of the two pressure control valves, Cadillac PC-2 and Moog Mod. 1526, were subject to the standard static tests and the no-load dynamic tests for purpose of obtaining valve constants as used in the transfer function and to compare the valves' performance. Static tests made were (1) pressure gain, (2) flow gain, (3) pressure-flow curves, and (4) quiescent flow. Results are shown in Figures 53 to 59, in Appendix V.

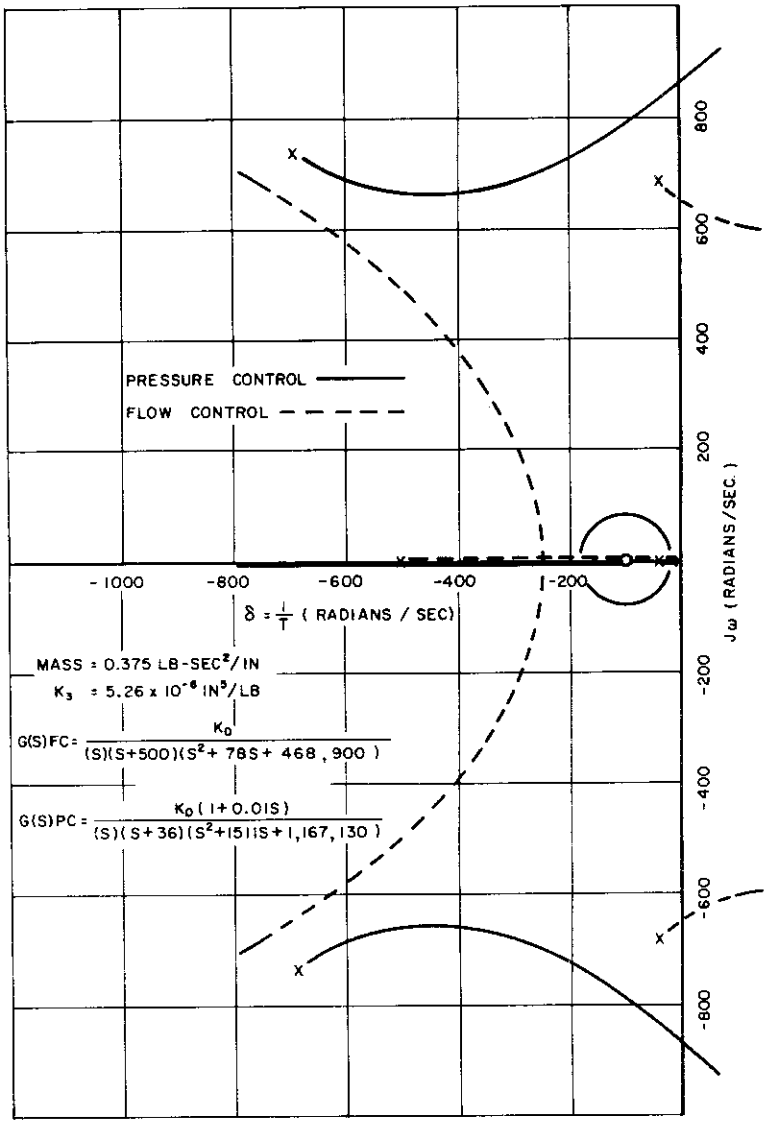

Figure 38. Root Locus Plot of Velocity Compensated Hydraulic Position Servo System

a. Static Tests

(1) Cadillac PC-2: Operation of this valve during all static tests was quite smooth with no indication of sticking or instability. Variation of pressure with differential current was linear except at points very close to rated

maximum current of 8 ma. Slope of the pressure flow curves was quite steep and linear over the range of pressure control. With 8.0 ma, differential current, maximum spool displacement was reached at low values of flow so that over most of the range of rated flow the valve acted as a conventional sharp edged orifice. With lower values of differential current this saturation effect occurs at higher values of flow.

Essentially constant quiescent flow was measured over the entire range of differential current. Since this test is run with blocked load, the only flow is leakage past the lands directly to drain or through the orifice connecting the two spools and then to drain. Because of no load flow, the spool moves very little and leakage conditions probably remain similar to those existing at null.

(2) Moog Pressure Control Mod. 1526: Performance of this valve was in the main similar to that of the PC-2 valve although some tendency for the spool to stick was noted. The pressure gain curve was linear from 0 to 4 ma differential current. Some departure from linear operation was noted from 4 to 6 ma. Pressure saturation was reached at 6 ma although the valve was rated at 8 ma. Quiescent flow was approximately 0.1 gpm for all values of differential current, but apparent spool sticking caused erratic operation during this test and the results were not plotted.

Pressure flow curves for this valve exhibit the familiar steep slope during operation over the range of pressure control although the slope was not as great as for the PC-2 valve. Also, some rounding-off of the slope was noted for small values of load flow.

When this valve was initially put on the test stand, it was found impossible to null the valve with 0 ma differential current. With 3 ma applied the valve would null. After discussion with the manufacturer it was agreed that the difficulty had been caused by mounting the valve with only three bolts instead of four. Apparently, this unsymmetrical mounting causes sufficient distortion of the torque motor magnetic field to prevent nulling in the usual manner. Use of four bolts of similar material corrected the trouble.

b. No-Load Test

The no-load test was conducted in a manner similar to that described in the WADC Technical Report 55-29, Part 2 with an addition, however, of pressure transducers on each side of the actuator. Purpose of this test for a pressure control valve was to determine values of T_1 and T_2. Results are shown in Figures 60 and 61 in Appendix V. Values of T_1 and T_2 are approximately equal for both valves with T_1 equal to 0.02 second and T_2 equal to 0.002 second.

2. Load Tests

a. Open Loop

Dynamic load tests consisted of frequency response runs using various values of mass and oil volume for each run. Results are presented in the form of Bode plots on Figures 62 to 66 in Appendix V. For purposes of comparing experimental and calculated results with similar load conditions, values of ω_c, ω_n and ζ were extracted from these Bode plots.

The first step in the procedure was to determine ω_c, the break frequency resulting from the system first order time constant. Attenuation effects of this time constant were then subtracted from the inital Bode plot, resulting in a plot of the remaining second order system. Both ω_n and ζ were then determined by comparing this altered Bode plot with a set of curves describing second order systems with various damping ratios. Such a set of curves is shown in Figure 8 of WADC Technical Report 55-29, Part 4.

Comparison of experimental and calculated results are presented in Table 4. It can be seen that as in the previous valve report, good agreement has been achieved between the experimental and calculated values of ω_n. In those runs where the resonant frequency was below 100 cps, agreement was within 9 percent. In the run with a calculated frequency of 160 cps, there was an error of 12.5 percent.

The agreement between experimental and calculated values of damping ratio, ζ, was not as good as for ω_n and ω_c. In all runs, the calculated value of ζ was greater than was obtained experimentally. An underdamped system was indicated, however,

TABLE 4

OPEN LOOP CHARACTERISTICS

Run	ω_c (cps)		ω_n (cps)		ζ	
	Exp.	Calc.	Exp.	Calc.	Exp.	Calc.
1	4.2	5.7	77	80	0.20	0.30
2	6.0	5.7	90	93	0.25	0.45
3	5	5.7	142	160	0.30	0.60
4	6	7.0	81	89	0.18	0.27
5	4.0	6.2	65	67	0.20	0.25

DESCRIPTION OF RUN

Run	Valve	Oil Volume (in^3)	Load Weight (lb)
1	Cadillac PC-2	11.56	150
2	Cadillac PC-2	8.05	150
3	Cadillac PC-2	2.70	150
4	Cadillac PC-2	11.56	90
5	Moog PC	11.56	150

for all runs, and agreement was within 50 percent. Although this agreement is poor, it is much better than had been obtained by the previous method of analysis.

Manufacturers' published data on pressure control valve dynamic response are generally given in part in the form of pressure gain vs. frequency for blocked load port conditions. Figure 39 shows the frequency response of the Cadillac PC-2

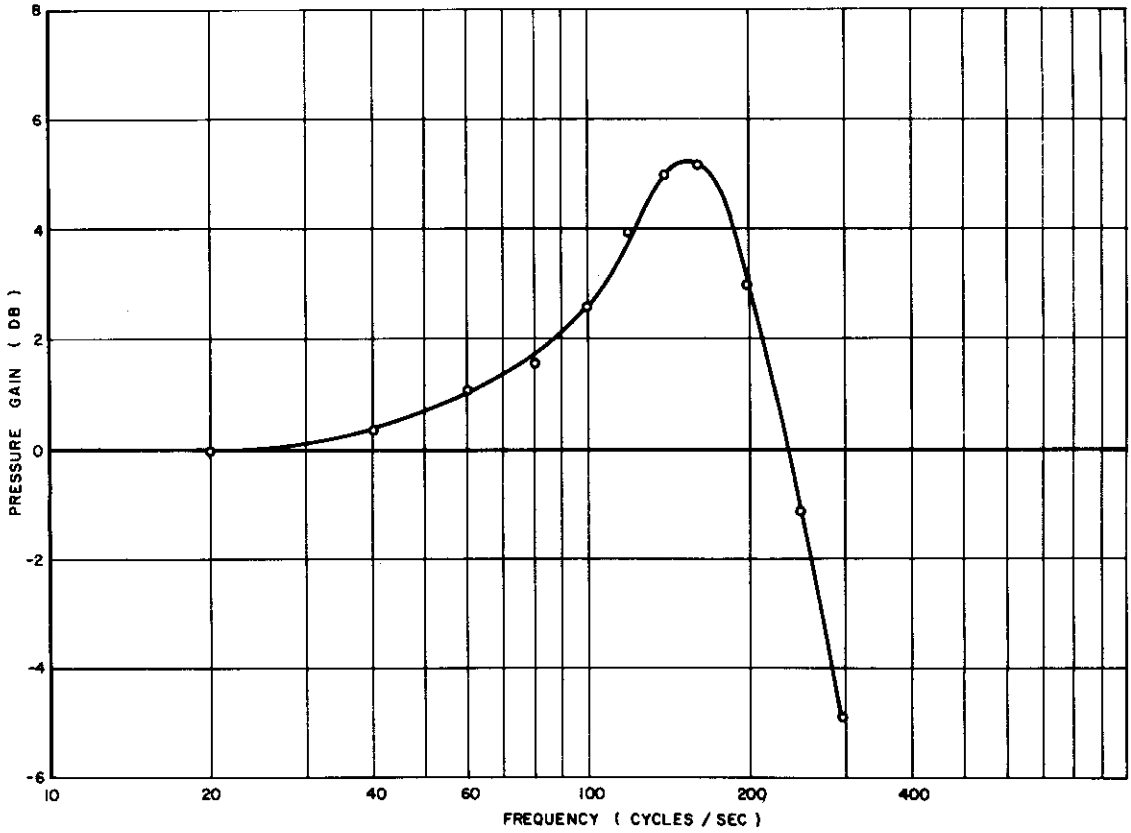

Figure 39. PC-2 Output Pressure vs. Frequency with Blocked Load

valve under such conditions. Analytically, a transfer function relating output pressure to differential current may be developed from the basic equations presented previously in this report. Blocking the load ports is analogous to an immovable load of infinite mass, so allowing M_L to go to infinity in the derived transfer function results in an expression which describes the test situation. The transfer function thus obtained is,

$$\frac{\Delta P}{\Theta_i} = \frac{\frac{K_1 C_1 A}{K_3 T_1}}{S^2 + \left[\frac{C_2}{K_3} + \frac{1}{T_1} + \frac{C_1}{K_3} \cdot \frac{T_2}{T_1}\right] S + \left[\frac{C_1 + C_2}{K_3 T_1}\right]} \qquad (38)$$

The characteristic equation of this function represents a second order system whose resonant frequency and damping are both determined by the volume of oil under compression and system leakage.

b. Closed Loop

Experimental comparison of the flow and pressure control valves in closed loop operation was accomplished by frequency response runs using loads similar to those studied by the root locus techniques described previously in this report. Results of these tests are shown in the form of Bode plots on Figures 40, 41, and 42.

Figure 40 shows the relatively low-frequency resonance

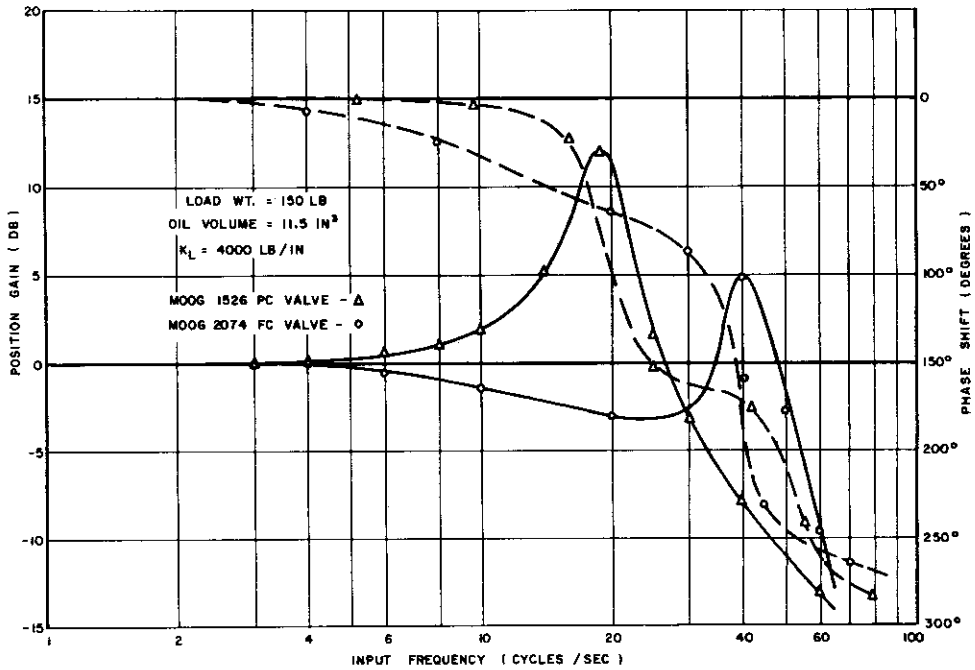

Figure 40. Hydraulic Position Servo Frequency Response

which exists in an uncompensated position servo system using a pressure control valve. Use of a flow control valve in the same system results in a resonance at higher frequency, although the reduction in gain produced by the two first order lags tends to mask the effect of this resonance.

Figure 41 demonstrates the somewhat greater bandwidth

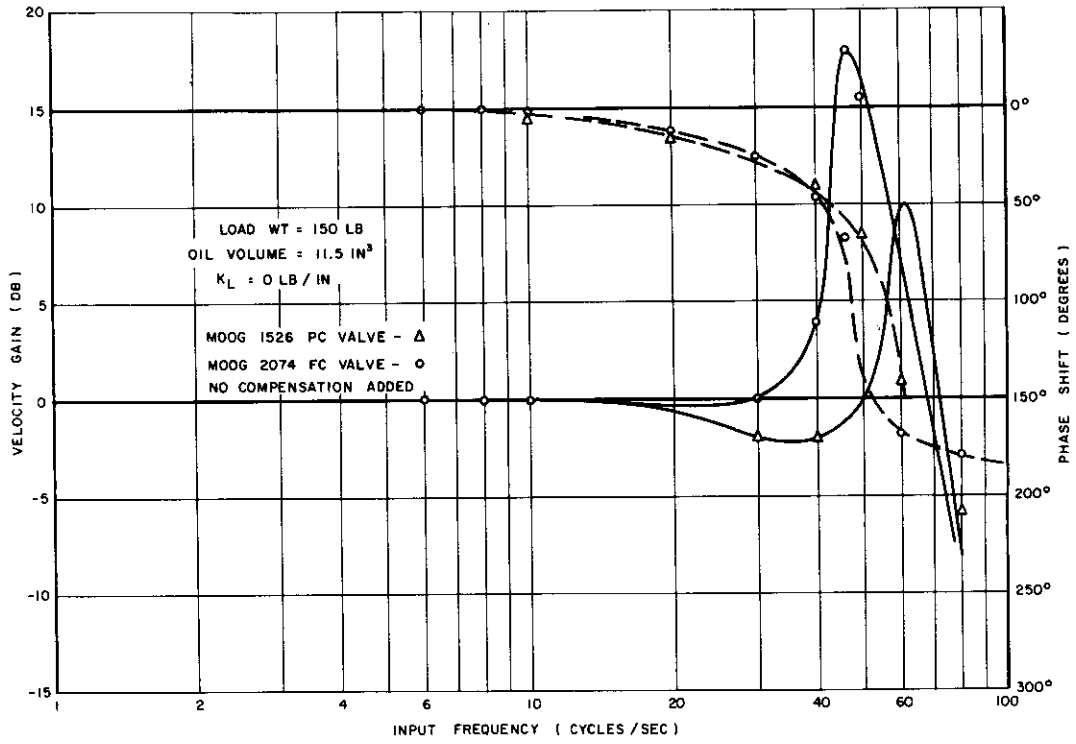

Figure 41. Hydraulic Velocity Servo Frequency Response

which can be expected from a velocity servo using a pressure control valve than can be obtained with the same system using a flow control valve. As noted previously, the pressure control valve system performance can be expected to be sensitive to outside disturbances on the load. Because of the linear (as opposed to rotary) nature of the test equipment, the experimental application of such disturbances could, however, not be mechanized in the velocity system tested.

The effect of adding velocity or proportional plus derivative feedback to a position servo is shown in Figure 42.

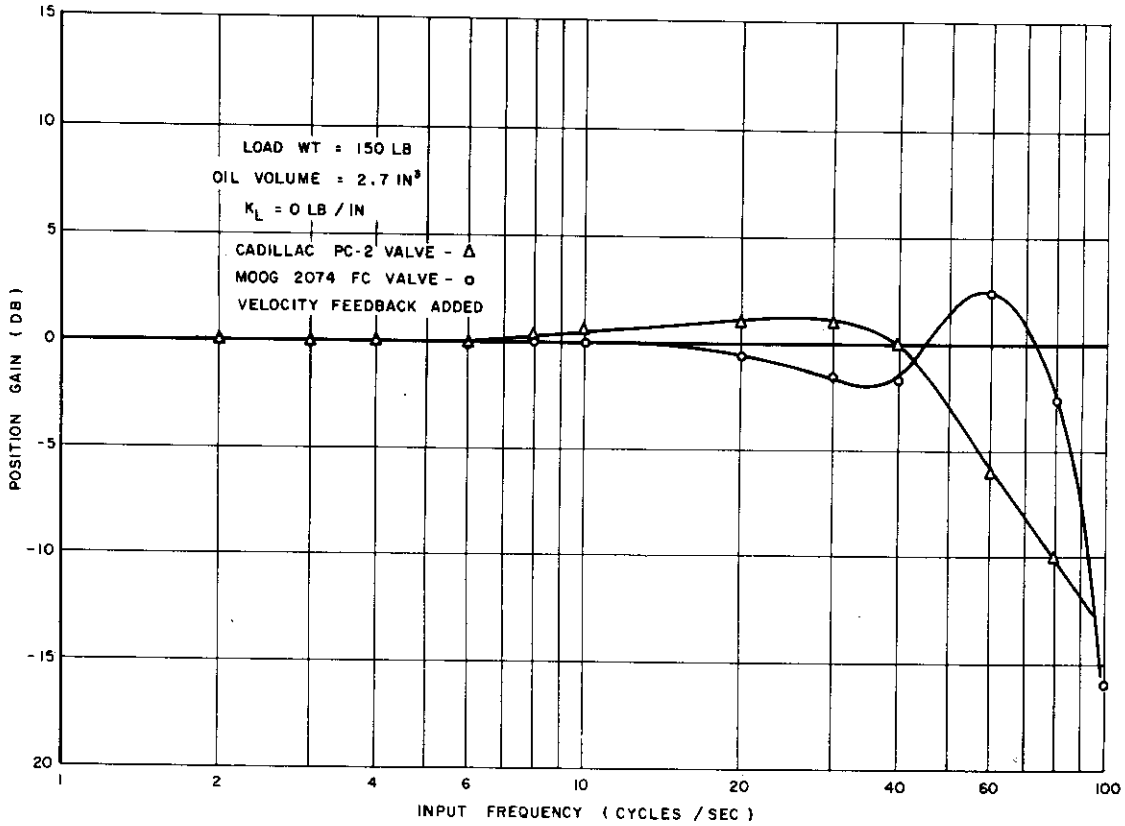

Figure 42. Velocity Compensated Hydraulic Position Servo Frequency Response

The presence of an effective single time constant producing a lag at approximately 50 cps is evident from the pressure control valve system frequency response. In accordance with the root locus diagram this system should have a resonance near 100 cps. Although such is not in evidence, it is apparently somewhat above the range of frequencies covered in the test. Resonance in the flow control valve system occurred at a lower frequency and essentially served to increase system bandwidth to a value slightly greater than that achieved by the pressure control system.

E. Conclusions

Presence of a large time constant in a pressure control valve system open loop response, in addition to the load dynamics, greatly deteriorates its performance with respect to a similar system using an ideal valve. Performance of the system is also adversely affected by the nonideal

pressure-flow characteristics similar to those of the two valves tested. As was discussed previously, an ideal pressure control system has definite frequency response and minimized error coefficient advantages when compared to a flow control system for position control. Any changes which could be made in the present valves to more nearly approach the ideal valve should be beneficial.

Forces acting on the pressure control valve spool are first-stage pressure, feedback pressure, and flow forces. If the flow forces could be reduced to zero or a negligible value, output pressure would be essentially independent of flow and ideal static pressure-flow characteristics should result.

In addition to the improvement in static characteristics, reduction of flow forces should also improve the valve's dynamic response. Examination of the controlling equations shows that a reduction in flow force spring constant, K_s, should decrease the value of the $\Delta P_2/\Delta I$ time constant, T_2, and increase the value of the $Q_L/\Delta I$ time constant, T_1. The over-all effect of these two changes, in conjunction with the increase in C_1, is to reduce the higher order coefficients of the resulting system characteristic equation. In the limit, the desired second order equation of a system using an ideal pressure control valve should result.

In light of the above, it appears desirable to attempt construction of a pressure control valve with minimized flow forces. Lee and Blackburn[2] have developed a means of doing this by appropriate shaping of the chambers formed between the spool and sleeve. Sinclair and Trumbull[3] point out that although practically all flow forces are eliminated by the shaping discussed in Reference 2, it would be expensive to manufacture. A slightly less effective but considerably less expensive means of spool shape manufacture is suggested. R. N. Clark[1] in another paper points out that Sinclair and Trumbull's scheme is only effective at high flow rates and has developed an alternate means of flow force reduction using radial holes as ports in the valve sleeve. It is believed that a similar approach could be applied to a pressure control valve and mechanization of same should result in a valve with greatly improved performance.

With the valves presently available, there appears to be no load configuration where use of a pressure control valve would result in a clearly superior performance. Conversely, use of a flow control valve does exhibit better dynamic response and less susceptibility to stiction in a noncompensated position servo. Use of velocity compensation with a pressure control valve with some loads can result in a position servo system having somewhat higher frequency response and appreciably greater

loop gain than for a similar system using a flow control valve. The advantages may be somewhat offset, however, by the adverse effects of stiction with pressure control.

Use of a pressure control valve in a velocity servo system results in a bandwidth equal to or slightly greater than can be obtained with flow control within the range of loads studied. Although the system gain tends to drop off at a relatively low frequency due to the valve's large time constant, the effect of load resonance extends system bandwidth to equal or exceed that obtainable from a flow control velocity system.

If reduction of flow forces in a pressure control valve results in the predicated characteristics, a valve of this type should see wide usage. At present, however, advantages of pressure control over flow control are marginal at best.

LIST OF SYMBOLS (CHAPTER III)

Symbol	Dimensions	Description
A_f	in^2	Spool pressure feedback area (Moog)
A_L	in^2	Load actuator area
A_s	in^2	Spool area open to first-stage pressure
B_L	lb-sec/in	Load viscous friction
B_v	$lb\text{-}sec/in^3$	Valve leakage coefficient (Cadillac)
C_1	$in^5/lb\text{-}sec$	Slope of valve pressure-flow curves
C_2	$in^5/lb\text{-}sec$	Load leakage coefficient
C_3	$in^5/lb\text{-}sec$	Slope of first-stage pressure-flow curves
C_4	$in^5/lb\text{-}sec$	Slope of spool orifice pressure-flow curve
ΔI	ma	Valve input current
K_1	$in^3/ma\text{-}sec$	First-stage flow gain
K_2	-	Ratio of feedback to output pressure
K_3	in^5/lb	Oil compressibility coefficient
K_4	in^2/sec	Spool flow gain
K_f	$in^3/ma\text{-}sec$	Flow gain of over-all valve
K_L	lb/in	Load spring constant
K_p	$lb/ma\text{-}in^2$	Pressure gain of over-all valve
K_s	lb/in	Flow force spring constant
M_L	$lb\text{-}sec^2/in$	Load mass
ΔP_1	lb/in^2	First-stage differential pressure

LIST OF SYMBOLS (cont'd)

Symbol	Dimensions	Description
ΔP_L	lb/in^2	Load differential pressure
Q_1	in^3/sec	First-stage flow
Q_L	in^3/sec	Flow out of valve to the load
S	1/sec	La Place Transform variable
T_1	sec	ΔQ / ΔI time constant
T_2	sec	ΔP / ΔI time constant
θ_o	in.	Load position
θ_s	in.	Spool position
ω_c	rad/sec	Break frequency of open loop first order time constant
ω_n	rad/sec	Undamped natural frequency of open loop system
ζ		Damping ratio of open loop resonance

CHAPTER IV

REQUIREMENTS AND DESIGN OF A HIGH-TEMPERATURE HYDRAULIC TEST FACILITY

A. Introduction

One of the most difficult problems confronting the designers of the next group of high-speed missiles and aircraft is that of coping with the extremely high-temperature environments on the external surfaces of the vehicles when flying at high speed. The source of this problem is absolute stagnation air temperature which is approximately linearly related to the vehicle Mach number.

The actual temperature of the vehicle surface is a function of the stagnation temperature, the heat transfer coefficient of the air film adjacent to the vehicle surface, and the emissivity of surface material. At low altitudes, where the air is dense, the heat transfer rate is quite high, and the surface temperatures are the closest to the stagnation temperatures. At high altitudes, the heat transfer coefficients are much lower so that the actual surface temperatures may range from, say one-third stagnation temperature (^{o}F) at 100,000 feet altitude to less than one-tenth stagnation temperature at 200,000 feet. In any case, it is not difficult to conceive of systems which will operate at surface temperature of 1000^{o}F or greater. For instance, an aircraft flying at Mach 3 at sea level and up to Mach 5 at 100,000 feet will be operating near the 1000^{o}F surface temperature range.

The ambient temperatures inside the vehicle will vary from one design to another and are dependent on such factors as duration of flight, amount and type of thermal insulation, the amount of refrigeration, if used, and whether the vehicle is manned. Generally speaking, it can be concluded that the refrigeration equipment should not be used in missiles unless absolutely necessary. It should be maintained at a minimum in manned aircraft to save space and weight. Thus, for example, in a hypersonic manned aircraft, while refrigeration may be required to protect the human occupant, the remaining equipment should be able to operate directly in the high-temperature environment, if possible.

Thus, there is a great need for equipment that can operate in high-temperature environments, and considerable development work is presently being directed in that direction, particularly with regard to hydraulic equipment with which this study is concerned. There are, for instance, servo

valves, actuators, and pumps currently commercially available capable of operation at temperatures up to 400°F. However, very little equipment exists for temperatures above this range.

Along with the need for high-temperature hydraulic components emerges the need for high-temperature testing facilities for developing and determining the capability of these components. Because of the wide ranges in temperatures, flows and simulated altitudes required of these facilities, they become quite expensive to build and maintain.

It is the purpose of this phase of the study to formulate the design of a high-temperature facility which could be utilized for the testing of hydraulic servo control valves and other hydraulic elements at fluid temperatures up to 750°F in combination with ambient temperatures up to 1200°F and at simulated altitudes up to 120,000 feet. The following sections briefly discuss the current and future high-temperature requirements of military airborne hydraulic systems, describe some high-temperature facilities presently available, set forth the over-all requirements of a practical high-temperature testing facility and describe in considerable detail the design of such a facility.

B. Temperature Requirements of Current and Projected Aircraft

A number of service vehicles currently under development have operational surface temperature environments exceeding 1000°F. However, in nearly all cases, the time duration of these high temperatures is so short that internal ambient temperatures within the vehicle do not approach critical values. Examples of these vehicles are the ballistic missiles and satellite launchers. However, in the case of ballistic missiles, extremely high surface temperatures are encountered during the terminal phase of flight, where presently no control is provided. The development of control systems capable of operating under these extremes in temperature would solve one of the problems of terminal guidance.

Other vehicles which will operate under the influence of high stagnation temperatures are the research vehicles such as X-15. Vehicles such as the North American Weapons System 110 and Convair B-58 will probably have maximum surface temperatures between 500°F and 800°F.

To our knowledge, no service vehicle is presently under design or development which will require operation under oil temperatures appreciably greater than 400°F. However, several present hydraulic systems require operation under oil temperatures up to 400°F.

As mentioned earlier, equipment is currently available that is capable of operating under these temperatures. Servo valves can be purchased from both Cadillac Gage and Moog Valve Company for operation in the 400°F oil environment. Actuators can be obtained from the Allison Division of General Motors and North American for these oil temperatures and considerably higher ambient temperatures. Pumps are available from Vickers and New York Air Brake which will operate at 400°F.

A great deal of effort is now being concentrated on components which will operate at temperatures above this range.

C. High-Temperature Facilities Presently in Use or Under Construction

A number of valve manufactures have constructed high-temperature testing facilities during the last two years. Among these are Moog Valve Company, Cadillac Gage, at both their Detroit and Costa Mesa Divisions, Hydraulic Research, Inc., Bendix Pacific Division, Minneapolis Honeywell, and Vickers, Inc. In all of these facilities, the oil from the test stand is cooled before it enters the pump and then reheated after it leaves the pump.

The Cadillac Gage facility at Detroit is quite small and capable of operating with oil temperatures up to 400°F. Calrod units are used as heaters. The Cadillac Gage Costa Mesa Division has about the same temperature capability at low flows. The oil is heated by passing a high current, provided by a three phase electrical power source through the tubing conducting the oil to the equipment being tested. Hydraulic Research has built a high-temperature facility capable of producing oil temperatures of 700°F and ambient temperatures of 1000°F with an oil flow of 10 gpm. The oil is heated by Calrod units and cooled by air. Ambient temperatures are maintained by electrical resistance heaters.

Bendix Pacific Division has recently completed a high-temperature facility capable of providing oil temperatures of 800°F and ambient temperatures of 1200°F. Calrod units are used for heating the oil while electric resistance heaters are used to maintain the ambient temperature. A water tower is used for cooling. The maximum flow capacity of the installation is 24 gpm and the maximum pressure capability is 5000 psi.

The Vickers test facility was designed primarily for their high-temperature pump development and they have several units capable of providing oil temperatures as high as 600°F.

Minneapolis Honeywell has a facility capable of operating at oil temperatures up to 400°F. The oil is heated electrically. A conventional

piston pump is operated at 300°F by using special high-temperature seals.

A number of missile and aircraft manufacturers also have installed high-temperature testing facilities, generally more elaborate than those described above. Such facilities are available at North American, Convair, San Diego Division, Republic Aircraft Corp., General Electric, MacDonnell Aircraft, and Bendix Missile Division. North American was the only one of these visited.

North American has an elaborate high-temperature test facility consisting of at least four ovens or testing enclosures capable of testing hydraulic equipment at oil temperatures of 600°F and ambient temperatures of 1150°F under sea level conditions. In addition, they have an oven that will provide the above temperatures at a simulated altitude of 100,000 feet. The latter employs a radiant heat source, consisting of electrical resistance heaters, which is absorbed and reemitted by a thin plate partition separating the heat source and the equipment under test.

The test area and ovens are housed in a remodeled concrete bomb shelter. Remote controls are employed for controlling the hydraulic equipment and a system of motorized mirrors and a closed circuit TV system are used for visual observation. Oxygen analyzers and CO_2 fire protection equipment are also provided.

D. Requirements of the High-Temperature Facility

As a result of the data gleaned during the survey phase and the previous discussions, it is concluded that the high-temperature facility should have the following characteristics.

Supply pressure	1000 to 5000 psi
Maximum flow capacity	40 gpm
Maximum oil temperature	750°F
Maximum ambient temperature	1200°F
Maximum simulated altitude	120,000 feet
Maximum temperature response from any equilibrium temperature	6° / sec

Range of temperature response gradient +155 °F

Automatic Temperature and Pressure Control

For reasons of economy, the flow capacity of 40 gpm is best met by using two separate 20 gpm units, as the capability of any one system under test will rarely exceed 20 gpm. Provision should be included, however, for paralleling the two units if more than 20 gpm is required for a single system. The following design considers only a 20 gpm capability.

E. Design of the High-Temperature Hydraulic Test Facility

1. General

As stated previously, the objectives of this design are to supply oil at pressures up to 5000 psi, at temperatures up to 750°F, and at flow rates up to 20 gpm to the test stand. Since the oil cannot be pumped at high temperatures, these requirements make it necessary to heat the oil after it is brought up to pressure and then to cool the drain oil before it is returned to the sump. The basic flow diagram for the system appears in Figure 43.

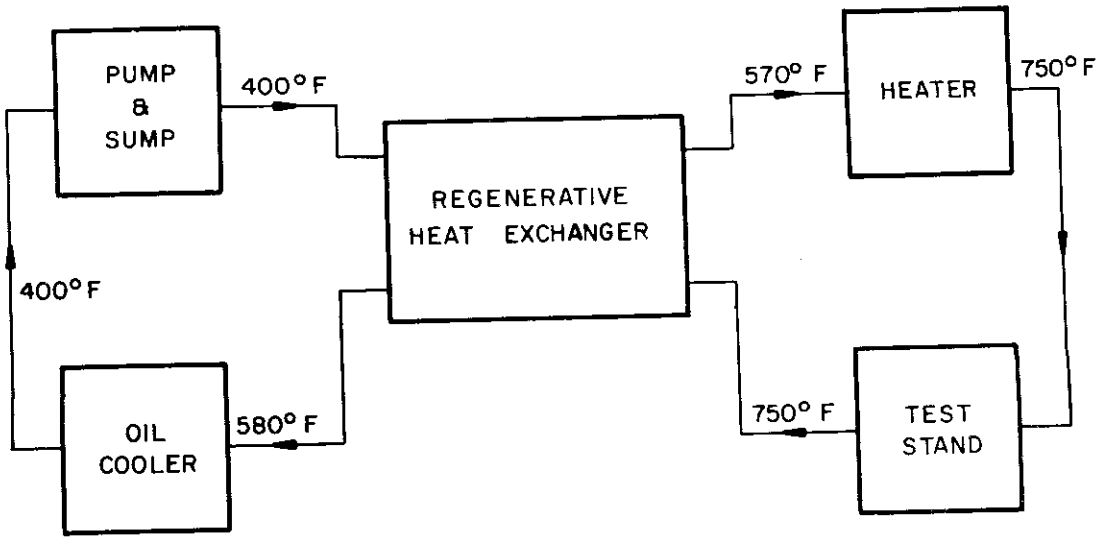

NOTE: THE TEMPERATURES SHOWN ARE THOSE THAT WILL APPEAR AFTER EQUILIBRIUM HAS BEEN REACHED WHEN OPERATING AT MAXIMUM OUTPUT TEMPERATURE.

Figure 43. Basic Block Diagram of High-Temperature Test System

a. Pump Selection

One of the first problems in the design involved the choice of a suitable hydraulic pump. For the economy of heating and cooling equipment, it is desirable to pump at as high a temperature as possible. An investigation of the field revealed that most hydraulic pumps are not recommended for operation above 200°F and, in fact, are not recommended at all for use with most of the high-temperature hydraulic fluids. This situation is due primarily to the poor lubricity of high-temperature fluids and to the decrease in lubricity with increasing temperature exhibited by all fluids. Thus, the solution to the high-temperature pumping problem depends on a pump design that does not rely on the pumped fluid for its lubrication. Such a pump must have its own lubrication system and exclude the pumped fluid from contact with any moving parts except the pumping plungers.

One group of pumps that meets these specifications is made by Kobe Inc. Their three cylinder, 1-1/8 inch bore, 4 inch stroke, and 400 rpm pump driven by a 60 hp motor, fulfills the pressure and flow requirements and has been operated in other installations at temperatures up to 600°F. This pump is of the fixed displacement type and hence an adjustable relief valve must be used for pressure control. Its plungers and liners are replaceable as assemblies and hence not only is replacement easily accomplished, but, also, it is possible to change the pump displacement by selecting different bore sizes. The only disadvantage of this pump is that its low angular speed and small number of pistons result in a lower than normal pump ripple frequency and higher than average ripple amplitude. This, however, is not too serious a problem in this design for, as will be seen latter, the large length of pipe between the pump outlet and the test stand, required for heat transfer purposes, serves as an excellent ripple filter. Hence, it is anticipated that little if any pressure pulsation will be present at the test stand.

Thus with a suitable pump selected, the system design pumping temperature was set at 400°F. While this is an admittedly conservative temperature for the pump in question, its choice was based on the fact that future needs for a higher test stand temperature could then be met by simply raising the pumping temperature. Also, it is to be noted that 400°F is

considerably above the maximum temperature limits of most hydraulic pumps.

b. Fluid Considerations

In order for the heat exchangers to be designed, it was necessary to know the physical properties of the fluid to be used. Hence, an investigation of the high-temperature hydraulic fluid field was made and a chart was prepared comparing the properties of interest of several of the most promising fluids (see Table 5). It is to be noted that in numerous instances extrapolation of the available data was necessary to finish this chart. The results show that while 750°F, the maximum proposed operating temperature, is somewhat above the maximum temperature for stable operation of any of the fluids, the silicones come closest to meeting this requirement. One such fluid is GE No. 81717 which ranks near the top in high-temperature stability and viscosity and, in addition, has fair lubricity. The physical properties of this fluid, as depicted graphically in Figure 44, were used in the heat transfer calculations.

c. Heating and Cooling System

Because of the cost of these special high-temperature fluids, (the GE silicones are priced at $40 to $50 per gallon), it was decided to keep the volume of the system to a minimum. In order to do this, the requirements on allowable pressure drop in the heat exchangers had to be raised. It was decided that a total piping pressure drop of 500 psi could be tolerated for the system. This loss will be compensated for by increasing the pump pressure 500 psi to 5500 psi and hence the design test stand pressure will not be affected.

(1) Regenerative Heat Exchanger

Thus, with these factors in mind, the design of the heat exchangers was started. The heart of the heating system is the regenerative heat exchanger. This device cools the drain oil and uses this heat to warm the oil as it leaves the hydraulic pump, thereby effecting a considerable saving in heater power. Basically, the unit consists of a shell and tube counterflow exchanger with high-pressure supply oil flowing through the tube and the low-pressure

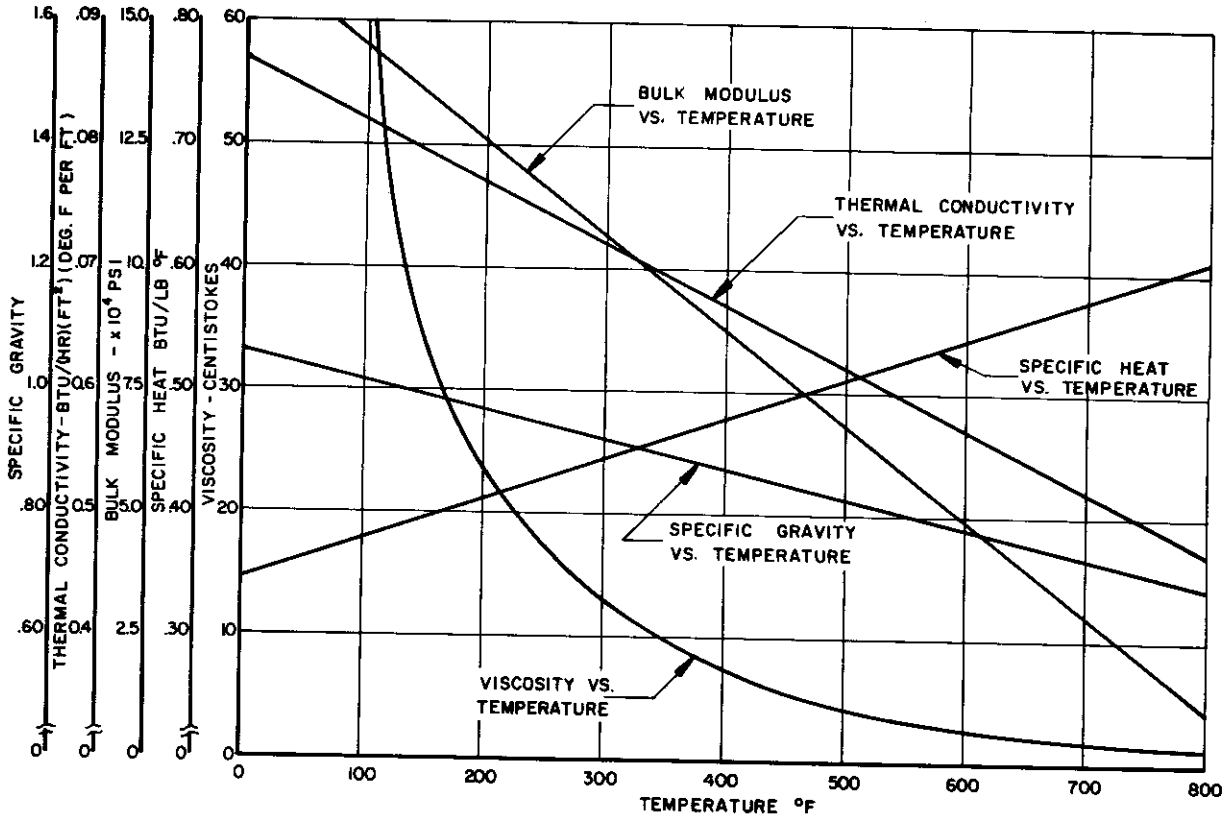

Figure 44. Physical Properties of GE Fluid 81717

drain oil flowing through the shell. Its expected performance specifications were that it heat the supply oil from 400°F to 600°F and that it cool the drain oil from 750°F to 550°F. Thus, the mean temperature gradient for heat transfer was 150°F. The design was based on standard heat exchanger sections and because of its relatively low volume, the 2 inch Brown Fintube section was used as a starting point. A cross-sectional view of this device is shown in Figure 68 in Appendix VI.

For the design calculations, the maximum system flow rate was employed. Since this is the condition requiring the maximum heat transfer, the resulting design will then be adequate for all possible flow rates. The first step was to determine the heat transfer coefficient for the flow inside the exchanger pipe. Calculations of the Reynolds and Prandtl numbers for this flow indicated the

proper formula to use for finding this coefficient (see Appendix VI). Application of this formula yielded a coefficient of 340 Btu/hr, ft^2, ^oF for the inner surface of the pipe. In order to calculate the heat transfer coefficient for the flow on the outer surface of this pipe, a formula for turbulent flow in concentric annuli was first applied. The result thus obtained was then multiplied by a fin effectiveness correction obtained from Brown Fintube data. The result was a coefficient of 265 Btu/hr, ft^2, ^oF.

By the use of these heat transfer coefficients, the required length of exchanger section was estimated to be 160 feet. Thus, the unit could be made up of four standard 40 feet Brown Fintube sections in series. Each of these units is approximately 22 feet long and they will be placed side by side in this installation. The resultant device has a total volume, including a 10 percent over-allowance for end connections, of 23.7 gallons. Its calculated performance is a 170^oF rise in the temperature of the 400^oF high-pressure supply oil and a 170^oF drop in the temperature of the 750^oF drain oil. It is to be noted that the specific heat of the oil increases with temperature. Thus, even though equal temperature changes are given for the heating and cooling operations, these figures allow for considerable heat loss to the surroundings. The tube side pressure drop of this unit was calculated to be 130 psi and the shell side drop was estimated to be 30 psi.

(2) Heater

From this regenerative heat exchanger, the supply oil is fed to a heater where it undergoes a rise in temperature of up to 180^oF, raising its temperature to a maximum of 750^oF. The power required to provide this temperature change at the maximum system flow rate is 208 Btu/sec, the heat equivalent of 220 kw. In order to provide the system with greater transient response, it was decided to use a heater of 250 kw capacity. With this input power the heater will be capable of a temperature rise of 205^oF. In addition, the transient temperature response of the system after reaching equilibrium at any operating point will be approximately $\pm 7^oF$ per second.

This heating will be accomplished by passing the oil through a length of stainless steel tubing to which electrical power is directly applied. In this manner, the heat is developed right in the tubing and hence not only are the heat transfer problems associated with a separate heat source eliminated, but, also, a system with greater transient response is the result. The use of stainless steel tubing of 7/8 O.D. with a 0.120 inch wall was found to be consistent with the strength and allowable pressure drop requirements of this system. Calculations based on the dimensions of this tubing and the maximum system flow rate produced a tube to oil heat transfer coefficient of 444 Btu/hr, ft^2, ^oF. By the use of this coefficient and the maximum required heat transfer rate, together with a maximum tube to oil temperature gradient of 40^oF, the required length of tubing was found to be approximately 300 feet. Thus, the volume and pressure drop for the unit were determined as 4.95 gallons and 240 psi, respectively.

Physically, the unit consists of 45, 2 foot diameter coils of tubing spaced on 1-1/2 inch centers, thus forming a cylindrically shaped object approximately 2 feet in diameter and 5 feet long. It will be made up of standard 22 foot lengths of tubing connected end to end. In addition to the mechanical connectors, copper bonding straps will be provided at each joint to eliminate the possibility of high electrical resistance at these points. Electrically, the unit will be connected in delta with two phases connected, respectively, at the 100 foot and 200 foot points, and the third phase connected to the input and output which is then established at ground potential. This three-phase delta connection is desirable not only because it allows the input and output to be at ground potential but, also, because of the inherent advantages in the use of a balanced three-phase load when high power levels are involved.

(3) Oil Cooler

The final heat exchanger in the system is the oil cooler. This device accepts drain oil from the regenerative heat exchanger at a maximum temperature of 580^oF and cools it to 400^oF, the oil pumping temperature. The design of this device was based on a shell and tube exchanger

configuration with oil flowing through the tube and cooling water flowing in the shell. Its cross-sectional dimensions are similar to those of the regenerative heat exchanger with the exception that a thinner tube wall was possible because of the lower fluid pressures involved. The heat transfer calculations revealed that 80 feet of exchanger section would be adequate for this unit and that a maximum cooling water flow rate of 10 gpm would be required. Such a unit could be made up of two 40 foot Brown Fintube exchangers in series. Its oil volume is approximately 2 gallons and its full flow oil pressure drop is roughly 29 psi.

(4) Materials

It is to be noted that the material used in the design of all of the foregoing heat exchangers was stainless steel. This material was chosen principally for its chemical inertness. Plain carbon steel is adequate from a strength standpoint, and, in addition, it has advantages over stainless steel in regards to cost and heat transfer capabilities. However, in an installation of this kind, any corrosive action of the contained fluid would soon render the system inoperative. Therefore, because the hydraulic fluids exhibit some corrosive properties at high temperatures, it is believed that the additional cost of stainless steel is warranted.

d. Over-all System Considerations

The over-all system resulting from the above design has a conservatively rated maximum output of 20 gpm at 750°F. Its total oil volume would be approximately 33 gallons, and the total pressure drop when operating at full flow and at maximum temperature output would be roughly 430 psi. As the output temperature is lowered, the pressure drop increases due to the increase in viscosity of the oil. However, as the required output temperature is reduced, less heat transfer capacity is needed and, hence, parts of the system can be bypassed, thus reducing the pressure drop. For example, output temperatures up to 580°F are possible without the regenerative heat exchanger. With this unit bypassed, the resultant system has a total volume of roughly 10 gallons and a pressure drop of maximum output temperature of 300 psi. In this manner, the system pressure

drops can be held to reasonable values throughout the useful temperature range; in addition, it is to be noted that when the regenerative heat exchanger is not used the system oil volume is considerably reduced.

Future needs for higher output temperatures from this installation could be met by simply increasing the pumping temperature. As previously mentioned, the proposed pump has been run at temperatures up to 600°F. With such a pumping temperature, this system would be capable of output temperatures up to 900°F when and if hydraulic fluids able to operate in this range become available.

e. Facility Control Systems

The purpose of this section is to discuss the control system necessary to maintain the oil supplied to the test stand at the specified temperature and pressure. A flow diagram showing the control elements required to accomplish this appears in Figure 45. Basically, there are three separate

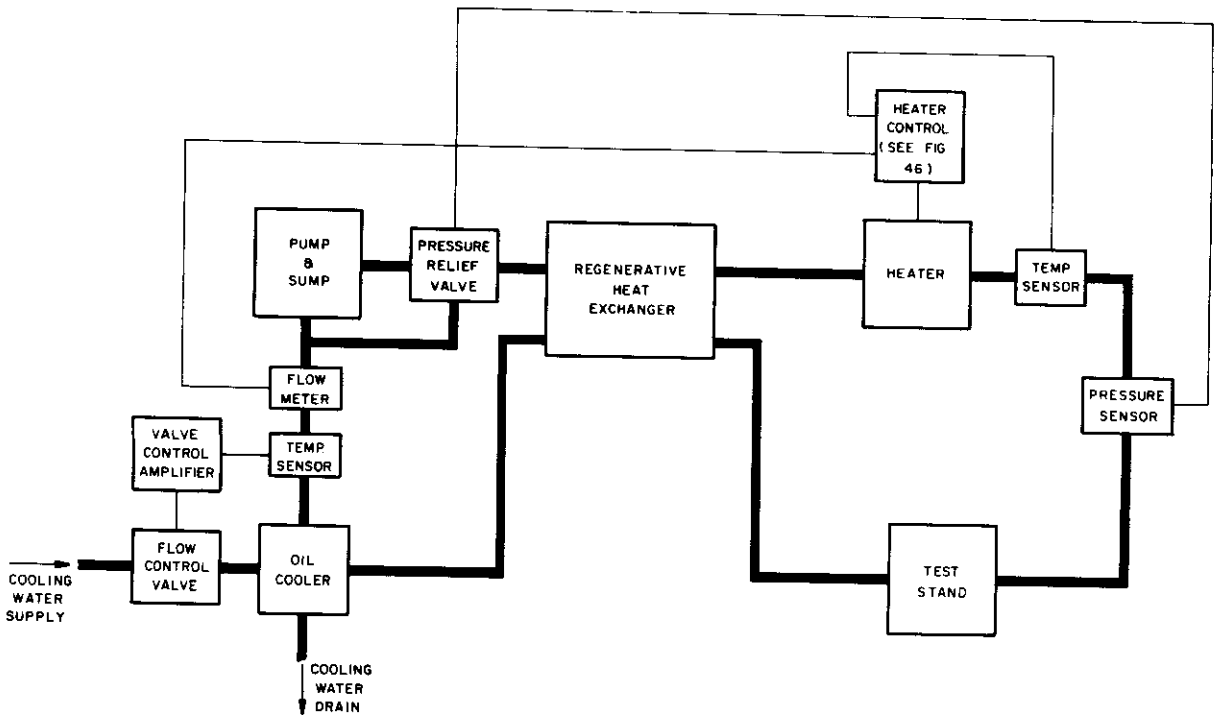

Figure 45. Block Diagram of High-Temperature Test System with Control Elements

control systems: one to control test stand pressure, one to control test stand temperature, and the third to control pump temperature.

(1) Pressure Control System

The pressure control system can take several possible forms. In the ideal configuration, the output of a pressure sensor located just before the test stand is used to control a servo-operated relief valve located at the pump output. Because the sensor is located at the test stand, this system is self-compensating for varying piping pressure drops as the flow rate changes. In addition, such a configuration is advantageous because the relief valve is located at a point of lowest oil temperature and, also, because only the oil fed to the test stand undergoes the heating cycle. A less complex pressure control system could consist simply of an adjustable relief valve located at the pump output. With such a system, the test stand pressure could vary as much as 400 psi due to variations in the piping pressure drop with flow rate. This problem could be solved by placing the relief valve just before the test stand. However, such a system would be uneconomical due to the fact that the entire pump output would always pass through the heating cycle. In addition, a relief valve capable of extreme high-temperature operation would then be required. Thus, it appears that the first system, even though it is the most complex, is the most desirable for this design.

Another aspect of pressure control involves the pump pulsations. As previously mentioned, the ripple frequency from the Kobe pump is approximately 20 cps and, in addition, because the pump is of three cylinder design, the pulsation amplitude is quite high. Thus, the need for some kind of pulsation damper is indicated. Fortunately, the large amount of pipe required for heat transfer in this design should serve as a very good damper. Calculations for the natural frequency of the oil between the pump and the test stand produced a fundamental value of approximately 3-1/4 cps. Since this is only about 1/6 the pump ripple frequency, the pump pulsations should be pretty well removed by the time the oil reaches the test stand. If, however, pulsation problems are encountered,

a piston type accumulator could be installed in the system to damp these pulsations.

(2) Temperature Control Systems

Basically, the oil temperature control system consists of a temperature sensor, located at the test stand, whose output is used to control the power flow to the oil heater previously described. However, in addition to controlling test stand oil temperature, this system must not allow the heater wall to oil temperature gradient to exceed $40^{\circ}F$. To do this, the output from a flow meter is fed to the oil heater controller. This signal limits the maximum power that can be applied to the oil heater, depending on the system flow rate and independently of the power called for by the temperature sensor. Thus, the heat input is never allowed to exceed the amount that will cause the allowable heater wall to oil temperature gradient to be reached. In addition, this flow rate information is useful to predict required changes in heater power. For example, if the system flow rate should suddenly increase, the temperature sensor would not indicate the need for any increase in heater power until a change in the output temperature occurred. However, the flow meter senses the required change immediately. Thus, by allowing flow rate information to govern the heater power during transient flow conditions, the output temperature variations can be reduced.

As a safety precaution, the control system should immediately shut off the heater power if the flow stops for any reason. This function can be provided by feeding some fraction of the flow rate voltage to a relay which drops out, shutting off the heater power whenever the flow drops below the normal minimum rate. In addition, as an added safety feature, an over-temperature switch will be provided on the heater. This device shuts off the power if the heater temperature ever rises above the prescribed maximum value.

A block diagram illustrating the mechanization of this heater control system appears in Figure 46. The recorder pictured in this diagram compares the temperature sensor signal to a set reference voltage and gives

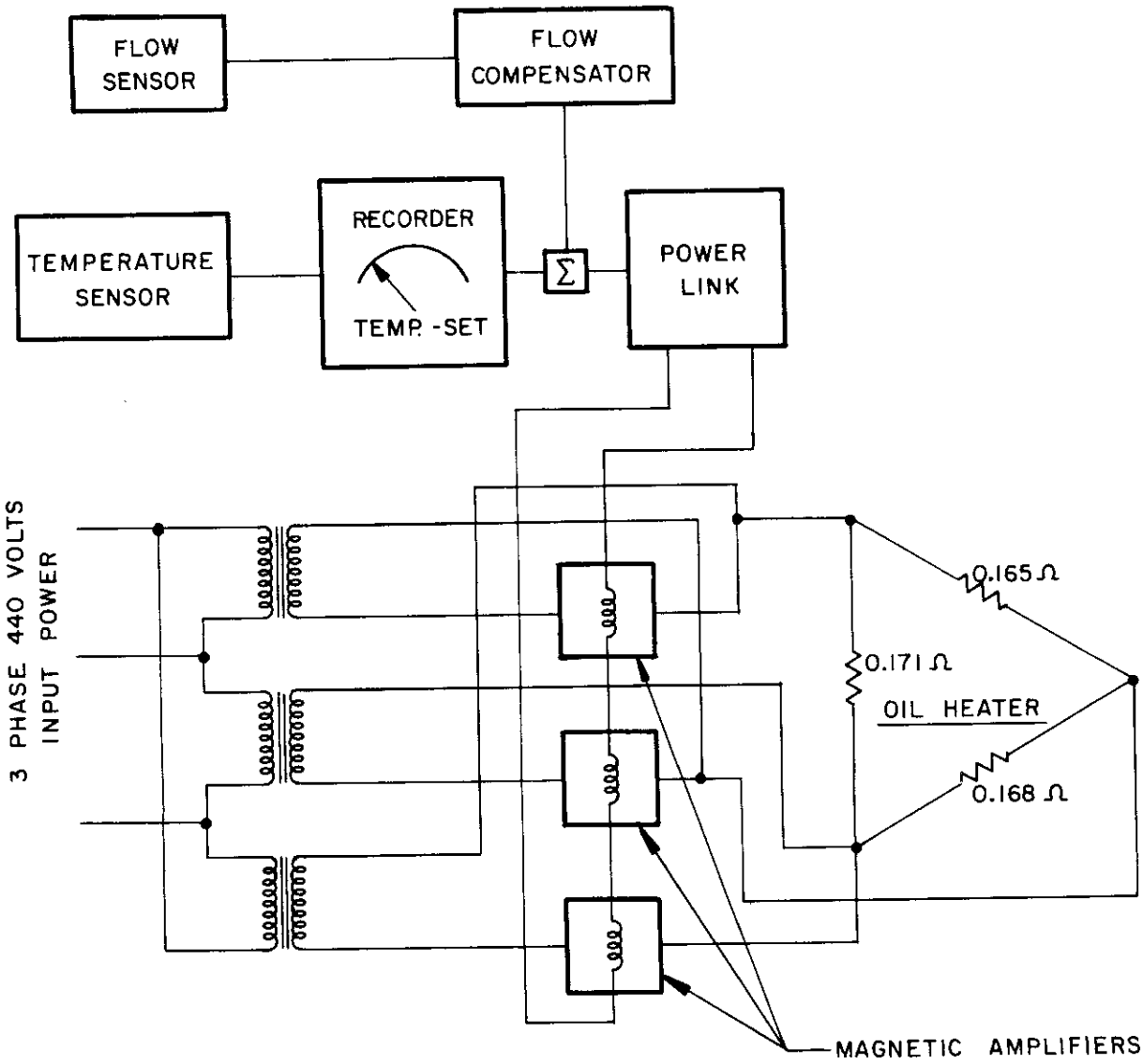

Figure 46. Block Diagram of Heater Control System

an output error signal proportional to the difference of these two voltages. This device also provides a graphical record of the variations of error signal with time. Since this error signal is proportional to the difference between the set temperature and the actual system output temperature, a record showing the accuracy of temperature control during the test period is thus provided.

The recorder output is modified by the flow rate information, as previously discussed, and then is fed to

the Power Link supplied by Vickers Electric Inc. This device amplifies this signal to provide control excitation to the magnetic amplifiers which, in turn, control the heater power flow. It is to be noted that an unbalanced load is shown in the diagram. This condition is due to the fact that a temperature gradient exists along the heater length and that the resistivity of the stainless steel tubing has a positive temperature coefficient. The illustrated case is for the system operating at maximum capacity and thus it represents a condition of maximum unbalance.

The purpose of the final control system in this design is to limit the sump oil temperature to approximately 400°F. Thus, until the drain oil temperature reaches 400°F, this control system is inoperative. The temperature control is accomplished by varying the flow of cooling water through the oil cooler according to the demands of a temperature sensor placed downstream of the cooler. No oil flow rate information was used in this design because high accuracy of temperature control is not necessary.

f. Test Stand

It is desired in the test stand to simulate the environmental conditions present in high-speed aircraft. These include temperatures up to 1200°F and pressures as low as those at 120,000 feet altitude. Thus, the test stand takes the form of several vacuum ovens in which the components under test are placed. The ambient temperature and pressure of each oven should be controlled independently. The required size of these ovens is dependent on the size of the components to be tested. However, their volumes should be kept to a minimum, not only for economy of evacuating equipment but, also, because the strength requirements of a vacuum chamber increase rapidly with the size of the unit. Basically, each oven will consist of a stainless steel inner chamber surrounded by electric heating elements and with an observation window and door on one side. The hydraulic lines are piped directly into these chambers which are located inside an insulated steel casing. Suitable ovens are manufactured by the K.H. Huppert Company of Chicago. The test stand control panel contains chamber temperature and pressure controls, together with gauges indicating these

quantities. In addition, recorders will be supplied to provide graphic records of chamber temperature and pressure during the testing period.

Due to the fact that temperatures above the autoignition point of the oil will often exist inside the test chamber, the danger of fire or explosion in case of an oil leak is quite high. This danger can be considerably reduced by charging the chamber with an inert gas at the start of the tests. While this is not so important if the test is to be run at or near the vacuum capacity of the unit, it is an absolute necessity if a high-temperature test is to be run near atmospheric pressure.

In addition, in order to minimize the effects of an explosion, the test chamber should contain a blowout plug which will open if the chamber pressure ever exceeds 10 psig. Thus, the effects of an explosion can be vented outside the building and mechanical damage to the test stand and surrounding objects is avoided. The operation of this blowout plug should also simultaneously trigger a carbon dioxide fire extinguishing system, inside the test chamber, and turn off all system power.

g. Over-all System Layout

In designing a hydraulic test facility, one of the prime considerations is for the safety of the testing personnel. This is especially true in a high-temperature facility where the temperature of the oil adds to the danger in the event of a leak in the system. The danger can be considerably reduced by having the pump and heat transfer equipment separated from the test area so that a minimum of piping is exposed to the test personnel. This arrangement also is advantageous in that it makes it possible to isolate much of the heat and pump noise from the test area. A system layout based on the above principles is illustrated in Figure 47. In this layout, three separate rooms are employed: one for the heat transfer equipment, one for the pump and heater magnetic amplifiers, and the third for the test stand. By providing a separate room for the pump and electrical equipment, the necessity of controlling the ambient temperature in the heat transfer room was avoided. It is to be noted that although this layout only shows one pump, room is provided for a dual installation of pumps and heat transfer equipment in case a 40 gpm capacity system is desired.

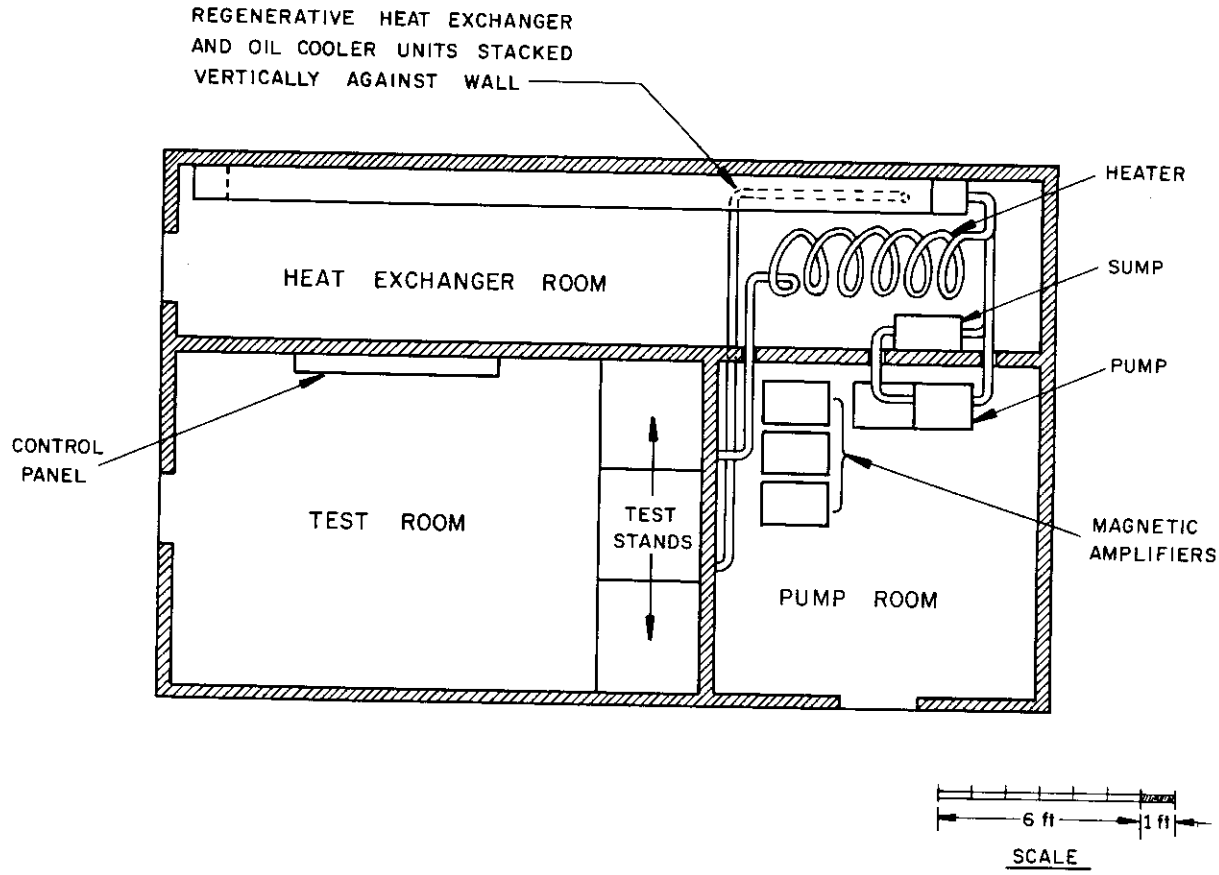

Figure 47. Suggested Floor Plan of High-Temperature Test Facility

Several safety devices should be provided to control the operation of the system. One of these is a leak detector which takes the form of a sump level indicator that shuts off all the system power if the sump level falls more than a prescribed amount. This device consists of a float controlled direction sensing switch. The latter is necessary because during normal system operation the sump level will rise due to the expansion of the oil with temperature. On the other hand, leakage would result in a liquid level falloff. Thus, it is desirable that the switch shut off the system if the level begins to fall from any starting point.

In addition, all the rooms should be provided with some method of fire protection. The danger is the greatest in the heat transfer room, and, hence, it is suggested that this room be equipped with an automatically triggered extinguishing system.

TABLE 5

PROPERTIES OF HIGH-TEMPERATURE HYDRAULIC FLUIDS*

	OS - 45	Oronite 8200	Oronite 8515	GE 81717	GE 81644
Density - lb/ft^3	55.9 At Room Temp.	43	43	53.5	53.5
Thermal Conductivity - Btu/hr ft°F K_b		0.0245	0.0389	0.0595	
Specific Heat - Btu/lb°F C_p	0.8	0.87	0.83	0.56	0.56
Viscosity - $\frac{lb}{hr\ ft}$ μ	0.975	2.08	1.96	4.99	5.6
Spontaneous Ignition Temperature °F	700	760	760	900	900
Bulk Modulus (Evaluated at 5000 psi) psi	253,000 At Room Temp.	56,000	56,000	100,000	100,000
Thermal Stability	Stable up to 400°F	Stable up to 400°F	Stable up to 400°F	Stable up to 600°F	Stable up to 600°F

*All Properties evaluated at 650°F except where otherwise noted.

APPENDIX I

DETERMINATION OF TORQUE MOTOR PARAMETERS

A. Preliminary Considerations

Torque motor parameters will be derived for the Moog Type 9126 valve. An identical procedure was used for the Type 942. In both cases, it was assumed that the torque motor operated without saturation.

Some of the torque motor parameters were determined from magnetic circuit geometry (Figure 48) and the plot of spool differential pressure

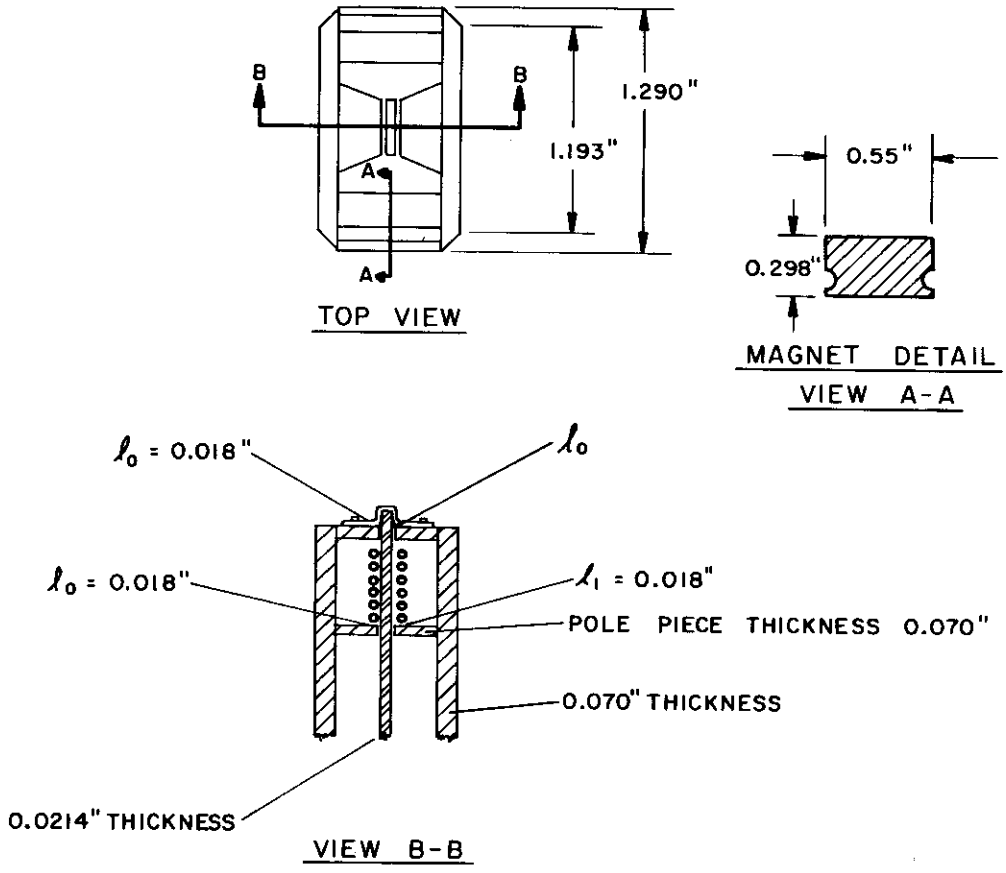

Figure 48. Magnetic Circuit Geometry Moog 9126

(blocked load) vs. flapper displacement ratio (Figure 49). It had been determined experimentally that with rated current of 8 ma applied to the valve, $\Delta P = 350$ psi; from Figure 49, $x/h = 0.46$.

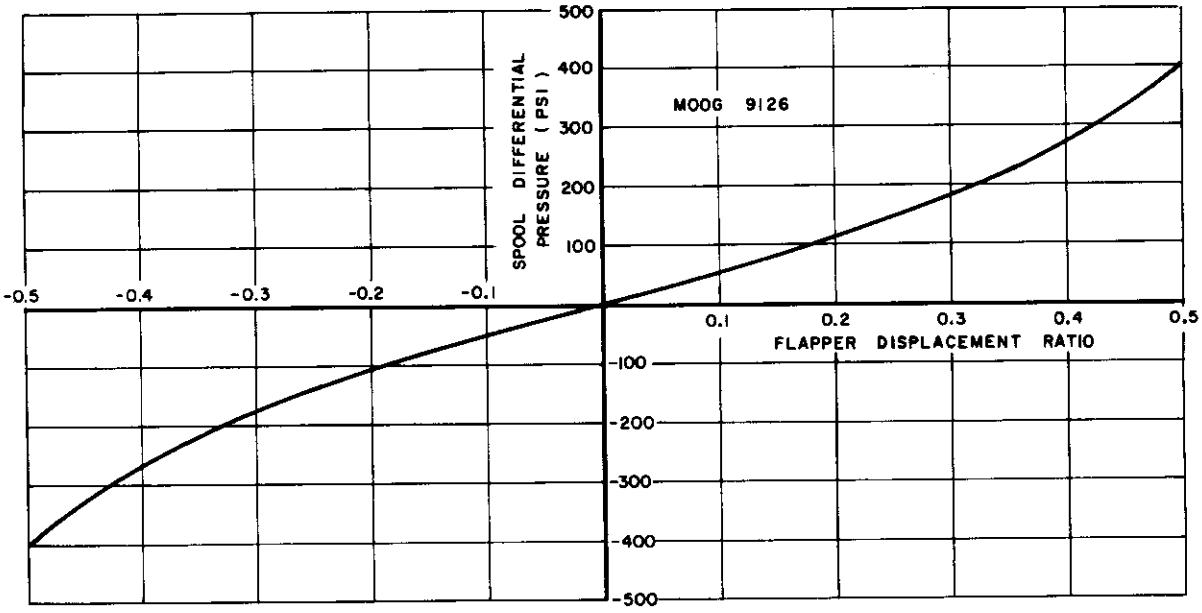

Figure 49. Blocked Spool Pressure vs. Flapper Displacement Ratio Moog 9126

The force F_1 exerted on the flapper by the static head of fluid at the nozzle can be written

$$F_1 = A_f \Delta P = 350 \times 2.54 \times 10^{-4} = 0.089 \text{ lb} \tag{1}$$

When reflected at the pole piece,

$$F_1 = 0.089 \times \frac{0.713}{0.551} = 0.115 \text{ lb} \tag{2}$$

The net force of magnetic attraction F_2 between flapper and pole pieces can be written

$$F_2 = 5.77 \times 10^{-7} (B_1^2 - B_2^2) A_g \tag{3}$$

with

$$B_1 = B_{pm} + B_{em} \tag{4}$$

and

$$B_2 = B_{pm} - B_{em} \tag{5}$$

Substituting (4) and (5) into (3) and neglecting for this analysis the flapper spring rate,

$$5.77 \times 10^{-7} \times 4B_{pm} B_{em} A_g = 0.115 \tag{6}$$

from which

$$B_{pm} B_{em} = 2.56 \times 10^6 \text{ gauss}^2$$

To determine B_{pm} and B_{em}, it is necessary to write the equations for total flux in the magnetic circuit and the total magnetomotive force required to overcome air gap reluctance:

$$\sigma_{pm} B_{pm} A_g = B_m A_m \tag{7}$$

$$1.3 H_{pm} L_g = H_m L_m \tag{8}$$

Application of the methods of References (6) and (7) for estimating magnetic leakage factors results in $\sigma_{pm} = 7$ and $\sigma_{em} = 3$. Then from (7)

$$B_{pm} = 1.2 B_m \tag{9}$$

Also, since $H_{pm} = B_{pm}$ for the air gap,

$$B_m/H_m = 7 \tag{10}$$

The intersection of (10) with the BH curve for Alnico VI yields $B_m = 4500$ gauss. Therefore from (9), $B_{pm} = 5400$ gauss; hence, $B_{em} = 475$ gauss.

For the electromagnet circuit,

$$\sigma_{em} B_{em} = \mu \frac{N\Delta I}{L_g} \tag{11}$$

Solving (11) for an 8 ma input, N = 4500 turns.

B. Back EMF Constant

The equation for the voltage induced by a magnetic field can be written as

$$e = N\frac{d\phi}{dt}\,10^{-8} = N\,\frac{\partial\phi}{\partial i}\,\frac{di}{dt}\,10^{-8} + N\,\frac{\partial\phi}{\partial x}\,\frac{dx}{dt}\,10^{-8} \qquad (12)$$

or as

$$e = L\frac{di}{dt} + K_v\frac{dx}{dt} \qquad (13)$$

Determination of K_v was accomplished by plotting normalized air gap flux vs. normalized flapper displacement (Figure 50) and determining the slope of this curve at the origin. This technique was based on the assumption that all of the air gap flux was due to the permanent magnet. For the Type 9126, the slope $\partial\phi/\partial x$ was 5.64×10^4 lines/in., from which $K_v = 2.54$ volt-sec/in.

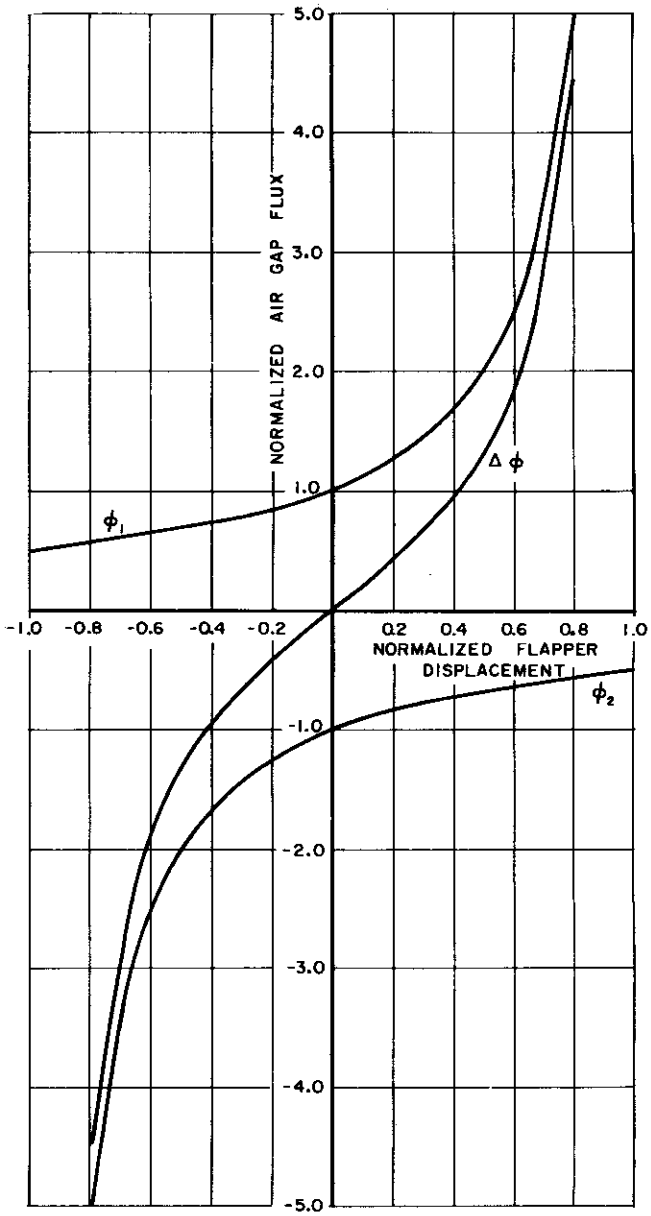

Figure 50. Normalized Air Gap Flux vs. Normalized Flapper Displacement

C. Flapper Magnetic Spring Rate

An equivalent circuit for the torque motor is presented in Figure 51. The equations for the fluxes linking the flapper can be written as

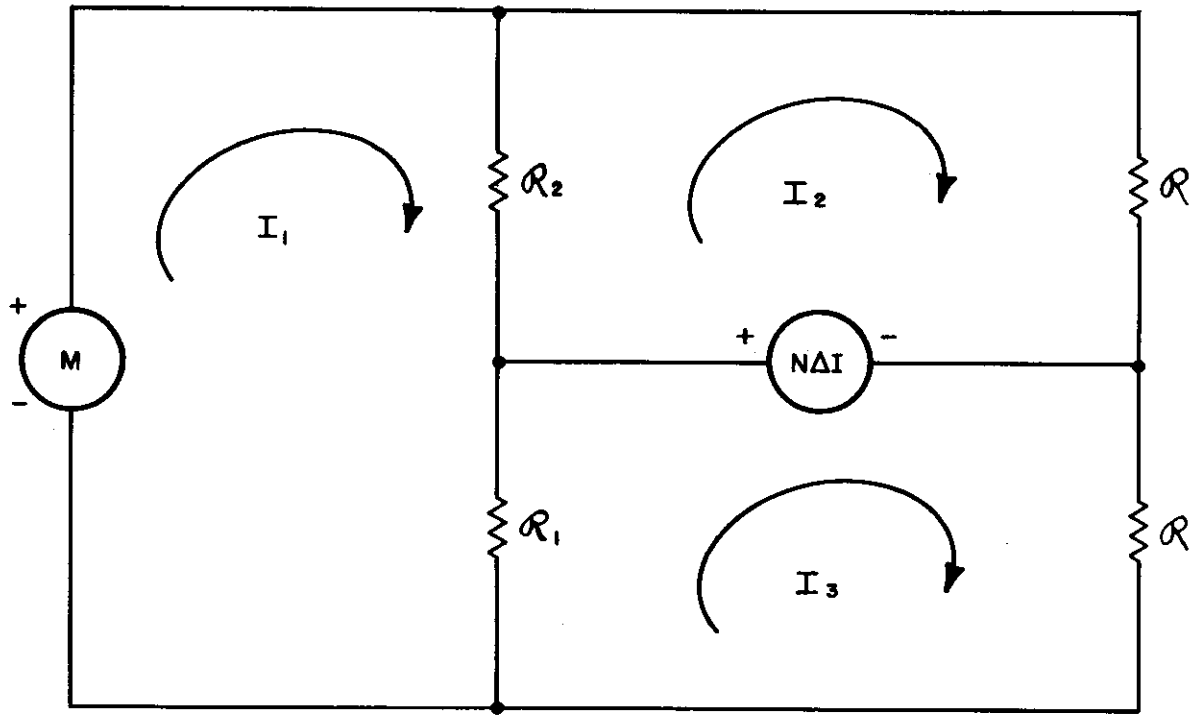

Figure 51. Equivalent Circuit to Torque Motor

$$\phi_1 = I_1 - I_3 = \frac{M_m}{\mathcal{R}_2 + \mathcal{R}_1\left[\frac{\mathcal{R}+\mathcal{R}_2}{\mathcal{R}+\mathcal{R}_1}\right]} + \frac{2\,N\Delta I}{(\mathcal{R}+\mathcal{R}_2) + \frac{\mathcal{R}_2}{\mathcal{R}_1}(\mathcal{R}+\mathcal{R}_1)} \tag{14}$$

$$\phi_2 = I_1 - I_2 = \frac{M_m}{\mathcal{R}_1 + \mathcal{R}_2\left[\frac{\mathcal{R}+\mathcal{R}_1}{\mathcal{R}+\mathcal{R}_2}\right]} - \frac{2\,N\Delta I}{(\mathcal{R}+\mathcal{R}_1 + \frac{\mathcal{R}_1}{\mathcal{R}_2}(\mathcal{R}+\mathcal{R}_2)} \tag{15}$$

where

$$\mathcal{R} = \ell_o/\mu A_g \tag{16}$$

$$\mathcal{R}_1 = (\ell_1 - x')/\mu A_g \tag{17}$$

$$\mathcal{R}_2 = (\ell_1 + x')/\mu A_g \tag{18}$$

$$M_m = \phi (\mathcal{R}_1 + \mathcal{R}_2) = 12.9\ B_{pm}\ \ell_1/\mu \tag{19}$$

Substituting (16) - (19) into (14) and (15) and writing in terms of normalized flapper displacement using numerical values of air gap lengths

$$\phi_1 = \frac{12.9\ B_{pm}\ A_g}{(1+x'/\ell_1) + (1-x'/\ell_1)\left[\frac{1.72+x'/\ell_1}{1.72-x/\ell_1}\right]} + \frac{2\ N\Delta I\ \mu\ A_g}{(1.72+x'/\ell_1) + (1.72-x'/\ell_1)\left[\frac{1+x'/\ell_1}{1-x'/\ell_1}\right]} \tag{20}$$

$$\phi_2 = \frac{12.9\ B_{pm}\ A_g}{(1-x'/\ell_1) + (1+x'/\ell_1)\left[\frac{1.72-x'/\ell_1}{1.72+x'/\ell_1}\right]} - \frac{2\ N\Delta I\ \mu\ A_g}{(1.72-x'/\ell_1) + (1.72+x'/\ell_1)\left[\frac{1-x'/\ell_1}{1+x'/\ell_1}\right]} \tag{21}$$

Now Equation (3) can be written in terms of flux rather than flux density, converting to English units and substituting the numerical values of A_g,

$$F = 7.13 \times 10^{-7} (\phi_1^{\,2} - \phi_2^{\,2}) \tag{22}$$

For various values of x/ℓ_1, (20) and (21) were solved for ϕ_1 and ϕ_2. Substitution into (22) resulted in a plot of F vs. x. The slope of this curve was the magnetic spring rate, 23 lb/in. Converting to rotational units, this rate was

$$23 \times (.55)^2 = 7 \text{ in-lb/rad}$$

As derived in Appendix II, the mechanical spring rate was 28 in-lb/rad. Hence, the net flapper spring rate was

$$K' = 21 \text{ in-lb/rad} \tag{23}$$

D. Torque Motor Constant

Considering Equation (43), Chapter II, under static conditions

$$aK_m \Delta I - bA_f \Delta P = K' \frac{x'}{a} \tag{24}$$

Using (3) of Chapter II and rearranging

$$K_m = \left[\frac{K'h(x/h)}{b} - b\, A_f\, \Delta P\right]\frac{1}{a\Delta I} \tag{25}$$

For 8 ma, $\Delta P = 350$ and $x/h = 0.46$. Therefore

$$K_m = 25 \text{ lb/amp} \tag{26}$$

Equation (24) can now be solved for ΔP as a function of differential current and flapper displacement.

$$\Delta P = 76 \times 10^3\, \Delta I - 562\, x/h \tag{27}$$

APPENDIX II

DETERMINATION OF FLAPPER PARAMETERS

A. Moment of Inertia

The flapper (Figure 52) was assumed to be a rectangle of length a

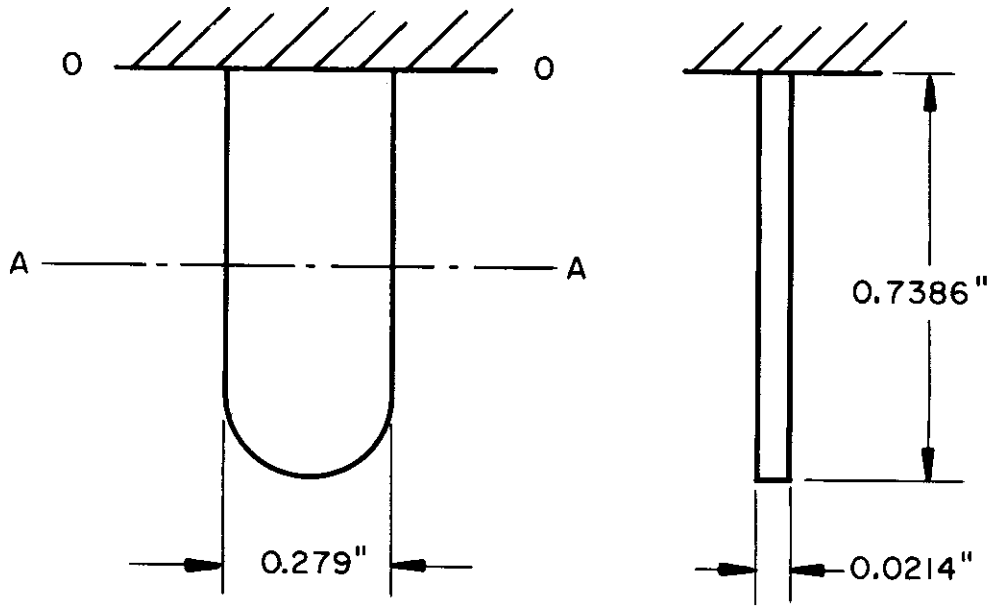

Figure 52. Flapper Geometry Moog 9126

and width b supported at one end. With respect to its center of gravity

$$J'_{A-A} = \frac{M a^3}{12} \tag{1}$$

with

$$M = wV \tag{2}$$

Assuming that w, the density of steel, is 0.28 lb/in^3,

$$J'_{A-A} = \frac{0.28 \times 0.7386 \times 0.0214 \times 0.279}{386} \times \frac{(0.7386)^2}{12}$$

$$= 1.45 \times 10^{-7} \text{ in-lb-sec}^2/\text{rad}^2$$

Translating with respect to the end of the flapper,

$$J'_{o-o} = 1.45 \times 10^{-7} + \frac{0.28 \times 0.7386 \times 0.0214 \times 0.279}{386} \times \frac{(0.7386)^2}{2} \quad (3)$$

$$= 6.81 \times 10^{-7} \text{ in-lb-sec}^2/\text{rad}^2$$

B. Mechanical Spring Rate

The flapper was assumed to be a steel ($E = 30 \times 10^6$) rectangular plate of width b, length l and thickness h. From Marks' Handbook, the spring rate for such a spring is $bh^3E/4l^3$. Substituting, the rate is 51 lb/in. or 28 in-lb/rad. As discussed in Appendix I-C, the net flapper spring rate is actually less by the amount of magnetic spring rate. That is,

$$K' = 28 - 7 = 21 \text{ in-lb/rad} \quad (4)$$

C. Viscous Damping

It was assumed that the flapper damping ratio was 0.6. The natural frequency of the flapper was

$$\omega_n = \sqrt{\frac{K'}{J'}} = 5500 \text{ rad/sec}$$

Hence

$$D' = 2\zeta\omega_n J' = 1.2 \times 5500 \times 6.81 \times 10^{-7}$$

$$= 4.5 \times 10^{-3} \text{ in-lb-sec/rad} \quad (5)$$

APPENDIX III

DETERMINATION OF FIRST-STAGE PARAMETERS

A. Upstream Orifices and First-Stage Drain Orifice

For a sharp edged circular orifice,

$$Q = C_q \frac{\pi D^2}{4} \sqrt{\frac{2\Delta P}{\rho}} \tag{1}$$

Now MIL-O-5606 oil has a mass density ρ of approximately 78×10^{-6} lb-sec^2/in^4. Assuming an orifice discharge coefficient $C_q = 0.65$ and substituting,

$$Q = 80\, D^2 \sqrt{\Delta P} \tag{2}$$

(This value of C_q is actually an average value, since C_q is really a function of Reynolds number. However, over the range of Reynolds numbers encountered (1500-3000), C_q is practically constant and equal to 0.65).

Therefore, both K_o and K_D can be evaluated from knowledge of the orifice diameters.

$$K_o = 80\, D_I^{\,2} = 80\, (6.2 \times 10^{-3})^2 = 3.03 \times 10^{-3} \text{ in}^4/\text{sec}\sqrt{\text{lb}} \tag{3}$$

$$K_D = 80\, D_D^{\,2} = 80\, (1.37 \times 10^{-2})^2 = 1.5 \times 10^{-2} \text{ in}^4/\text{sec}\sqrt{\text{lb}} \tag{4}$$

B. Flapper-Nozzle Orifice

The flapper and nozzle form a cylindrical orifice, for which

$$Q = C_q \pi\, D_o h \sqrt{\frac{2\Delta P}{\rho}} \tag{5}$$

Data obtained from tests indicate that $C_q = 0.5$ for this type of discharge configuration. Substituting,

$$Q = 250\, D_o h \sqrt{\Delta P} \tag{6}$$

Hence,

$$K_N = 250\, D_o = 250 \times 1.94 \times 10^{-2} = 4.85 \text{ in}^3/\text{sec}\sqrt{\text{lb}} \tag{7}$$

C. First-Stage Hydraulic Lags

Assume that the pressure changes at the nozzle will be transmitted to the spool at the velocity of sound in MIL-O-5606. The speed of sound can be expressed

$$u = \sqrt{\beta/\rho} \tag{8}$$

from which

$$u = 5.3 \times 10^{4} \text{ in/sec} \tag{9}$$

Assuming that the total passage length is about 1 inch, the hydraulic time lag is about 20 μsec. Hence, as long as the valve operates at frequencies appreciably below $1/(20 \times 10^{-6})$rad/sec or 8 kc, these lags can be neglected.

APPENDIX IV

DETERMINATION OF SECOND-STAGE PARAMETERS

A. Spool Mass

The spool weighed 3.582 grams. The two restraining springs weighed 1.272 grams. On the average, about one-third of the spring mass contributes to the spool dynamics. Hence, the total effective mass was 4 grams or 2.17×10^{-5} lb-sec^2/in.

B. Restraining Springs

The springs were steel ($G = 11.5 \times 10^6$) helixes, one with four turns and one with five turns. The wire thickness d and the given radius r were known. From Marks' Handbook, for the five-turn spring

$$K = \frac{d^4 G}{64 n r^3} = \frac{(.048)^4 (11.5 \times 10^6)}{(64)(5)(0.091)^3} = 253 \text{ lb/in} \quad (1)$$

For the four-turn spring,

$$K = 253 \times \frac{5}{4} = 316 \text{ lb/in} \quad (2)$$

The total restraining spring rate is

$$K = 570 \text{ lb/in} \quad (3)$$

C. Spool Damping

It was assumed the spool damping ratio was 0.5. The natural frequency of the spool was:

$$\omega_n = \sqrt{\frac{K}{M}} = 5100 \text{ rad/sec}$$

Hence

$$D = 2\zeta\omega_n M = 5100 \times 2.17 \times 10^{-5} = 0.111 \text{ lb-sec/in} \quad (4)$$

D. Bernoulli Spring Rate

It has been shown by Lee and Blackburn Reference (4) that the Bernoulli forces on the spool can be written

$$F_B = 0.43\ w\ x\ P_v \tag{5}$$

Hence, the spring rate is

$$\frac{F_B}{x} = 0.43\ w\ P_v = K_B\ P_v \tag{6}$$

The sleeve diameter is 0.198 inch and the peripheral slots occupy one-half the sleeve circumference. Hence

$$K_B\ P_v = (0.43)\ (\frac{0.198\pi}{2})\ P_v = 0.133\ P_v \tag{7}$$

E. Compressibility

In determining the compressibility for the fluid in the spool end chambers, the fundamental relation is:

$$K_c = V/2\beta \tag{8}$$

The volume V is composed of the volume of the spool chamber plus the volume of the end cap less the volume occupied by the spring and spring guide. Experimentally, $V = 0.015\ in^3$.

Hence

$$K_c = \frac{0.015}{2x2.225x10^5} = 3.3 \times 10^{-8}\ in^5/lb \tag{9}$$

F. Leakage

It was estimated that $0.05\ in^3/sec$ leaked past the spool lands, with a null pressure of 540 psi. Hence

$$K_c = \frac{Q_c}{P_o} = \frac{0.05}{540} = 9.3 \times 10^{-5}\ in^5/lb\text{-}sec \tag{10}$$

G. Spool Friction

No value for spool friction was used. It was planned to vary this parameter in the analog to determine acceptable limits for its values.

H. Output Flow Relations

Equation (41), Chapter II, relates spool displacement and differential current statically.

$$y = \frac{K_1 A}{K^* (K_L + K_2)} \tag{41}$$

Equation (31), Chapter II, describes the first-stage pressure flow curves as

$$Q_c = K_1 \Delta I - K_2 \Delta P \tag{31}$$

From these curves,

$$K_1 = 0.022 \text{ in}^3/\text{ma-sec} \tag{11}$$

and

$$K_2 = 5.36 \times 10^{-4} \text{ in}^5/\text{lb-sec} \tag{12}$$

A typical value of K* was 750 lb/in and $A = 3.05 \times 10^{-2}$ in^2. Hence

$$y = \frac{2.2 \times 10^{-3} \times 3.05 \times 10^{-2}}{(750)(5.36 + 0.93)(10^{-4})} \Delta I = 1.42 \times 10^{-3} \Delta I \tag{13}$$

where ΔI is measured in milliamperes. At 8 ma, the Type 9126 valve was able to port 10 gpm. Hence

$$10 \times 3.85 = 8 \times 1.42 \times 10^{-3} K_F \sqrt{3000} \tag{14}$$

From (14), $K_F = 60 \text{ in}^3/\text{sec} \sqrt{\text{lb}}$

Therefore

$$Q_v = 60y \sqrt{3000 - P_L} \tag{15}$$

Experimentally, it had been observed that for $\Delta I < 0.4$ ma, the maximum load differential pressure attainable was less than 3000 psi. It was assumed that static inputs less than 0.4 ma would cause the valve to operate open centered

$$Q_v = C_1 y - C_2 P_L$$

From the leakage curves, at $\Delta I = 0.4$ ma,

$$Q_v = (0.275 - 0.13)(3.85) = 0.56 \text{ in}^3/\text{sec}$$

Hence,

$$C_1 = \frac{0.56}{0.4 \times 1.42 \times 10^{-3}} = 982 \text{ in}^2/\text{sec} \tag{16}$$

and

$$C_2 = \frac{0.56}{3000} = 1.87 \quad 10^{-4} \text{ in}^5/\text{lb-sec} \tag{17}$$

Hence,

$$Q_v = 982y - 1.87 \times 10^{-4} P_L \tag{18}$$

APPENDIX V

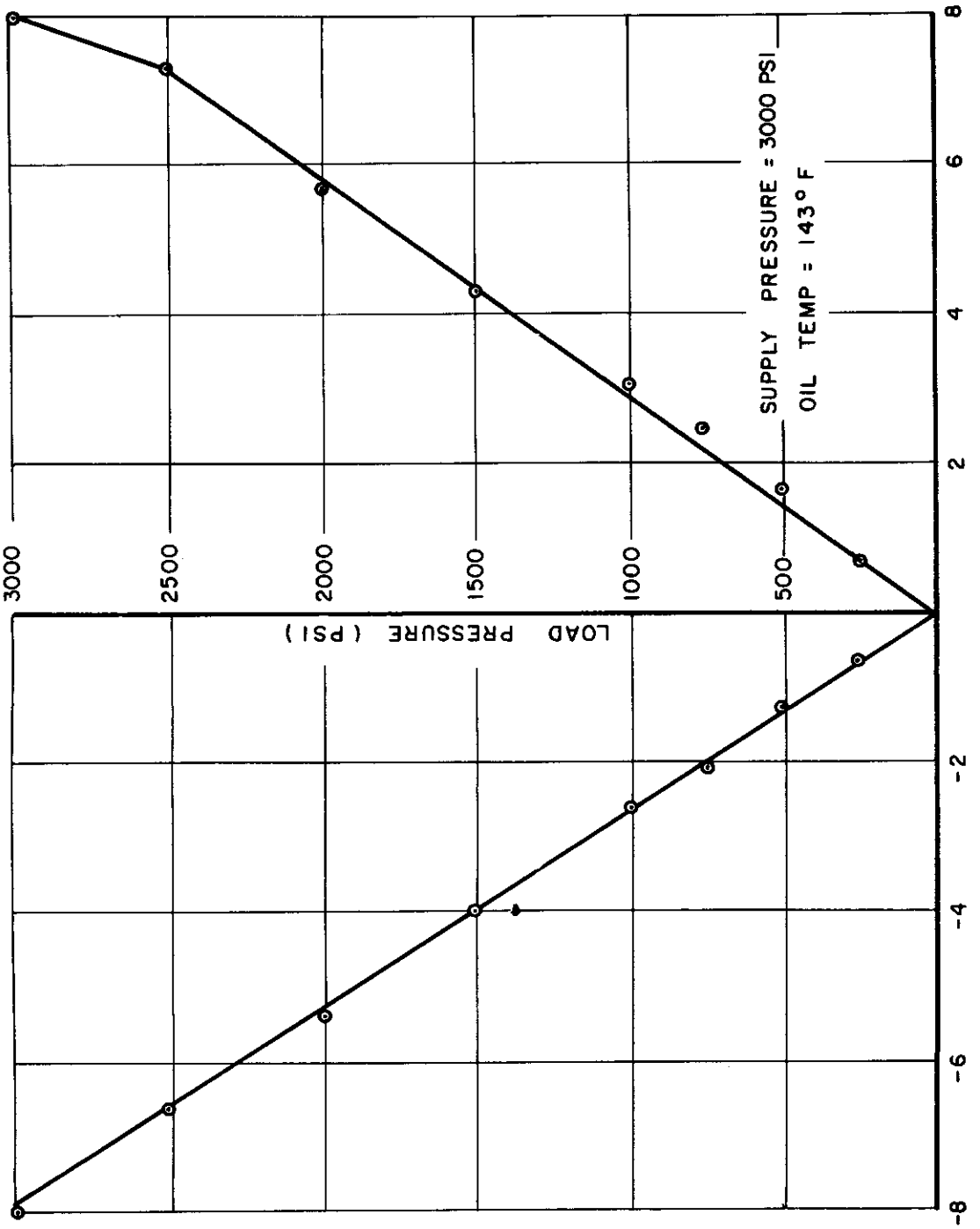

Figure 53. Cadillac Gage PC-2 Load Pressure vs. Differential Current

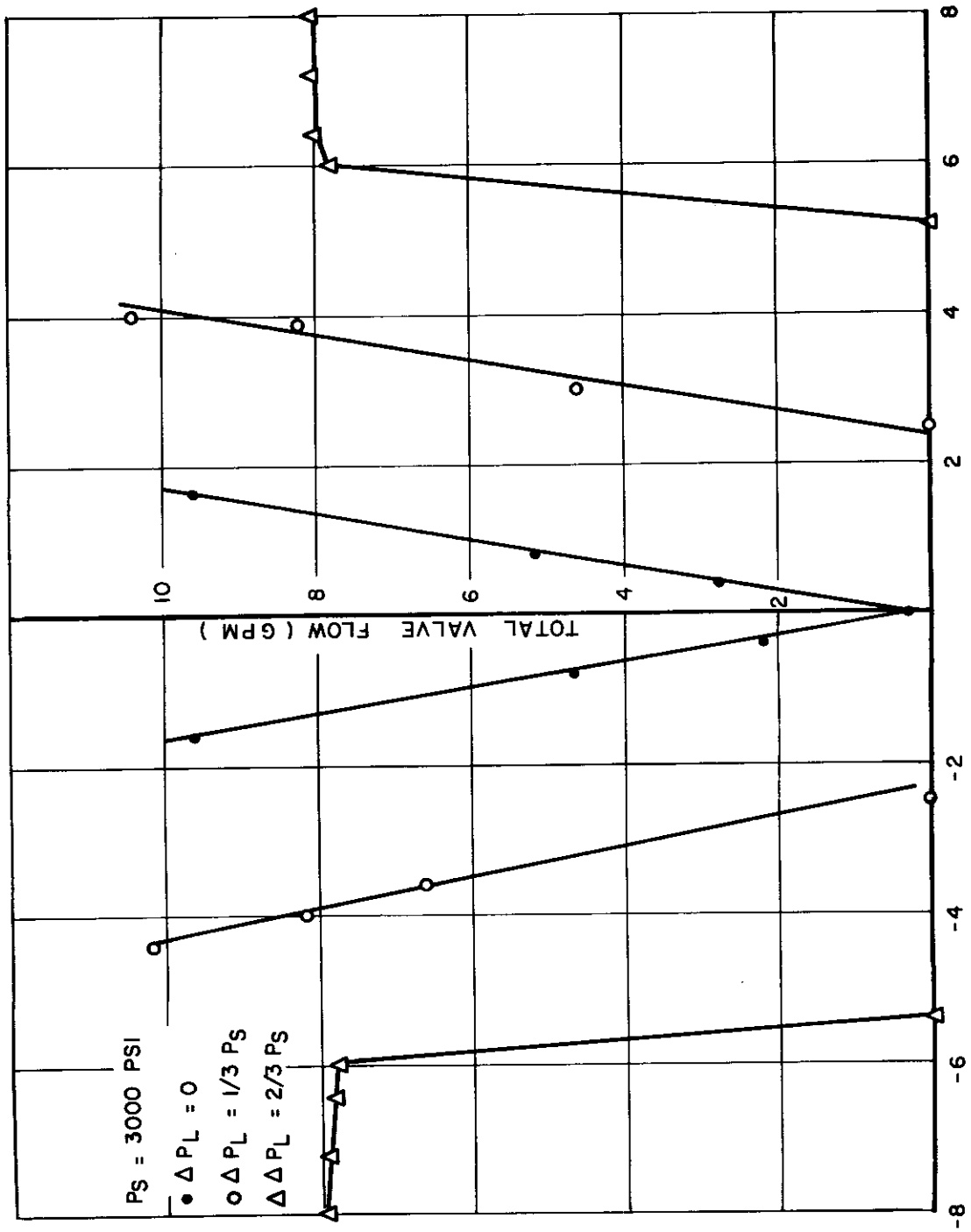

Figure 54. Cadillac Gage PC-2 Load Flow vs. Differential Current

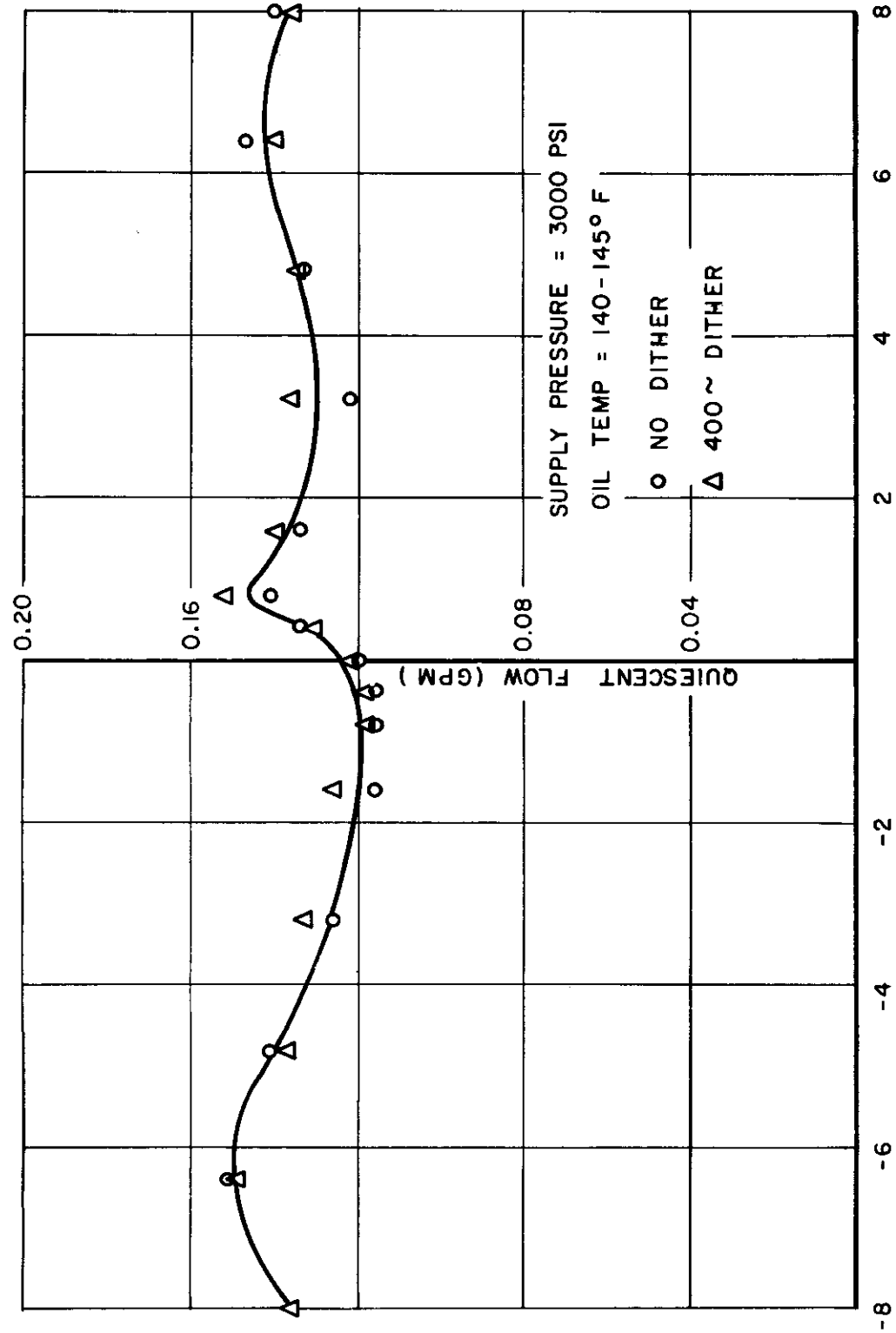

Figure 55. Cadillac Gage PC-2 Quiescent Flow vs. Differential Current

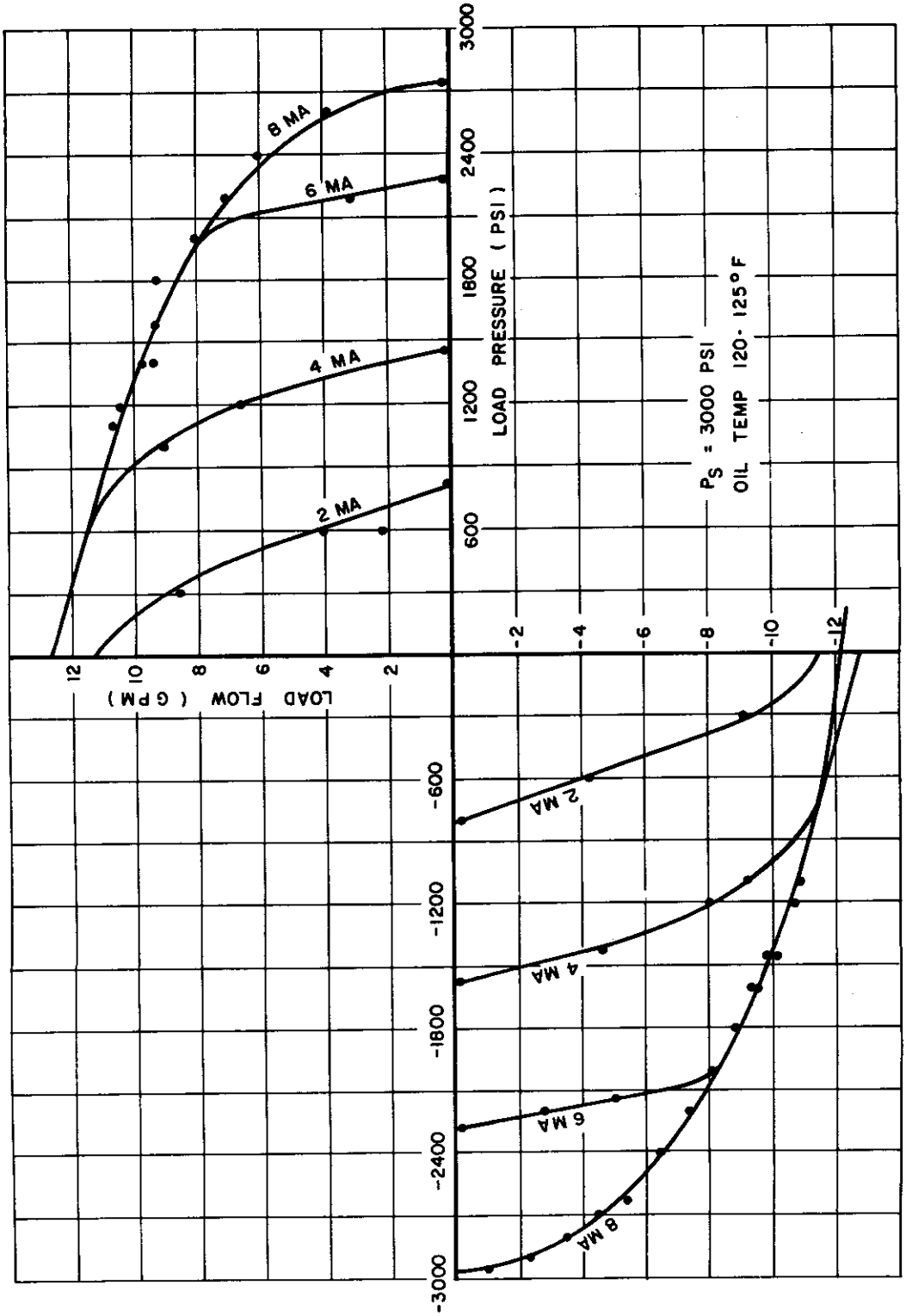

Figure 56. Cadillac Gage PC-2 Load Flow vs. Load Pressure

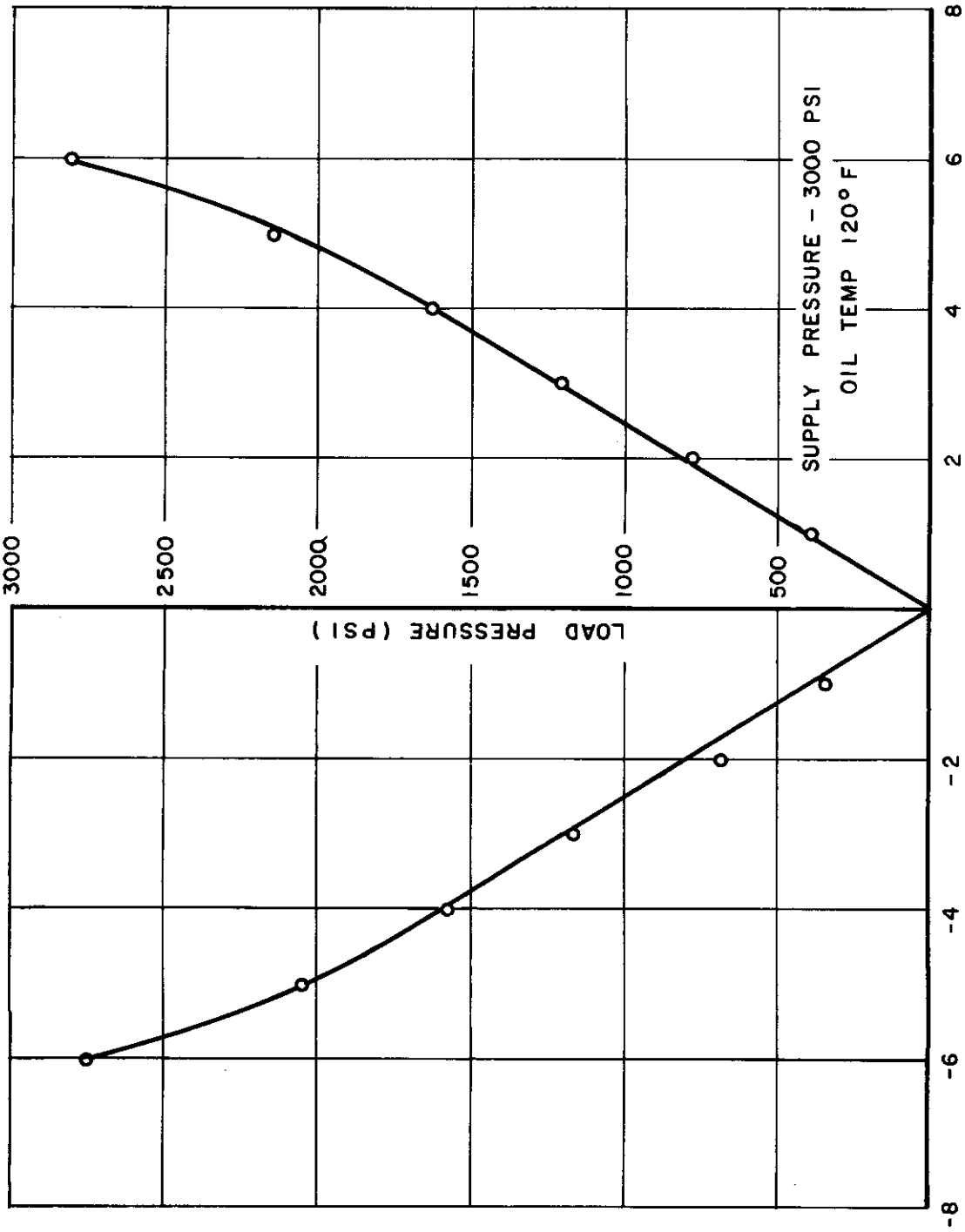

Figure 57. Moog Model 1526 Load Pressure vs. Differential Current

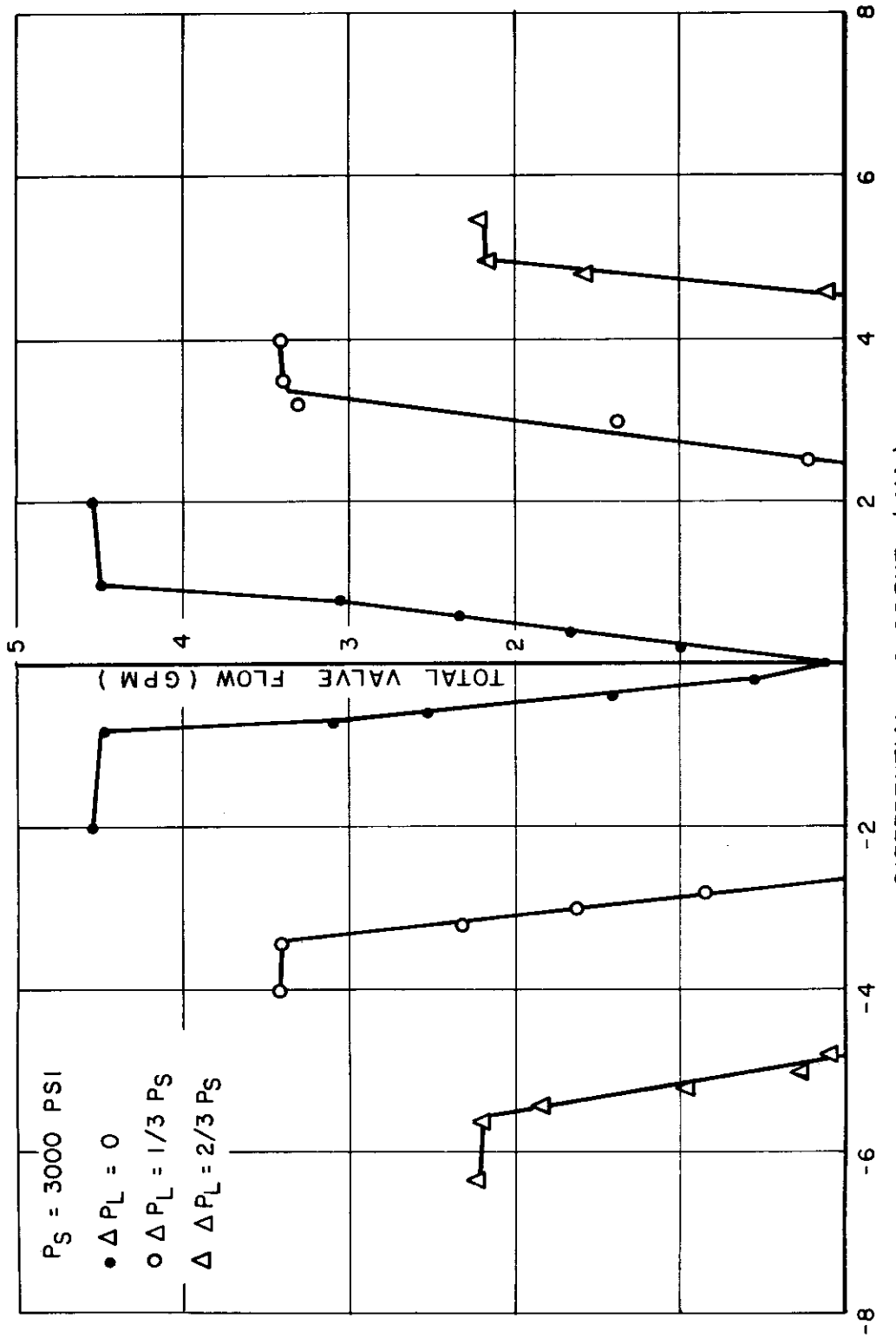

Figure 58. Moog Model 1526 Load Flow vs. Differential Current

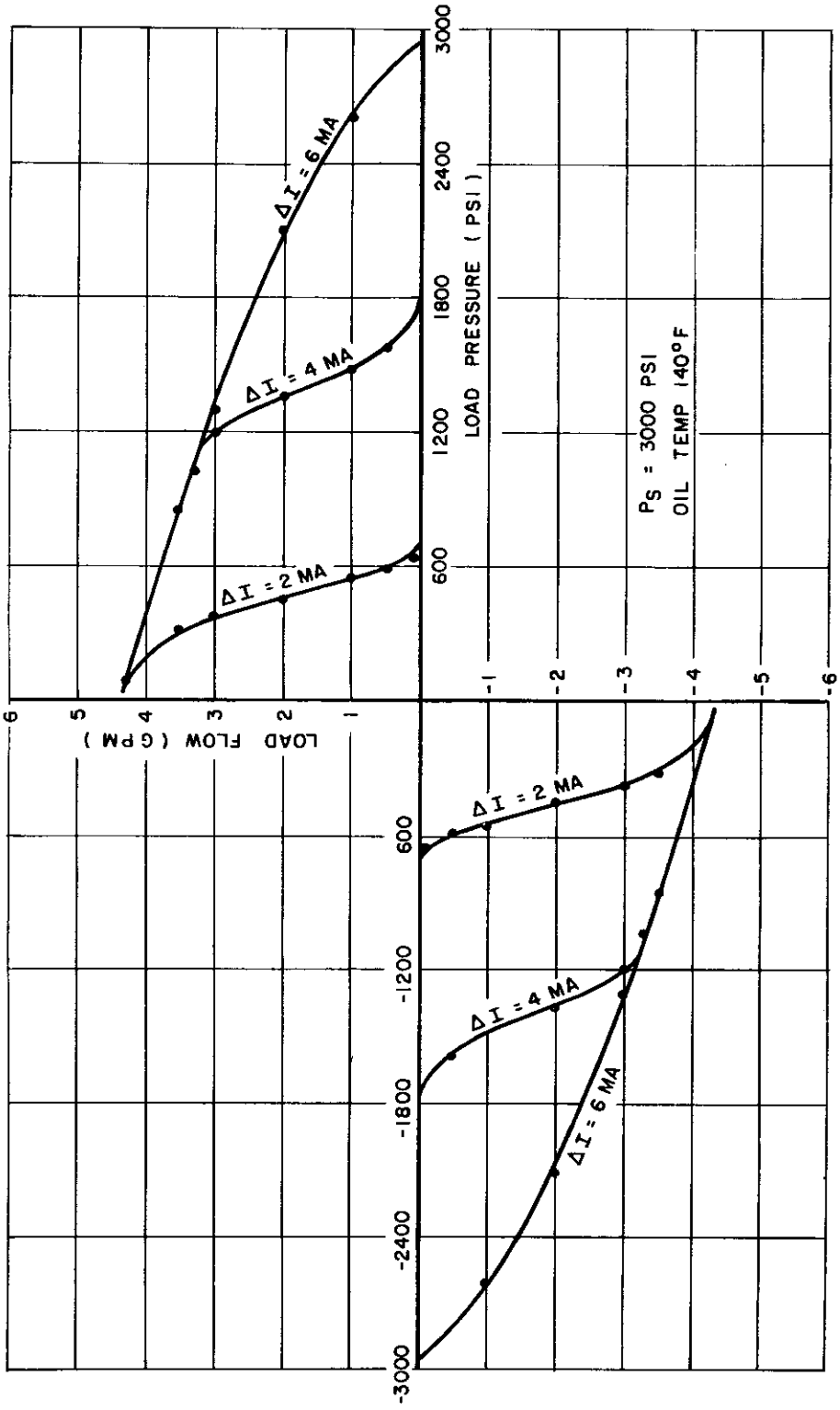

Figure 59. Moog Model 1526 Load Flow vs. Load Pressure

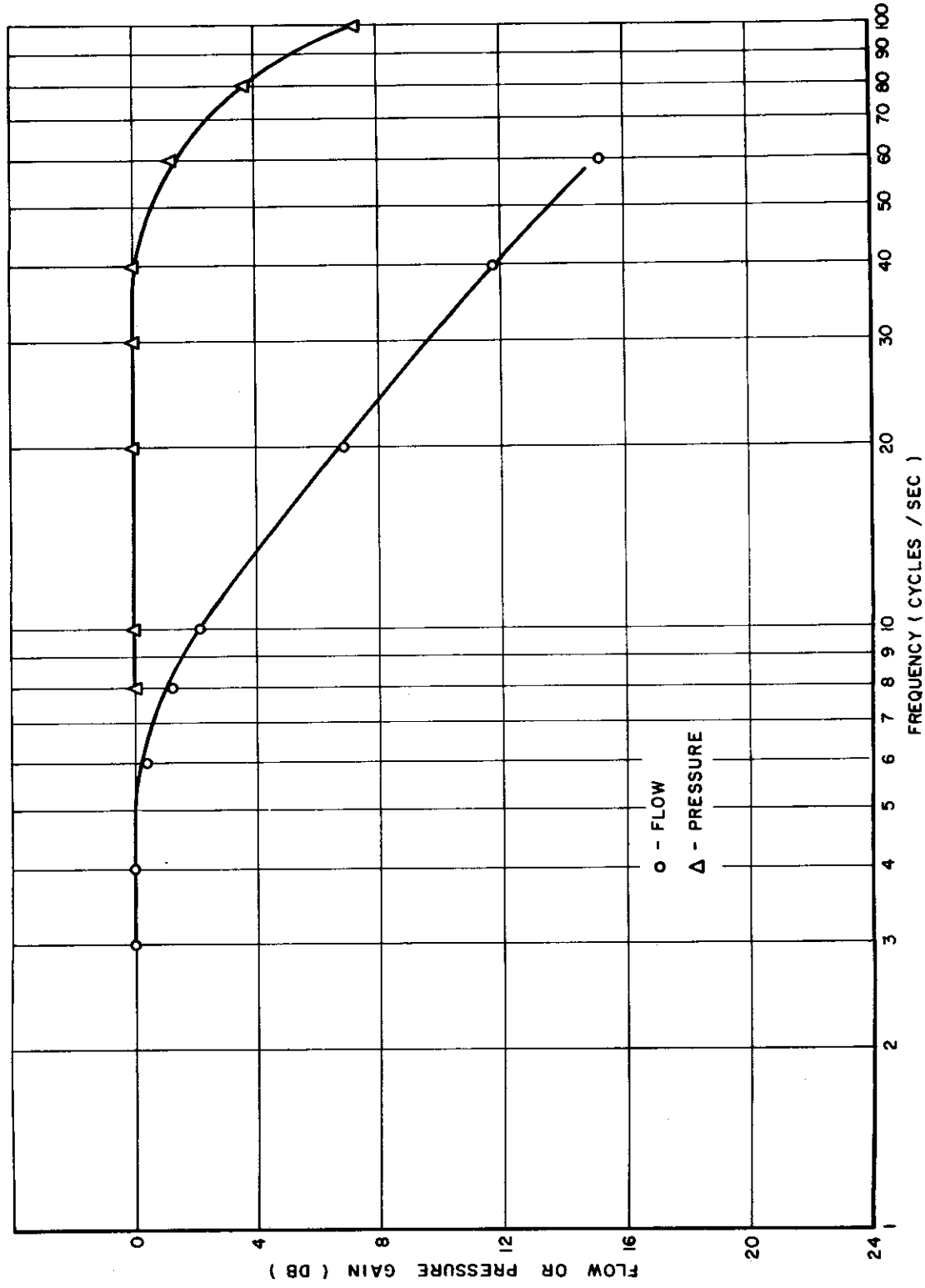

Figure 60. Cadillac Gage PC-2 No-Load Frequency Response

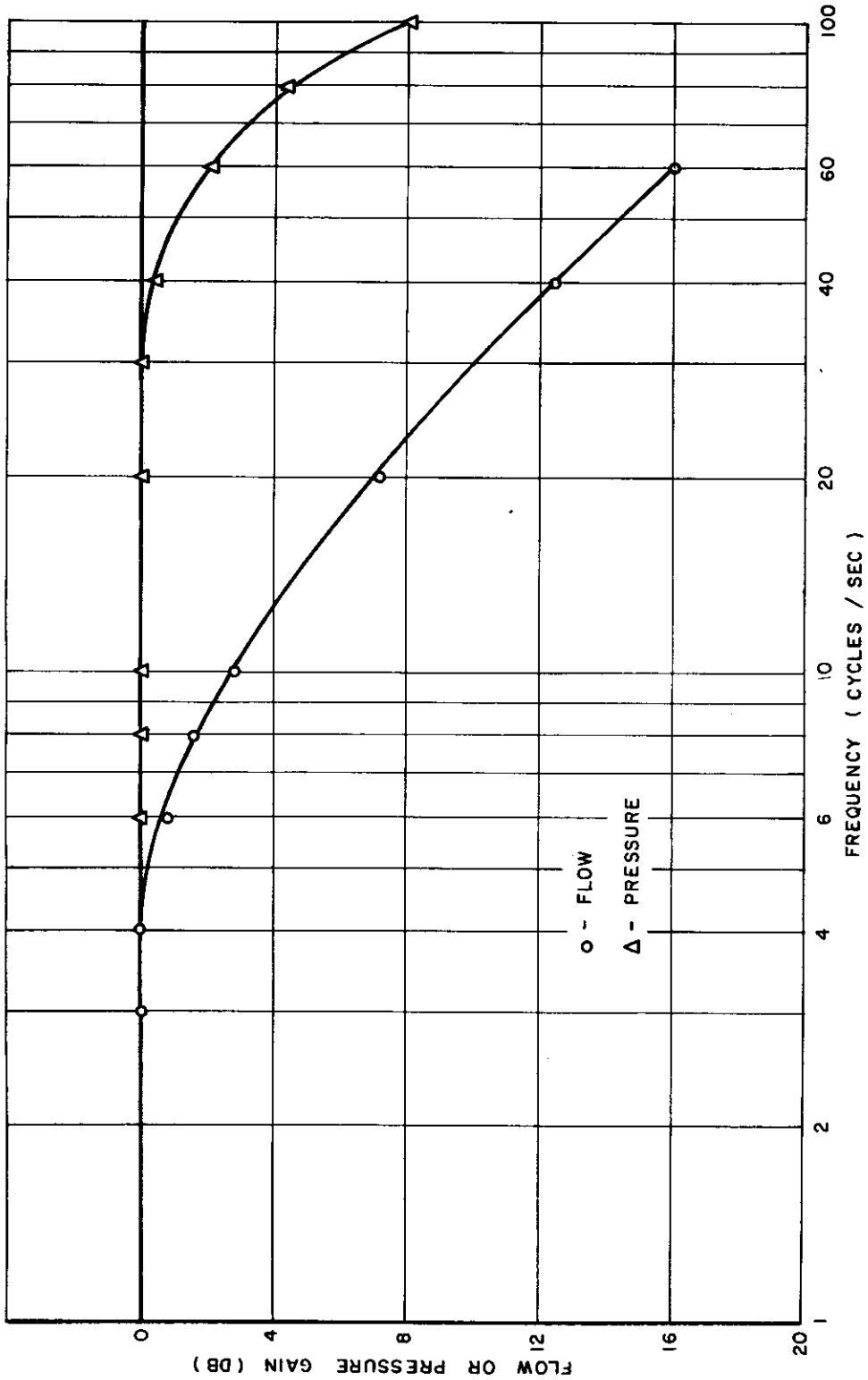

Figure 61. Moog Model 1526 No-Load Frequency Response

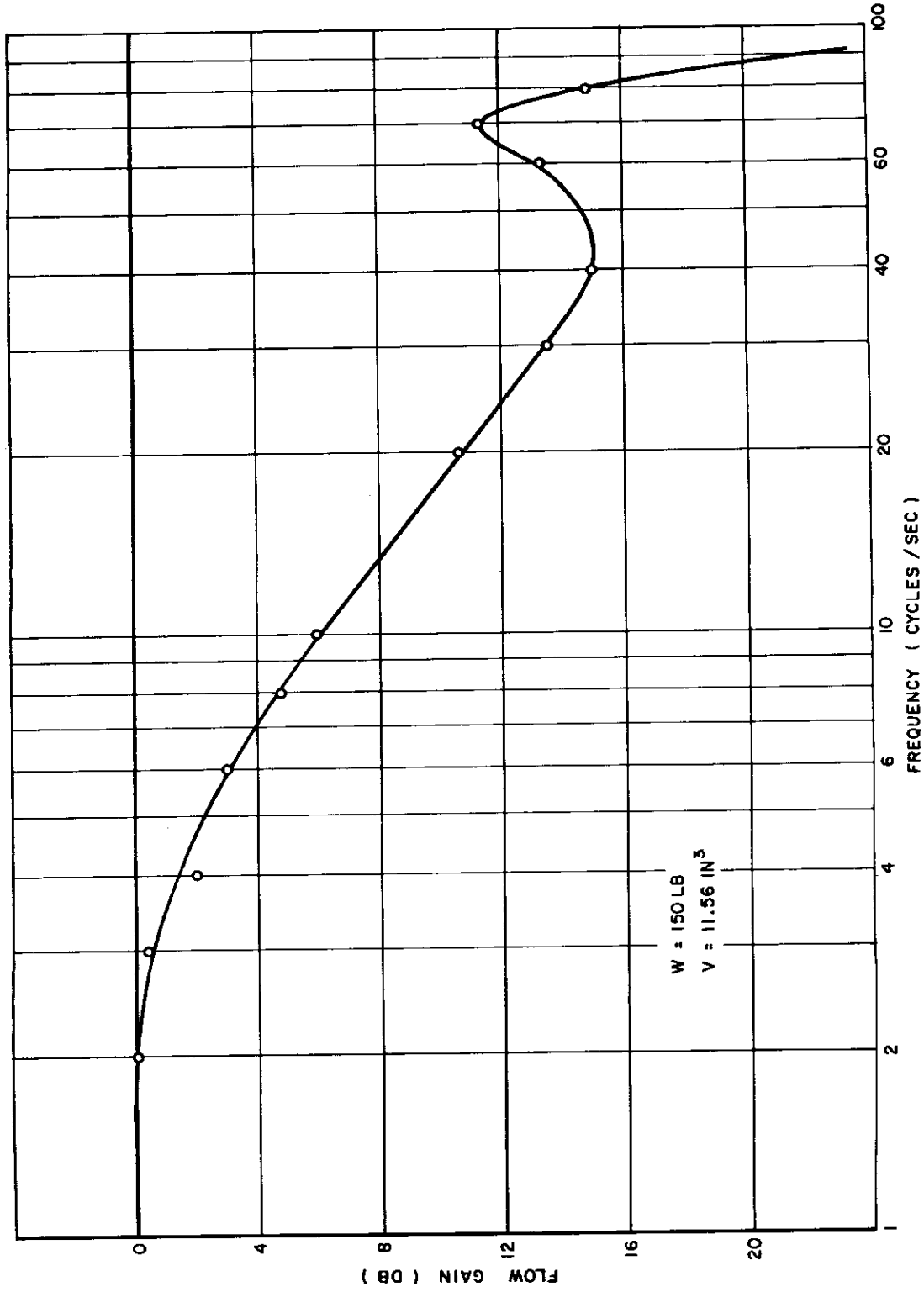

Figure 62. Cadillac Gage PC-2; Open Loop Frequency Response for Run 1

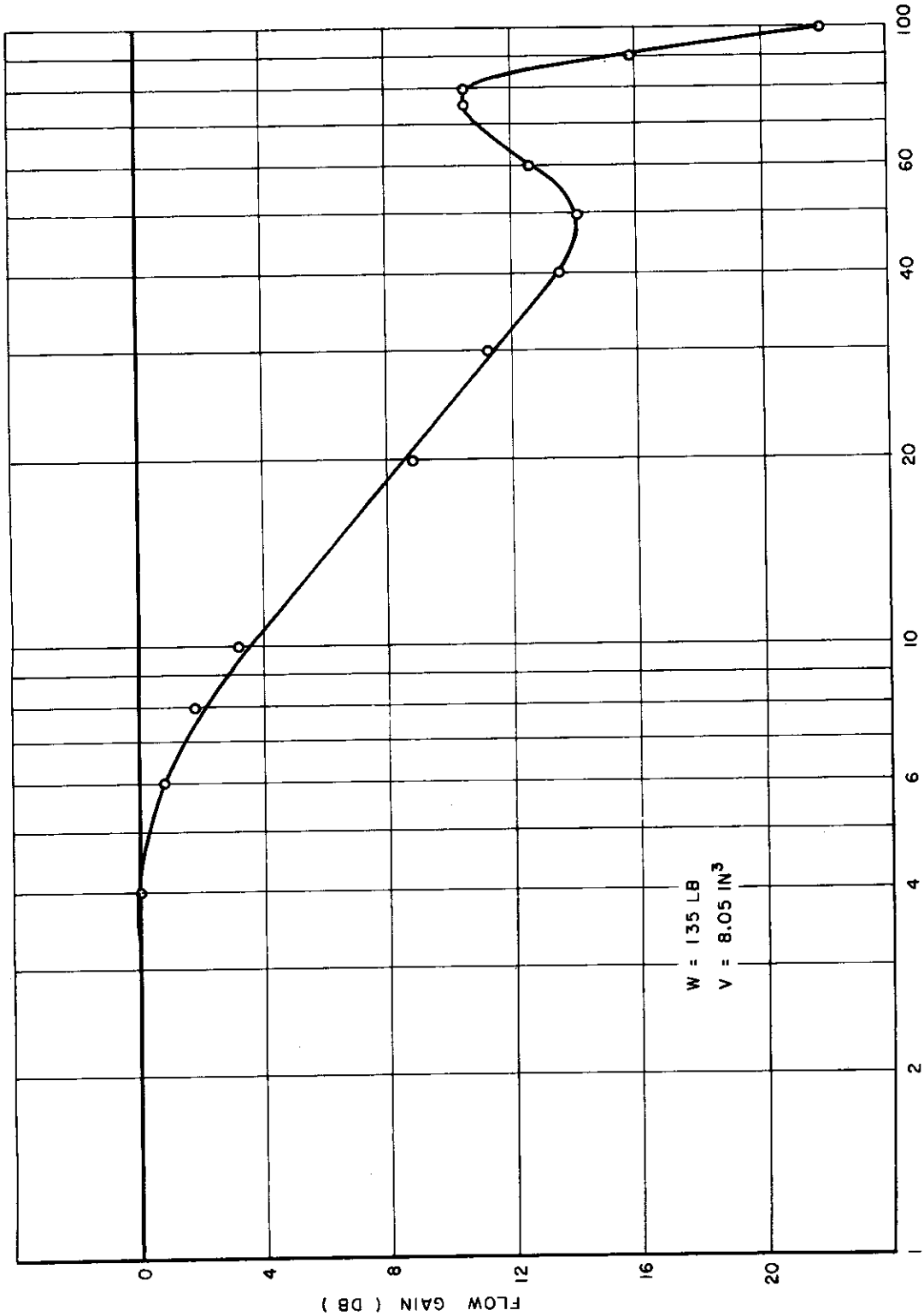

Figure 63. Cadillac Gage PC-2; Open Loop Frequency Response for Run 2

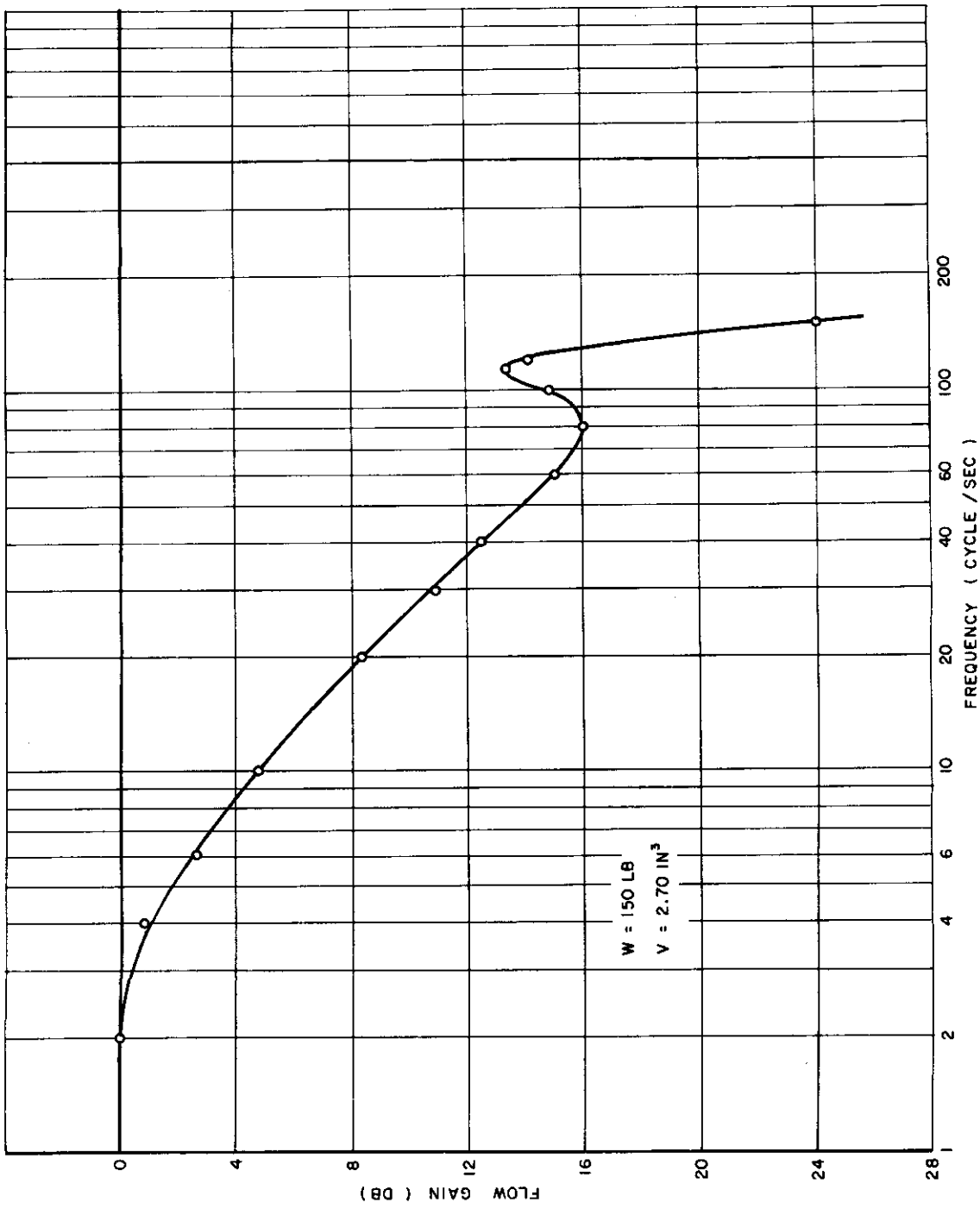

Figure 64. Cadillac Gage PC-2; Open Loop Frequency Response for Run 3

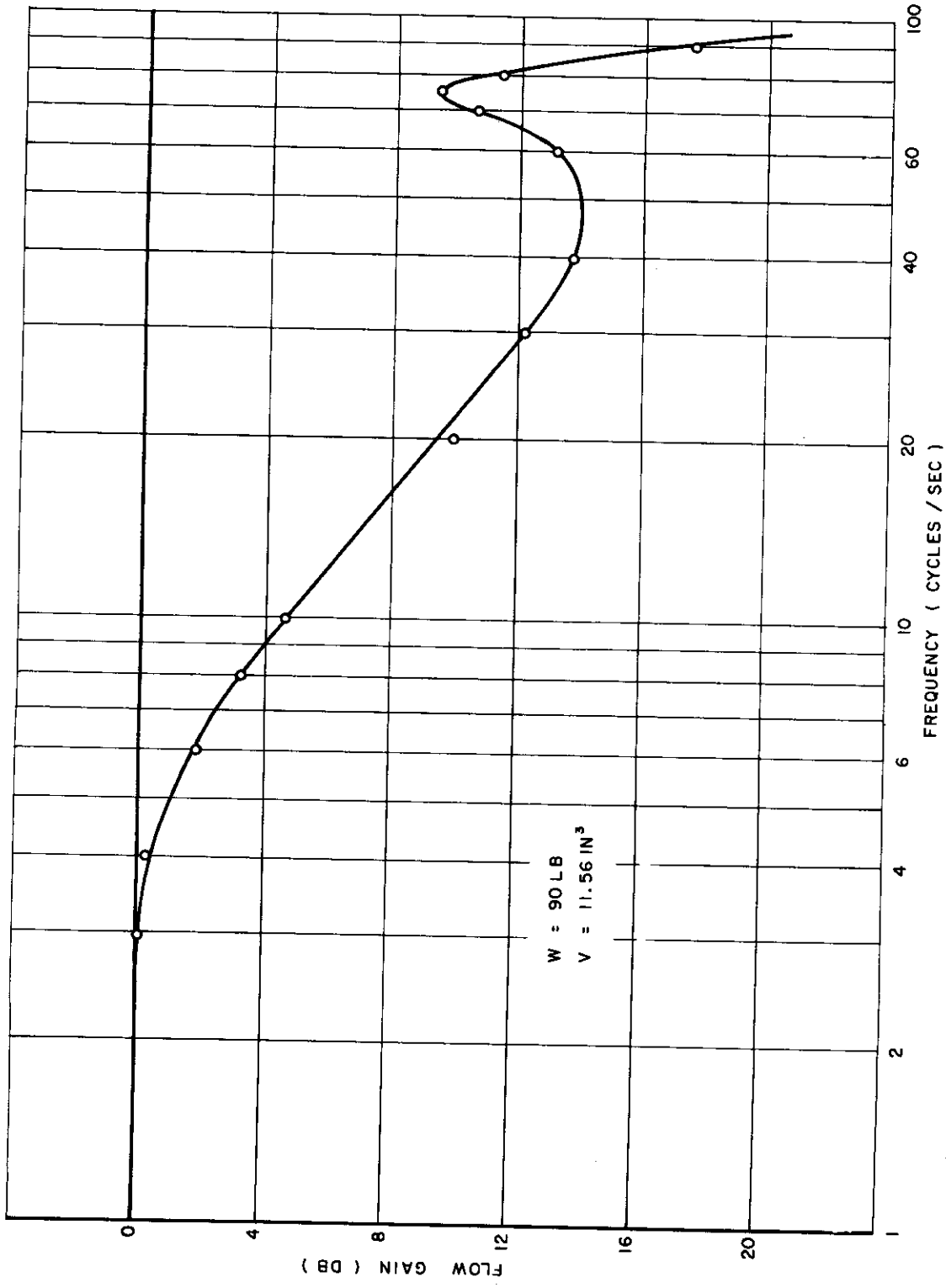

Figure 65. Cadillac Gage PC-2; Open Loop Frequency Response for Run 4

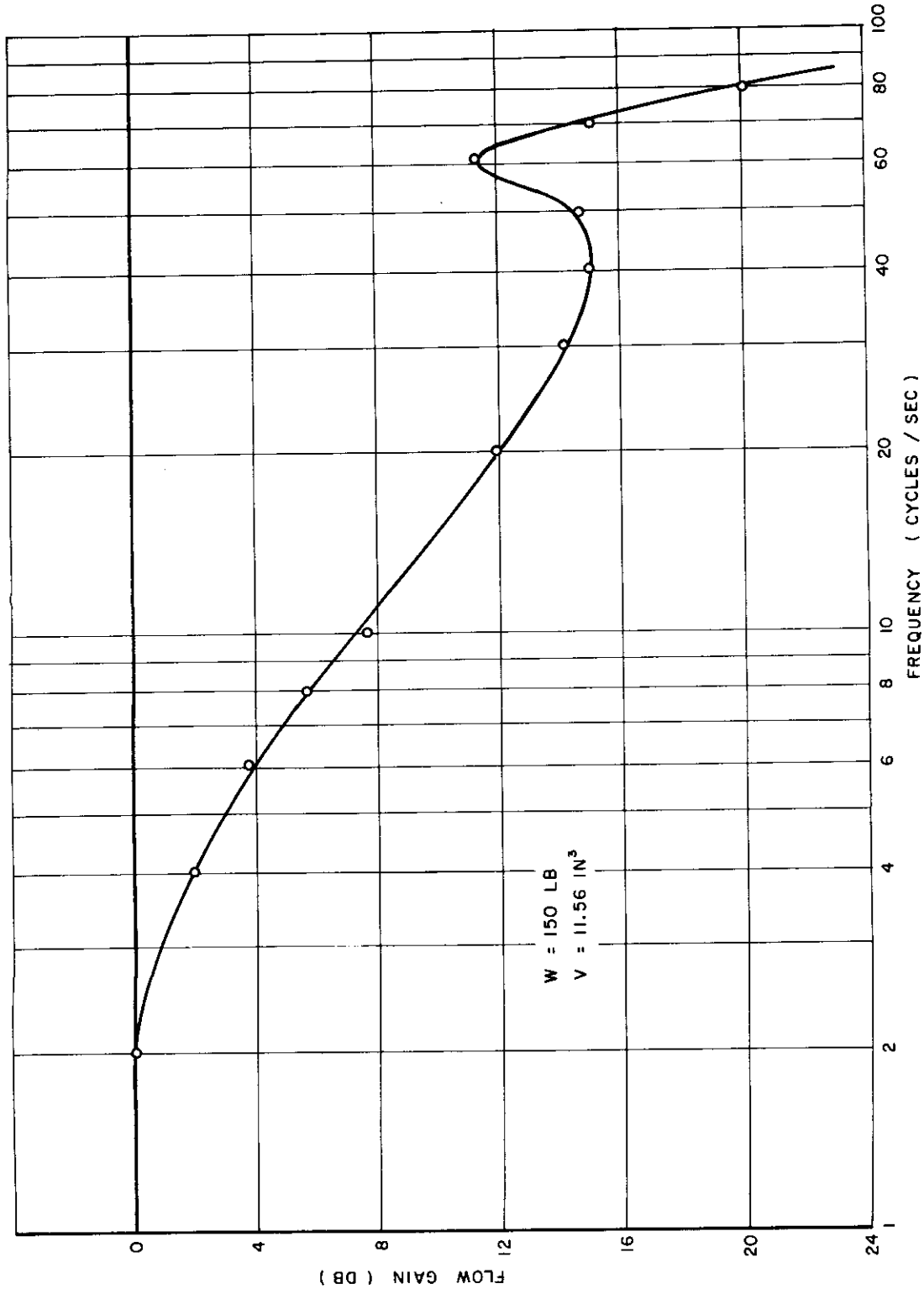

Figure 66. Moog Model 1526; Open Loop Frequency Response for Run 5

APPENDIX VI

HEAT TRANSFER CALCULATIONS

A. Nomenclature

C_p Specific heat at constant pressure - Btu/lb °F

D Diameter - feet

D_e Equivalent diameter, = 4 r_h

f **Friction** factor, dimensionless

G Mass Velocity - lb/(hr)(sq ft of cross-section)

g_c Conversion factor in Newton's Law of motion = 4.17×10^8 feet x $\frac{\text{lb matter}}{(\text{hr})^2 \text{ lb force}}$

h Coefficient of heat transfer between fluid and surface - $\frac{\text{Btu}}{(\text{hr})(\text{ft}^2)(^\circ\text{F})}$

K Thermal conductivity - Btu/(hr)(sq ft)(°F per ft)

L Length - ft

m Mass - lb

Q Heat transfer rate - Btu/hr

r_h Hydraulic radius, feet, equals cross-section divided by total wetted perimeter

t Temperature-degrees Fahrenheit

μ Viscosity - lb/(hr)(ft)

V_m Specific volume = $\frac{1}{\rho}$ - ft^3/lb

ρ Density - lb fluid per ft^3

N_{Re} Reynolds number $= \frac{DG}{\mu}$

N_{Pr} Prandtl number $= \frac{C_p \mu}{K}$

Subscripts

b Bulk

f Film $t_f = (t_b + t_w)/2$

w Wall

All references were taken from "Heat Transmission" by William H. McAdams, McGraw-Hill Book Company, Inc., 1954, Third Edition.

B. Regenerative Heat Exchanger

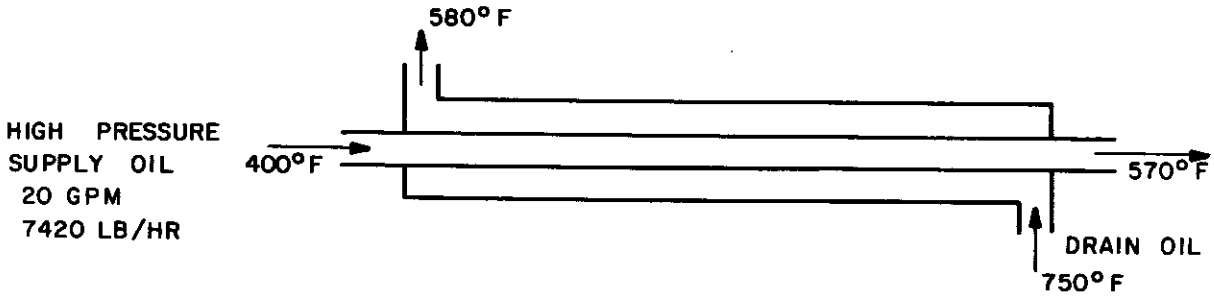

Fig. 67. Flow Diagram - Regenerative Heat Exchanger

1. Flow Inside Tube

a. Heat Transfer Coefficient

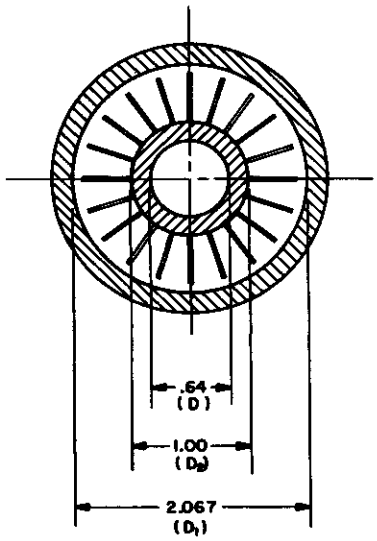

Figure 68
Cross Section -
Regenerative
Heat Exchanger

$D = 0.0533$ ft

Bulk Temp = 485°F

Wall Temp = 550°F

Film Temp = 527°F

$C_{pb} = 0.505$ = Btu/lb °F

$C_{pf} = 0.518$ Btu/lb °F

$\mu f = 7.7$ lb/hr ft

$K_f = 0.0655$ Btu/(hr) (ft^2) (°F per ft)

$\rho = 53.7$ lb/ft^3

$G = 3.33 \times 10^6$ lb/hr ft^2

$$N_{Re} = \frac{DG}{\mu} = 2.31 \times 10^4$$

$$N_{Pr} = \frac{C_p \mu}{K} = 60.9$$

Equation (9-10b), page 219, for turbulent flow applies to this situation.

$$h = \frac{0.023\, C_{pb}\, G}{\left(\frac{DG}{\mu f}\right)^{0.2} \left(\frac{C_p \mu}{K}\right)_f^{2/3}} = 340 \frac{\text{Btu}}{\text{hr ft } ^\circ\text{F}}$$

b. Pressure Drop

$f_m = 0.0063$, from Figure 6-11, page 156 ("Friction Factors For Flow in Pipe")

For incompressible flow, Equation (6-9a), page 157, applies

$$\Delta P = \frac{f_m G^2 V_m L}{2 g_c r_h 144} = 0.813L \text{ psi}$$

2. Heat Transfer Coefficient for Flow in Annular Space

Bulk Temperature = 665°F

Wall Temperature = 590°F

$C_{pb} = 0.565$ Btu/lb °F

$\mu_b = 3.94$ lb/hr ft

$\mu_w = 5.35$ lb/hr ft

$K_b = 0.0586$ Btu/(hr) (ft^2) (°F per ft)

$D_e = D_2 - D_1 = 0.0889$ ft

$$N_{Re} = \frac{D_e G}{\mu_b} = 1.075 \times 10^4$$

$$N_{Pr} = \frac{C_p \mu}{K} = 38$$

Equation (9-32c), page 243, applies

$$h = \frac{0.023\ C_{pb}\ G}{\left(\frac{C_p \mu}{K}\right)_b^{2/3} \left(\frac{\mu_w}{\mu_b}\right)^{0.14} \left(\frac{D_e G}{\mu_b}\right)^{0.2}} = 89.9\ \frac{\text{Btu}}{\text{hr ft}^2\ ^\circ\text{F}}$$

To this answer a fin efficiency correction factor was added. The result - $h_f = 265.$ Btu/hr ft^2 $^\circ$F.

3. Over-all Exchanger Performance

Heating Q = Flow Rate x $C_p \Delta t = 6.37 \times 10^5$ Btu/hr

Using this heat flow rate and the previously calculated coefficients, the length of exchanger section was estimated to be 160 feet. The calculated performance figures based on this length are:

	Required Temp. Gradient for Heat Transfer	Pressure Drop
Flow Inside Tube $\Delta t = Q/Ah$	70°F	130 psi
Flow Inside Annulus $\Delta t = Q/Ah_f$	91°F	30 psi
Tube Wall Conductivity $\Delta t = \frac{Q \ln \frac{D_2}{D_2}}{2 \pi LK}$	26°F	
Total	187°F	160 psi

It is to be noted that 187°F is very close to the design total temperature gradient for heat transfer of 180°F. Thus, 160 feet of exchanger section is adequate for this unit.

C. Oil Heater

This design is based on the use of 7/8 inch outside diameter stainless steel tubing with 0.120 inch wall thickness.

$$Q = m\, C_p \Delta t = 7.51 \times 10^5 \text{ Btu/hr} = 220 \text{ kilowatts}$$

In order to provide for transient response, the design was based on a heater of 250 kilowatt capacity.

Figure 69. Flow Diagram - Oil Heater

1. Fluid to Wall heat Transfer Coefficient

$D = 0.0529$ ft

Bulk Temperature = 660°F

Wall Temperature = 700°F

Film Temperature = 680°F

$C_{pb} = 0.562$ Btu/lb. °F

$C_{pf} = 0.569$ Btu/lb. °F

$\mu_f = 3.96$ lb/hr ft

$K_f = 0.058$ Btu/(hr) (ft^2) (°F per ft)

$\rho = 48.7$

$G = 3.37 \times 10^6$ lbs/hr ft^2

$$N_{Re} = \frac{DG}{\mu} = 4.50 \times 10^4$$

$$N_{Pr} = \frac{C_p \mu}{K} = 38.8$$

Equation (9-10b), page 219, for turbulent flow applies to this situation.

$$h_L = \frac{0.023\ C_{pb}\ G}{\left(\frac{DG}{\mu f}\right)^{0.2}\left(\frac{C_p \mu}{K}\right)_b^{2/3}} = 444 \text{ Btu/hr ft}^2\,^{\circ}\text{F}$$

Using this heat transfer coefficient and the criterion that the tube to wall temperature gradient is not to exceed 40°F, the required length of tubing was determined as 300 feet.

2. Pressure Drop

$f_m = 0.0054$, from Figure 6-11, page 156 ("Friction Factors For Flow in Pipe")

For incompressible flow, Equation (6-9a), page 157, applies.

$$\Delta P = \frac{f_m G^2 V_m\ L}{2 g_c\ r_h\ 144} = 240 \text{ psi}$$

D. Oil Cooler

Required Heat Transfer Rate = Q = 6.7×10^5 Btu/hr

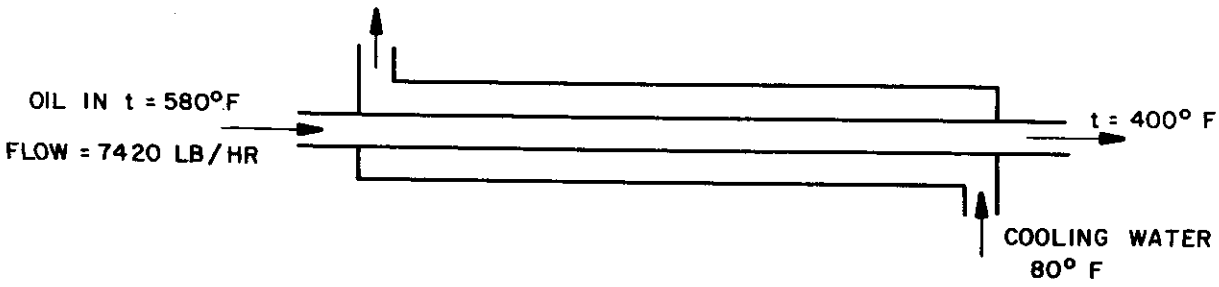

Figure 70. Flow Diagram - Oil Cooler

1. Flow Inside Tube

a. Heat Transfer Coefficient

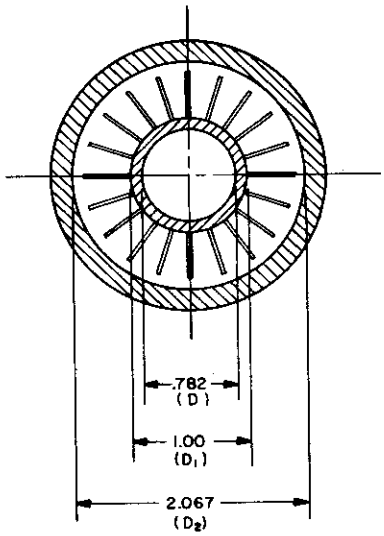

Figure 71. Cross Section - Oil Cooler

D = 0.0652 ft

Bulk Temperature = 490°F

Wall Temperature = 290°F

Film Temperature = 390°F

C_{pb} = 0.505 Btu/lb °F

C_{pf} = 0.474 Btu/lb °F

μf = 15.7 lb/hr ft

K_f = 0.0724 Btu/(hr)(ft^2)(°F per ft)

ρ = 53.4 lb/ft^3

G = 2.225 x 10^6 lb/hr ft^2

$$N_{Re} = \frac{DG}{\mu} = 9.23 \times 10^3$$

$$N_{Pr} = \frac{C_p \mu}{K} = 102.8$$

Equation (9-10b), page 219, for turbulent flow applies.

$$h_L = \frac{0.023\ C_{pb}\ G}{\left(\frac{DG}{\mu_f}\right)^{0.2} \left(\frac{C_p \mu}{K}\right)^{2/3}} = 189 \text{ Btu/hr ft}^2\ ^\circ\text{F}$$

b. Pressure Drop

f_m = 0.0079, from Figure 6-11, page 156 ("Friction Factor for Flow in Pipe")

For incompressible flow Equation (6-9a), page 157, applies.

$$\Delta P = \frac{f_m \, G^2 \, V_m \, L}{2g_c \, r_h \, 144} = 0.365L \text{ psi}$$

2. Heat Transfer Coefficient for Flow in Annular Space

Assume 10 gpm water flow rate

Bulk Temperature = $147^{\circ}F$

Wall Temperature = $200^{\circ}F$

$C_{pb} = 1$ Btu/lb $^{\circ}F$

$\mu_b = 1.11$ lb/hr ft

$\mu_w = 0.70$ lb/hr ft

$K_b = 0.378$ Btu/(hr) (ft^2) ($^{\circ}F$ per ft)

$D_e = D_2 - D_1 = 0.01817$ ft

$G = 3.21 \times 10^5$ lb/hr ft^2

$$N_{Re} = \frac{D_e G}{\mu} = 5.26 \times 10^3$$

$$N_{Pr} = \frac{C_p \mu}{K} = 2.94$$

Equation 9-32C, page 243, applies

$$h = \frac{0.023 \; C_{pb} \; G}{\left(\frac{C_p \mu}{K}\right)_b^{2/3} \left(\frac{\mu_w}{\mu_b}\right)^{0.14} \left(\frac{D_e G}{\mu_b}\right)^{0.2}} = 692 \; \frac{\text{Btu}}{\text{hr ft}^2 \, ^{\circ}F}$$

To this answer, a fin efficiency correction factor was added.

The result:

$$h_f = 1000 \ \frac{\text{Btu}}{\text{hr ft}^2\ ^\circ\text{F}}$$

3. Over-all Cooler Performance

Using the maximum heat transfer rate and the transfer coefficients, the length of exchange section was estimated to be 80 feet. The calculated performance figures based on this length are:

	Required Temp. Gradient for Heat Transfer	Pressure Drop
Flow Inside Tube $t = Q/Ah$	216°F	29 psi
Flow Inside Annulus $t = Q/Ah_f$	41°F	
Tube Wall Conductivity $\Delta t = \frac{Q \ln \frac{D_2}{D_1}}{2\pi LK}$	30°F	
Total	287°F	29 psi

It is to be noted that 287°F is less than the design total temperature gradient for heat transfer of 343°F. Thus, 80 feet of exchanger section is more than adequate for this unit.

LIST OF CITED REFERENCES

Chapter II

(1) Johnson, B. A. and Schmid, L.; An Investigation of a Number of Representative Electrohydraulic Servo Valves; WADC TR 55-29, Part 2, August 1956.

(2) Johnson, B. A. and others; Research on Servo Valves and Servo Systems; WADC TR 55-29, Part 4, August 1957.

(3) Johnson, C. L.; Analog Computer Techniques; McGraw-Hill Book Co., 1956, p 31.

(4) Lee, S. Y. and Blackburn, J. F.; "Steady-State Axial Forces on Control Valve Pistons", Trans ASME V 74 No. 6 August 1952, pp 1005-1011.

(5) Lee, S. Y. and Blackburn, J. F.; "Transient Flow Forces and Valve Instability", Trans ASME V 74 No. 6 August 1952, pp 1013-1016.

(6) Maynard, C. A.; "Analysis and Design of Permanent Magnet Assemblies," Machine Design April 18, 1957, pp 122-143.

(7) Tenzer, R. K.; "Estimating Leakage Factors of Permanent Magnets from Geometry of Magnetic Circuit"; Electrical Manufacturing; February 1957, pp 94-97.

LIST OF CITED REFERENCES

Chapter III

(1) Clark, R. N.; "Compensation of Steady-State Flow Forces in Spool Type Hydraulic Valves"; Trans ASME; V 79 No. 8, November 1957; pp 1784-1788.

(2) Lee, S. Y. and Blackburn, J. F.; "Steady-State Axial Forces on Control Valve Pistons", Trans ASME V 74 No. 6, August 1952 pp 1005-1011.

(3) Sinclair, R. I. and Turnbull, D. E.; "Reducing Static Reaction in Spool Type Valves"; Applied Hydraulics; August 1957; pp 106-109.